STUDIES ON THE EXCITATION MECHANISMS IN THE POSITIVE COLUMN He-Cd^+ LASER

Masakazu Mori

STUDIES ON THE EXCITATION MECHANISMS IN THE POSITIVE COLUMN $He-Cd^+$ LASER

by

Masakazu Mori

Nagoya University, 1978

Table of Contents

Chapter 1. Introduction

§1.1. Metal Ion Lasers

Many gas lasers have been developed since the discovery of the He-Ne laser.[1,2] Among them, only the rare gas ion lasers and the positive column metal ion lasers have many laser lines in the visible and ultraviolet spectral regions. They are the most important light source in the color holography, the color display, the printing, the laser metrology, or the Raman spectroscopy because of their good stability, relatively high output power, and manageability.

In the rare gas ion lasers, the active media consist of the rare gas discharges of the high discharge current densities,[3,4] and the laser output powers of the order of several watts can be obtained. Because of the high discharge current operation, however, thermal problems, bore erosion, a gas clean up, and a gas pumping are considerable. Then a cooling system, expensive materials, a gas reservoir, and a return path are needed, and the whole systems are usually rather huge and expensive. On the contrary, the positive column metal ion lasers using the rare gas-metal mixture discharges as the active media have much lower threshold discharge currents and higher quantum efficiencies than the rare gas ion lasers,[5] because ionization potentials of metals are low. The additional equipments are not necessary.

In 1964, the pulsed laser oscillation was obtained in the Hg(II) 6150 and 5678 Å lines.[6] This was the first metal ion laser. Later, pulsed and continuous oscillations were obtained

in the ionic spectra of metals such as Cd, Zn, Se, and I.[5,7-12] Among them, the positive column He-Cd^+ laser exhibited a high efficiency, and a relatively high laser output power was obtained at the Cd(II) 4416 Å line.[5] Moreover, laser oscillation was obtained at the Cd(II) 3250 Å ultraviolet line without any modification of the laser tube.[9,10]

In the early years, this positive column He-Cd^+ laser was realized with the oven type discharge tube; the Cd grains were placed in pockets along the tube axis and they were heated with heat tapes. This structure is, however, not suitable for making practical type lasers, and the control of the Cd vapor pressure is rather difficult at high discharge currents. In 1969, a cataphoresis type laser tube was developed, with which a uniform axial distribution of the Cd atom density was obtained by means of the cataphoresis effect.[13-15] Most of the practical laser tubes used at present are the cataphoresis type. Some technical improvements have been done in the laser tube thereafter,[16-18] and the positive column He-Cd^+ laser has become the most convenient and practical laser among the metal ion lasers.

Laser oscillation can be obtained also with a He-Cd discharge tube of a hollow cathode structure, which utilize the negative glow as the active medium.[19] In the hollow cathode discharge, one can obtain more laser lines and higher laser output powers than in the positive column discharge.[19,20] A practical hollow cathode laser system has, however, not been constructed yet because of the complicated structures, difficulties in controlling the Cd vapor pressure, rather unstable

laser output powers, and difficulties in preventing possible arcings accompanied with an extensive sputtering which leads to deteriorations of insulations and to the starvation of gas.

In view of the positive column He-Cd^+ laser being the most important metal ion laser at present as mentioned above, it becomes of an urgent interest to understand the excitation mechanisms in it thoroughly not only from a physical standpoint but also from a practical standpoint.

§1.2. Some Problems as to the Excitation Mechanisms in the Positive Column He-Cd^+ Laser

In the early stage of the studies on the positive column He-Cd^+ laser, it has been observed that the Cd(II) 4416 or 3250 Å laser output power shows a behavior similar to that of the Cd(II) 4416 or 3250 Å sidelight intensity,[5,21] which is proportional to the population density of the laser upper state. It has been concluded from this experimental result that the population densities of the laser lower states are negligibly small compared with those of the laser upper states. Since then, in the study of the positive column He-Cd^+ laser, the saturations of the laser output powers have been interpreted as the saturations of the population densities of the laser upper states, and only the excitation mechanisms to the laser upper states have been studied by many investigators.[21-26]

It seems rather difficult, however, to interpret the discharge current or He pressure dependence of the laser output powers by taking only the population densities of the laser

upper states into account. In the He pressure dependence of the laser output powers, for instance, the optimum He pressure for the Cd(II) 4416 Å laser output power is somewhat different from the He pressure where the Cd(II) 4416 Å sidelight intensity has a maximum. This may show that the contribution of the population density of the laser lower state is not negligible. There has been reported only one data concerning the population densities of the laser lower states under the optimum condition for the laser action.[27] They are insufficient to estimate the influence of the population densities of the laser lower states on the laser output powers. Moreover, as they were obtained with the absolute line-intensity measurements using the standard lamp and with the laser gain measurements, the errors in the experimental results may be large. Therefore, it has not been made clear whether the population densities of the laser lower states have the significant influence on the laser output powers or not.

The interest as to the excitation mechanisms in the positive column He-Cd^+ laser discharge so far is mostly directed to the excitation processes to the upper states of the Cd(II) 4416 and 3250 Å laser lines. Silfvast has proposed that the Penning excitation process between He atoms in the He(I) metastable states and Cd atoms in the ground state, as described in eq.(1.1), is the dominant excitation process to the laser upper states.[5]

$$He(2^3S \text{ or } 2^1S) + Cd \rightarrow He + (Cd^+)^* + e + K.E., \qquad (1.1)$$

where $(Cd^+)^*$ is the Cd(II) excited states, e is the ejected

electron, and K.E. is the kinetic energy. Later, the collision cross sections of the Penning excitation process have been measured with the after-glow technique, and it has been found that they are very large ($10^{-15} \sim 10^{-14}$ cm^2).[28-31]

In the next step, the population densities of the He(I) metastable states in the positive column He-Cd^+ laser discharge have been determined with the absorption method[23,24] and with the Hook method.[26] The Cd atom density dependence of the population density of the upper state of the Cd(II) 4416 or 3250 Å laser line could be explained fairly well with the measured population densities of the He(I) metastable states by assuming only the Penning excitation process. However, a considerable discrepancy was found between the discharge current dependences of the population densities of the He(I) metastable states and those of the laser upper states. The population densities of the He(I) metastable states are saturated in the low discharge current region, while those of the laser upper states are saturated in the much higher discharge current region.

On the other hand, the calculated population density of the He(I) 2^3S state increased linearly up to a discharge current around 100 mA.[32,33] Therefore, a complete discrepancy was found between the measured population density of the He(I) 2^3S state and the calculated one.

These discrepancies may come from defects in the measurement and calculations, or may be caused by neglecting excitation processes other than the Penning excitation process.

From the experimental results mentioned above, Miyazaki et al. have supposed that the He atoms in the He(I) 2^3P and 2^1P states also come into the Penning collisions with Cd atoms in the ground state, and proposed to take the sum of the population densities N_m of the He(I) first excited states (2^3S, 2^1S, 2^3P, 2^1P).[26] But the discharge current dependence of N_m was still insufficient to explain those of the population densities of the laser upper states.

In order to make clear whether the Penning excitation process is the dominant excitation process to the laser upper states or not, it is necessary to carry out accurate measurements as to the population densities of the He(I) metastable states, and to give theoretical interpretations for the dependences of them on various experimental parameters. Especially, the discharge current dependences of them have to be made clear theoretically, because a complete discrepancy exists between the experimental and theoretical results at present as mentioned above.

On the other hand, Jánossy et al. have proposed that the collisions between electrons and Cd^+ ions in the ground state have to be taken into account as well as the Penning collisions in the high discharge current region.[34] They supposed that the Cd(II) ground state was excited most dominantly by the Penning excitation process. The population densities of the Cd(II) ground state and the He(I) 2^3S state were calculated with rate equations, and it was derived that the population density of the Cd(II) ground state as well as that of the He(I) 2^3S state was saturated in the low discharge current region.

This contradicts the discharge current dependences of the ion densities obtained with the double probe measurement.[35)]

To make clear whether the stepwise excitation process from the Cd(II) ground state is the dominant excitation process to the laser upper states or not, we must measure the population density of the Cd(II) ground state accurately. However, there is no reliable method to determine it at present.

In the calculation of excitation rates to the He(I), Cd(I), or Cd(II) excited states by stepwise or direct excitation process, the electron energy distribution function as well as the electron density must be known. Assuming the Maxwellian electron energy distribution, the electron temperature and density in various positive column He-metal discharges have been measured with the double probe method.[36-38)] But it seems difficult to explain the dependences of the measured population densities of the He(I) or Cd(I) excited states on various experimental parameters by using the Maxwellian electron energy distribution function. Actually, it has been observed that the electron energy distribution in a discharge at medium pressures is far from the Maxwellian one.[39-41)] It has also been assured from the theoretical calculations based on the Boltzmann equation.[42-45)] The reliabilities of the measured or calculated electron energy distribution function have, however, not been verified yet. We have to examine the electron energy distribution more quantitatively.

§ 1.3. Purpose and Composition of the Dissertation

Since the positive column He-Cd^+ laser is the most valuable commercial type He-metal laser at present, investigations of the excitation mechanisms of it are significant from the not only physical but also practical points of view. However, sevaral problems as to the excitation mechanisms in the positive column He-Cd^+ laser still remain unresolved as mentioned in the preceding section.

The purpose of this dissertation is to resolve those problems and to make the excitation mechanisms of the laser upper and lower states in the positive column He-Cd^+ laser clear, and then to interpret the characteristics of the laser output power quantitatively. Although the laser oscillation is attained at the Cd(II) 4416 Å and 3250 Å lines, the excitation mechanisms of the Cd(II) 4416 Å laser is discussed mainly in this dissertation because it can be considered that the excitation mechanism of the Cd(II) 3250 Å laser is the same as that of the Cd(II) 4416 Å laser.

To accomplish the above purpose, the following experiments and calculations have been carried out. (1) A new absorption method "modified absorption method" is developed, with which the absorption coefficients can be measured accurately even in the ultraviolet region. (2) With the modified absorption method, the population densities of the Cd(II) and Cd(I) ground state are measured, and also those of various excited states except for the laser lower state. (3) The electron energy distribution function in the discharges used for the He-metal lasers is calculated with using the Boltzmann equation, and the reliability

of it is examined. (4) The population density of the lower state of the Cd(II) 4416 Å line is measured under the various conditions for the laser action by combining the modified absorption method with the laser gain measurement, and the contribution of it to the laser power is estimated. (5) Theoretical explanations are given for the dependences on various experimental parameters, particularly on the discharge current, of the population densities of the He(I) metastable states. (6) Finally, the excitation mechanisms in the positive column He-Cd^+ laser are discussed quantitatively with using the results (1) to (5).

This dissertation is composed as follows. In Chapter 2, we describe the principle of the modified absorption method and the results on the population density of the Cd(II) ground state. In Chapter 3, we describe a method to determine the population densities of highly excited states with the modified absorption method. In Chapter 4, it is shown that the electron density in the He-metal discharge at medium pressures can be determined with the modified double probe method even though the electron energy distribution in it is non-Maxwellian. The measured electron density is presented. In Chapter 5, we describe the results on the He^+ and Cd^+ ion densities separated by combining the modified absorption method with the modified double probe method. The ionization mechanisms are also discussed. In Chapter 6, the population densities of the He(I) excited states measured under the various experimental conditions are presented, and the saturation mechanisms of the population densities of the He(I) metastable states are discussed in detail. In Chapter 7, we describe the results on the population densities of the upper

and lower states of the Cd(II) 4416 Å line. In Chapter 8, the excitation mechanisms to the upper and lower states of the Cd(II) 4416 Å line are discussed with using rate equations and the results presented in Chapters 3 to 7.

References in Chapter 1.

1) A.Javan, W.R.Bennett,Jr., and D.R.Herriott,"Population inversion and continuous optical maser oscillation in a gas discharge containing an He-Ne mixture,"Phys.Rev.Lett.,vol.6, p.106,1961.

2) A.D.White and J.D.Rigden,Proc.IRE,vol.50,p.1697,1962.

3) W.B.Bridges,Appl.Phys.Lett.,vol.4,p.128,1964.

4) L.Dana and P.Laures,Proc.IEEE,vol.53,p.78,1965.

5) W.T.Silfvast,"Efficient cw laser oscillation at 4416 Å in Cd(II),"Appl.Phys.Lett.,vol.13,pp.169-171,Sep.1968.

6) W.E.Bell,Appl.Phys.Lett.,vol.4,p.34,1964.

7) G.R.Fowles and W.T.Silfvast,"Laser action in the ionic spectra of zinc and cadmium,"IEEE J.Quantum Electron.,vol.QE-1, p.131,1965.

8) W.T.Silfvast, G.R.Fowles, and B.D.Hopkins,"Laser action in singly ionized Ge, Sn, Pb, In, Cd and Zn,"Appl.Phys.Lett., vol.8,pp.318-319,June 1966.

9) J.P.Goldsborough,"Continuous laser oscillation at 3250 Å in cadmium ion,"IEEE J.Quantum Electron.,vol.QE-5,p.133,1969.

10) W.T.Silfvast,"New cw metal-vapor laser transitions in Cd, Sn, and Zn,"Appl.Phys.Lett.,vol.15,pp.23-25,July 1969.

11) G.R.Fowles and R.C.Jensen,"Visible laser transitions in the spectrum of singly ionized iodine,"Proc.IEEE,vol.52,pp.851-852,July 1964.

12) W.T.Silfvast and M.B.Klein,"CW laser action on 24 visible wavelengths in SeII,"Appl.Phys.Lett.,vol.17,pp.400-403,Nov.1970.

13) J.R.Fendley,Jr., I.Gorog, K.G.Hernqvist, and C.Sun,"Characteristics of a sealed-off He^3-Cd^{114} laser,"RCA Review,vol.30,

pp.422-428,Sep.1969.

14) J.P.Goldsborough,"Stable long life cw excitation of helium-cadmium lasers by dc cataphoresis,"Appl.Phys.Lett.,vol.15, pp.159-161,Sep.1969.

15) T.P.Sosnowski,"Cataphoresis in the helium-cadmium laser discharge tube,"J.Appl.Phys.,vol.40,pp.5138-5144,Dec.1969.

16) T.P.Sosnowski and M.B.Klein,"Helium cleanup in the helium-cadmium laser discharge,IEEE J.Quantum Electron.,vol.QE-7, pp.425-426,Aug.1971.

17) D.J.Brink and V.Hasson,"Application of controlled cathodic sputtering to a helium-cadmium laser,"J.Phys.D:Appl.Phys., vol.8,pp.L35-L38,1975.

18) T.F.Lohnston,Jr.,and W.P.Kolb,"The self-heated 442-nm He-Cd laser: Optimizing the power output, and origin of beam noise," IEEE J.Quantum Electron.,vol.QE-12,pp.482-493,Aug.1976.

19) W.K.Schuebel,"New cw Cd-vapor laser transitions in a hollow-cathode structure,"Appl.Phys.Lett.,vol.16,pp.470-472,June 1970

20) T.Salamon, L.Csillag, M.Jánossy, and K.Rózsa,"Single mode operation in a hollow-cathode transverse discharge He-Cd ion laser,"Phys.Lett.,vol.46A,pp.17-18,Nov.1973.

21) T.G.Giallorenzi and S.A.Ahmed,"Saturation and discharge studies in the He-Cd laser,"IEEE J.Quantum Electron.,vol.QE-7, pp.11-17,Jan.1971.

22) L.Csillag, M.Jánossy, K.Kántor, K.Rózsa, and T.Salamon, "Investigation on a continuous wave 4416 Å cadmium ion laser," J.Phys.D:Appl.Phys.,vol.3,pp.64-68,1970.

23) W.T.Silfvast,"Penning ionization in a He-Cd dc discharge," Phys.Rev.Lett.,vol.27,pp.1489-1492,Nov.1971.

24) P.G.Browne and M.H.Dunn,"Metastable densities and excitation processes in the He-Cd laser discharge,"J.Phys.B:Atom.Molec. Phys.,vol.6,pp.1103-1117,June 1973.

25) G.J.Collins,"Excitation mechanisms in He-Cd and He-Zn ion lasers,"J.Appl.Phys.,vol.44,pp.4633-4652,Oct.1973.

26) K.Miyazaki, Y.Ogata, T.Fujimoto, and K.Fukuda,"Excitation mechanism of 3250 and 4416 Å laser lines in the cataphoretic He-Cd laser discharge,"Japan.J.Appl.Phys.,vol.13,pp.1866-1874,Nov.1974.

27) D.T.Hodges,"Helium-cadmium laser parameters,"Appl.Phys.Lett., vol.17,pp.11-13,July 1970.

28) L.D.Schearer and F.A.Padovani,"De-excitation cross section of metastable helium by Penning collisions with cadmium atoms,"J.Chem.Phys.,vol.52,pp.1618-1619,1970.

29) G.J.Collins, R.C.Jensen, and W.R.Bennett,Jr.,"Charge-exchange excitation in the He-Cd laser,"Appl.Phys.Lett.,vol.19,pp.125-128,Sep.1971.

30) L.A.Riseberg, W.F.Parks, and L.D.Schearer,"Penning ionization of Zn and Cd by noble-gas metastable atoms,"Phys.Rev.,vol.A8, pp.1962-1968,Oct.1973.

31) J.M.Green and C.E.Webb,"The production of excited metal ions in thermal energy charge transfer and Penning reactions, J.Phys.B:Atom.Molec.Phys.,vol.7,pp.1698-1711,1974.

32) J.K.Mizeraczyk,"On saturation mechanisms in PC He-Cd^+ lasers," IEEE J.Quantum Electron.,vol.QE-11,pp.218-220,May 1975.

33) S.Watanabe, K.Kuroda, and I.Ogura,"Linewidth measurement and population calculation of a He-Cd laser,"J.Appl.Phys., vol.47,pp.4887-4895,1976.

34) M.Jánossy, V.V.Itagi, and L.Csillag,"On the excitation mechanism and operation parameters of the 4416 Å He-Cd laser,"Acta Phys.Hungar.,vol.32,pp.149-163,Jan.1972.

35) J.K.Mizeraczyk, Z.Zakrzewski, T.Goto, and S.Hattori, "Ionization mechanisms in positive-column He-Cd^+ laser discharge,"Proc.Twelfth Int.Conf.Phen.Ion.Gases,Eindhoven (North-Holland,Amsterdam,1975).

36) T.Goto, A.Kawahara, G.J.Collins, and S.Hattori,"Electron temperature and density in positive column He-Cd^+ lasers," J.Appl.Phys.,vol.42,pp.3816-3818,Sep.1971.

37) T.Goto, H.Kano, and S.Hattori,"Plasma parameters in gas discharges for positive-column He-Se^+ lasers,"J.Appl.Phys., vol.43,pp.5064-5068,Dec.1972.

38) J.K.Mizeraczyk,"A simple method of determination of electron density in positive-column He-metal laser discharges," J.Appl.Phys.,vol.46,pp.1847-1848,April 1975.

39) N.A.Vorobéva, Yu.M.Kagan, and V.M.Milenin,"Electron velocity distribution function in the positive column in a mixture of gases,"Sov.Phys.-Tech.Phys.,vol.9,pp.632-634,1964.

40) J.Y.Wada and H.Heil,"Electron energy spectra in neon, xenon, and helium-neon laser discharges,"IEEE J.Quantum Electron., vol.QE-1,pp.327-335,1965.

41) M.I.Ciobanu, A.I.Ciura, Eva Cojocaru, and I.M.Popescu, "Electron energy distribution function in the positive column of a helium-cadmium laser,"Rev.Roum.Phys.,vol.20, pp.29-41,1975.

42) J.A.Smit,"Berechnung der Geschwindigkeitsverteilung der Elektronen bei Gasentladungen in Helium,"Physica,vol.3, pp.543-560,1936.

43) A.J.Postma, "Calculated electron energy distribution functions for discharges in helium and helium-argon mixtures,"Physica, vol.43,pp.581-595,1969.

44) E.Vokatý and K.Mašek,"Glow discharge in rare-gas and metal vapour mixture I.Distribution functions and kinetic coefficient in He-Cd mixture discharge,"Czech.J.Phys.,vol.B22,pp.776-789,1972.

45) K.Mašek and E.Vokatý,"Solution of the Boltzmann equation for electrons in the discharges in metal vapour-helium mixtures," Czech.J.Phys.,vol.B24,pp.267-283,1974.

Chapter 2. Modified Absorption Method[1)]

§2.1. Introduction

In order to calculate collisional rates of various excitation processes to the laser states in the positive column (PC) He-Cd^+ laser discharge, it is indispensable to measure exactly the He^+ and Cd^+ ion densities and the population densities of the various excited states of He(I), Cd(I), and Cd(II) which relate to the laser states. The population densities of the He(I) metastable states, the Cd(I) ground state, the low lying Cd(I) excited states, and the upper state of the Cd(II) 3250 Å line have been determined experimentally with spectroscopic methods.[2,3)] On the other hand, there are no reliable experimental data on the ion densities at present. Silfvast tried to determine the population density of the Cd(II) ground state with the Ladenburg-Reiche method.[4)] This method employs two identical but separate discharges, one of which is the plasma to be investigated and the other acts as a light source.[5)] In the case of the He-metal gas mixture discharges, however, it is difficult technically to realize an equal metal vapor pressure in the two discharge tubes. Therefore, the results obtained with this method may contain large uncertainties. Moreover, the inner diameter of the discharge tube used in ref.4 was very large (10 mm) in comparison with those used for the He-metal lasers, and the control of the Cd atom density was probably not good. The measured results in ref.4, therefore, cannot be used in the quantitative study of the PC He-Cd^+ laser.

Although the ion densities were obtained from the double

probe measurement in ref.6, they contain large uncertainties because the mobility of Cd^+ ions is not known exactly. Therefore, we must develop a new method to determine the ion densities as well as the population densities of the He(I) metastable states.

An absorption method has been developed as one convenient method to determine population densities of various excited states in gas discharges.[5,7,8] The principle of it has been summarized in ref.7. There are three measuring methods according to what type of light source is used. (1) The Ladenburg-Reiche method which was used by Silfvast in ref.4. As mentioned above, however, this method is not suitable for the measurements in the He-metal discharges. (2) A method using a completely different light source from the plasma to be investigated.[9] This needs additional equipment and information about the spectra of the light source. (3) A self-absorption method developed by Harrison[10] in which one discharge tube and a reflective mirror are used. The discharge itself is a light source and at the same time, is the plasma to be investigated. Browne and Dunn used this method to determine population densities of several excited states in the PC He-Cd^+ laser discharge.[2] Although this method is simple and good, it is necessary to estimate a reflectivity of the mirror and a transmissivity of a window of the tube exactly. The estimation of them is very difficult. Moreover, the reflectivity or the transmissivity may change in the course of the experiment.

By modifying a conventional type of discharge tube, a simple absorption method has been developed, with which we

can obtain exact absorption coefficients of visible and ultraviolet lines in a cataphoresis type of discharge without any mirror or different light source.[1)]

§2.2. Principle of the Method

Figure 2-1 shows the diagram of the actual discharge tube and other experimental arrangement of the modified absorption method. The principle of the method is as follows. The discharge tube has one anode A and two identical cathodes K1 and K2. First the discharge is obtained between A and K1. From the schematic diagram of the optical arrangement shown in Fig.2-2, the light intensity I_{A-K1} from the plasma I of ℓ in length, which reaches a monochoromator through two identical apertures AP1 and AP2 of d in diameter, is given by eq.(2.1) when the plasma is spacially uniform and $d \ll a$, b, and ℓ.[10)]

$$I_{A-K1} = C' \frac{\theta^2 d^2}{16} F_q \int_0^\infty d\nu' \int_0^\ell dx\, f(\nu') \exp\{-k_0 f(\nu') x\}$$

$$= C \frac{\theta^2 d^2}{16} F_q \int_0^\infty d\nu' \left[1 - \exp\{-k_0 f(\nu')\ell\}\right]. \qquad (2.1)$$

Here, C' and C are constants relating to the ratio of the emission and absorption coefficients, and $C' = k_0 C$. θ is the half angle subtended at the center of AP2 by AP1, F_q is the transmissivity of the window, $f(\nu)$ is a function giving the line profile, and k_0 is the difference of the absorption coefficient and the induced emission coefficient at a certain frequency within

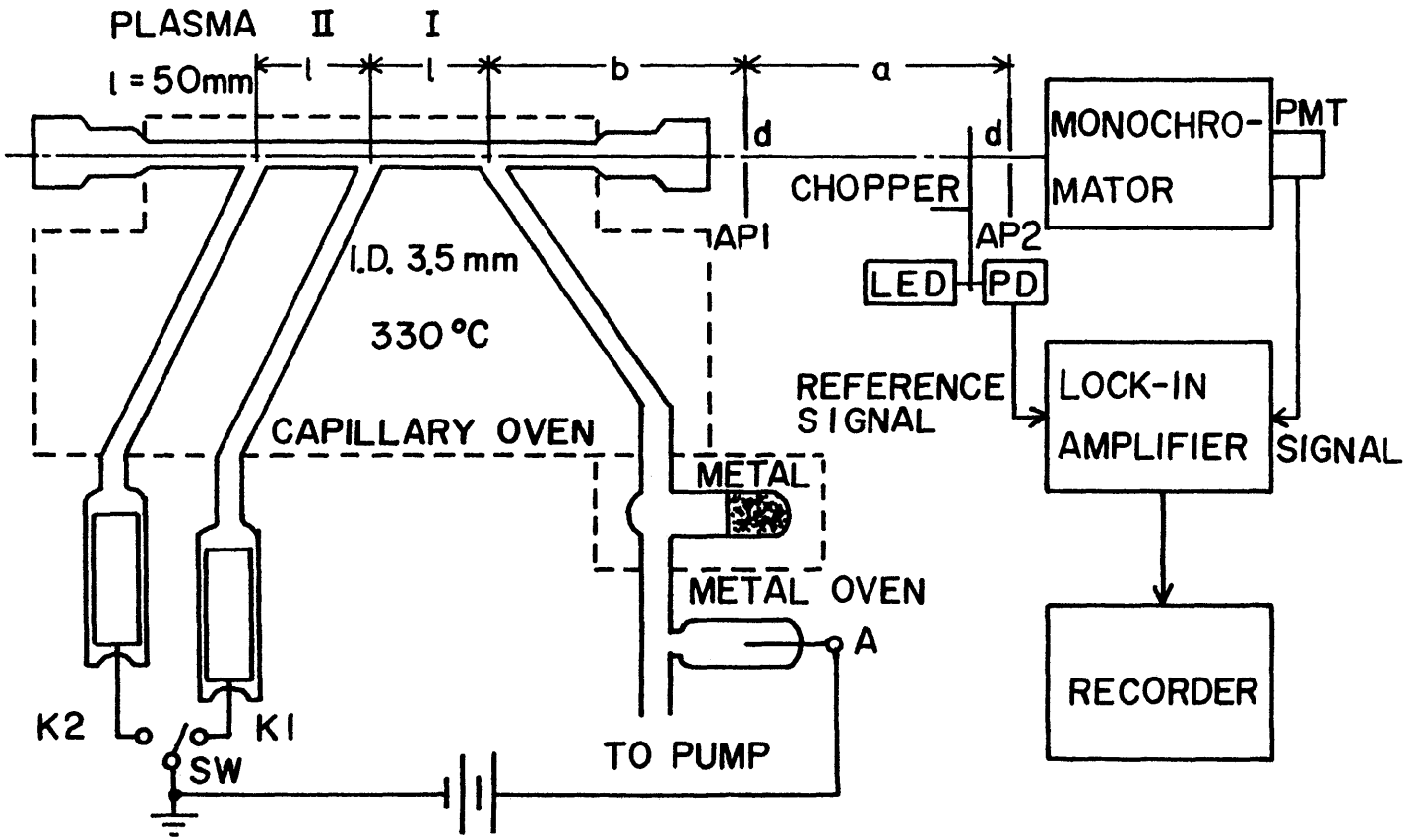

Fig.2-1. Schematic diagram of the modified absorption method.

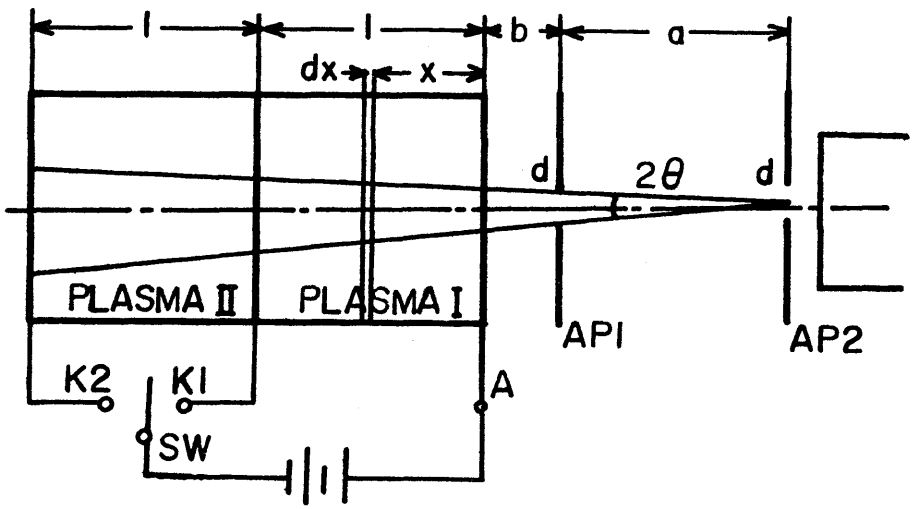

Fig.2-2. Optical arrangement of the modified absorption method.

the line profile. Next, the discharge is switched from A-K1 to A-K2. The light intensity from the plasma I + II of 2ℓ in length, I_{A-K2}, is obtained by replacing $\exp\{-k_0 f(\nu)\ell\}$ by $\exp\{-2k_0 f(\nu)\ell\}$ in eq.(2.1) merely. Therefore, we obtain that

$$G(k_0\ell) = I_{A-K2}/I_{A-K1} - 1$$

$$= \frac{\int_0^\infty [1 - \exp\{-k_0 f(\nu')\ell\}]\cdot\exp\{-k_0 f(\nu')\ell\}d\nu'}{\int_0^\infty [1 - \exp\{-k_0 f(\nu')\ell\}]\, d\nu'} . \qquad (2.2)$$

In deriving eq.(2.2), the multiple reflection on the tube wall has been neglected because it is negligibly small in our optical system. Note that the transmissivity F_q of the window never appears in eq.(2.2). Generally, $f(\nu)$ is a profile composed of several hyperfine splitting and isotope shift components. It is extremely important to know accurate $f(\nu)$ in order to get exact population densities. From eq.(2.2), we can calculate $G(k_0\ell)$ as a function of $k_0\ell$. It can be seen that $G(k_0\ell)$ is a single valued function of $k_0\ell$, and that $G(k_0\ell)$ decreases as $k_0\ell$ increases. Figure 2-3 shows $G(k_0\ell)$ as a function of $k_0\ell$ in the case of the single Doppler broadened profile $f_D(\nu)$, which is so normalized at the line center ν_0 that $f_D(\nu_0) = 1$.

On the other hand, it has been shown that[7)]

$$N_1\left(1 - \frac{g_1 N_2}{g_2 N_1}\right) = \frac{8\pi g_1 k_0 \ell \int_0^\infty f(\nu')\, d\nu'}{\lambda_0^2 g_2 A \ell} . \qquad (2.3)$$

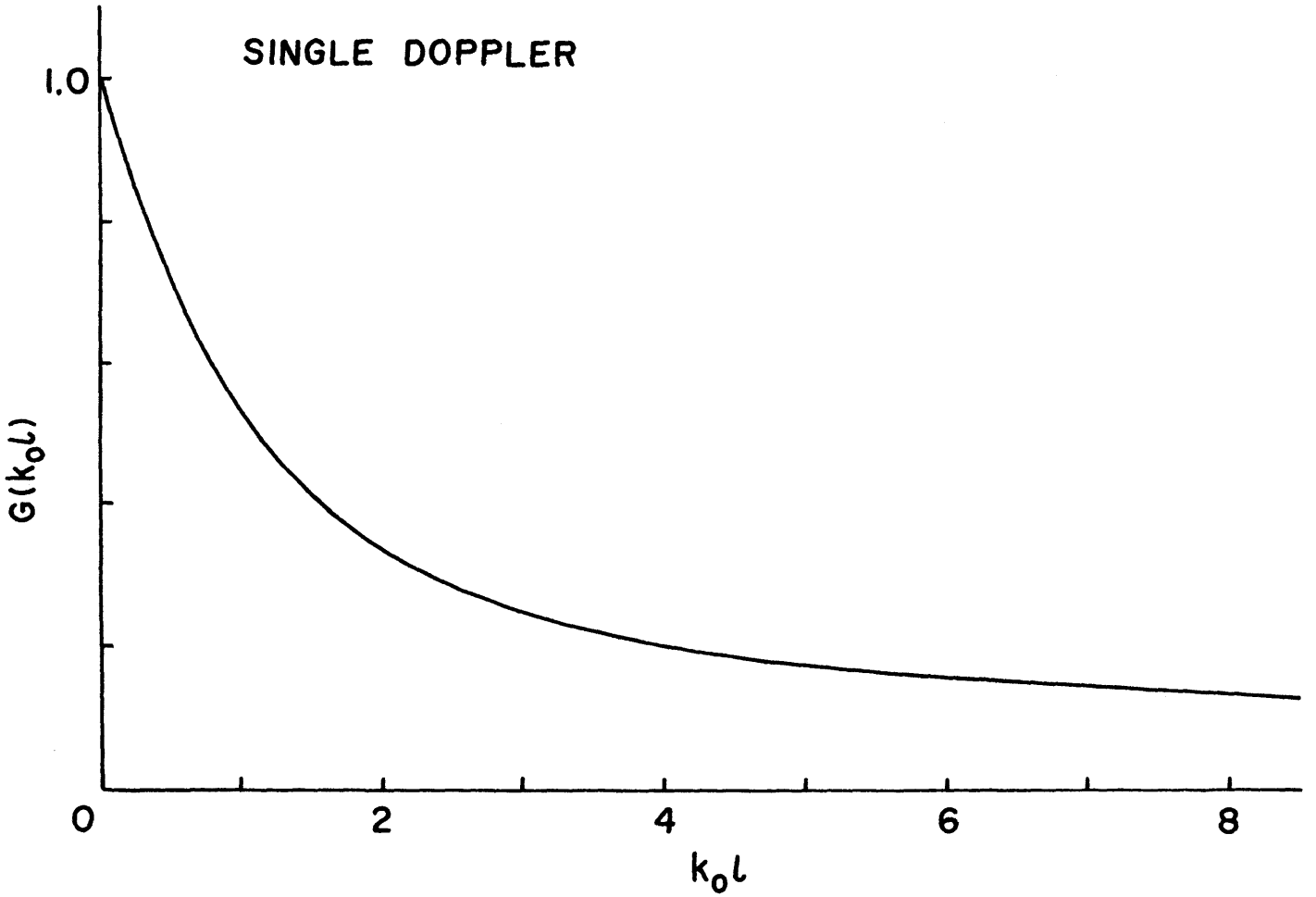

Fig.2-3. $G(k_0\ell)$ as a function of $k_0\ell$ in the case of the single Doppler broadened profile.

Here, the subscripts 1 and 2 denote the lower and upper states of the optical transition, respectively, N is the population density, g is the statistical weight, λ_0 is the wavelength, and A is the transition probability.

By measuring the ratio I_{A-K2}/I_{A-K1} of the endlight intensities, we obtain $k_0\ell$ from the functional dependence of $G(k_0\ell)$ on $k_0\ell$ in eq.(2.2). Provided that g_1N_2/g_2N_1 can be neglected compared with unity (in most cases $g_1N_2/g_2N_1 \lesssim 0.02$), N_1 can be determined from eq.(2.3) with $k_0\ell$ obtained above.

§2.3. Experimental Setup

A discharge tube of 3.5 mm inner diameter (I.D.) was used mainly in this experiment, but also a tube of 3 mm I.D. was used. The length of the plasma I was 5 cm in the tube of 3.5 mm I.D., and it was 3 cm in the tube of 3 mm I.D.. The diameters of the apertures AP1 and AP2 were both 0.4 mm. Since a = 30 cm and b = 10 cm, only the light emitted from the region of about 0.9 mm in diameter of the plasma column could enter into the entrance slit of the monochoromator. The change of the population density within that region is less than 10 % assuming that the radial distribution of it is given by the Bessel function of the zeroth order.

The capillary part of the tube was put in an oven of 600 K and the tube was connected to a flask of large volume at room temperature to keep constant the He atom density N_0 in the capillary part irrespective of the discharge current. Then N_0 is given by

$$N_0 = 1.78 \times 10^{16} p_0 \quad cm^{-3}, \tag{2.4}$$

where p_0 is the initial He pressure in Torr at room temperature. The Cd source was heated by a separate oven and the temperature was controlled within $\pm 1\,^{\circ}C$.

In this method, the switching from A-K1 to A-K2 of the discharge could be done with keeping constant the temperature of the Cd source, that is, the Cd vapor pressure. At one and a half minutes after switching at the longest, the discharge condition attained was completely the same as before switching. This could be easily observed from the relative change of the intensities of spectral lines of the He(I), Cd(I), and Cd(II), which were measured from the side of the discharge tube with a monochromator and a photomultiplier tube. We call the intensity of a spectral line measured from the side of the discharge tube "sidelight intensity" for convenience in this dissertation. When the discharge A-K2 was obtained, the leakage of Cd vapor to the branch K1 was very slight. It was checked with the Cd(II) 4416 Å sidelight and also endlight intensities at the optimum condition for the laser action, which had a low gain for the 5 cm or 3 cm plasma. Then it was concluded that the lights emitted from the plasmas I and II were equal in intensity, line profile, and frequency.

§2.4. Application to the Determination of the Population Density of the Cd(II) Ground State

This method was applied to the PC He-Cd^+ laser discharge,

and the population density of the Cd(II) ground state, the Cd(II) $5s^2S_{1/2}$ state, in the PC He-Cd^+ laser discharge has been determined directly from the measurement of the absorption coefficient of the Cd(II) 2265 Å line and also from that of the Cd(II) 2144 Å line. Those lines are shown in Fig.2-4 together with other Cd(II) lines.

In the case of the spectral lines of Cd of natural isotopic abundance, which consists of six even isotopes and two odd isotopes, the line profile is complicated due to the isotope shifts and hyperfine splittings. Assuming that each component in the profile had a Doppler broadened profile and also that the natural width was very small compared with the Doppler width, the line profile $f(\nu)$ was calculated. The ion temperature of the Cd(II) line was assumed to be about 1000 K from the data in refs.11 and 12. For the sake of convenience, the profile $f(\nu)$ of each Cd(II) or Cd(I) line is so normalized that $f(\nu_{112}) = 1$ in this dissertation, where ν_{112} is the center frequenc of the isotope Cd^{112} component.

Figure 2-5(a) shows the line profile $f(\nu)$ of the Cd(II) 2265 Å line, and Fig.2-5(b) shows $G(k_0\ell)$ as a function of $k_0\ell$. Those for the Cd(II) 2144 Å line are shown in Figs.2-6(a) and 2-6(b). The data concerning the isotope shifts and hyperfine splittings for the two lines were obtained from ref.13. The transition probabilities were quoted from ref.14.

The population density of the Cd(II) ground state determined with the Cd(I) 2265 and also 2144 Å line is shown in Fig.2-7

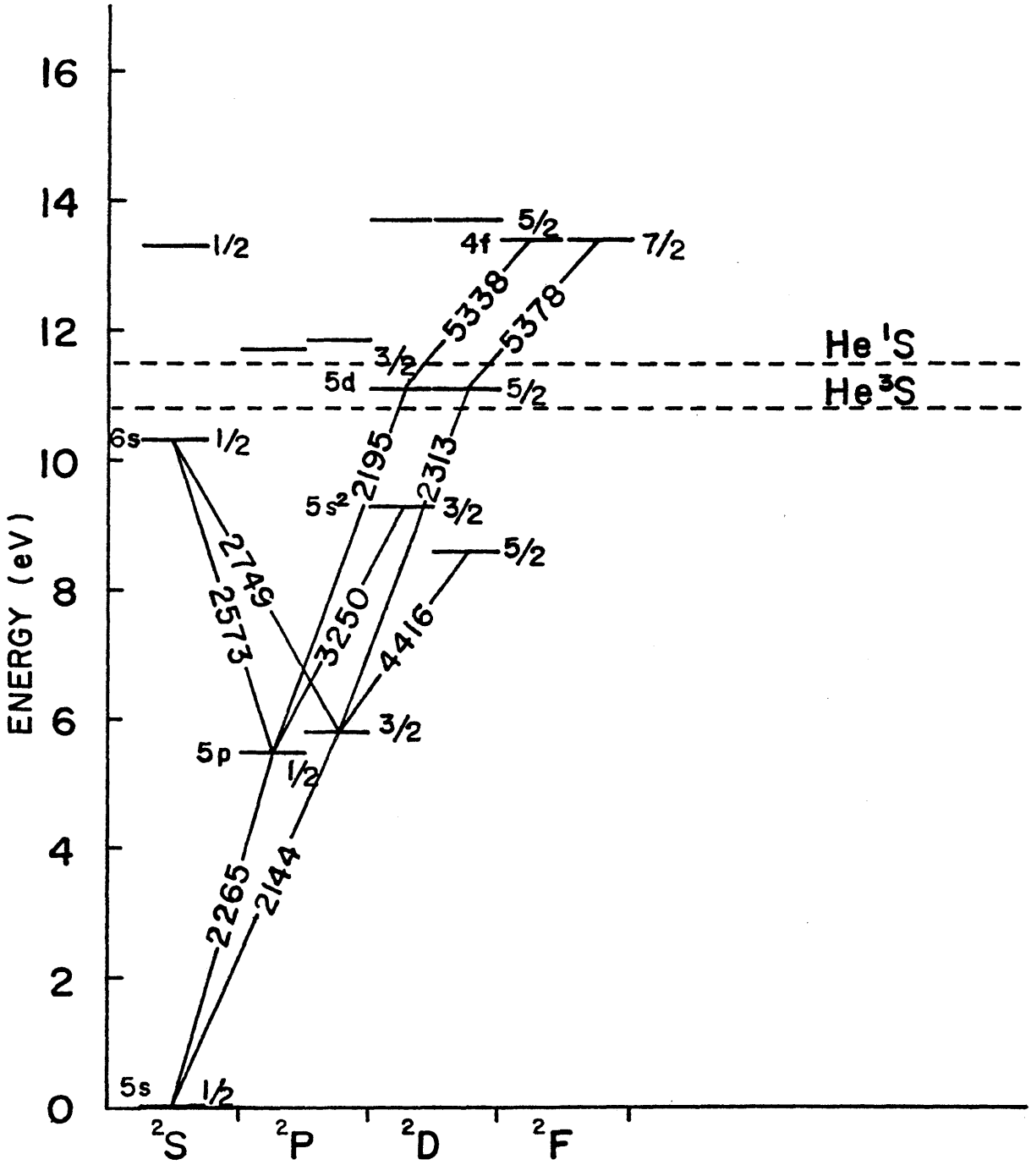

Fig.2-4. Energy level diagram of Cd(II).

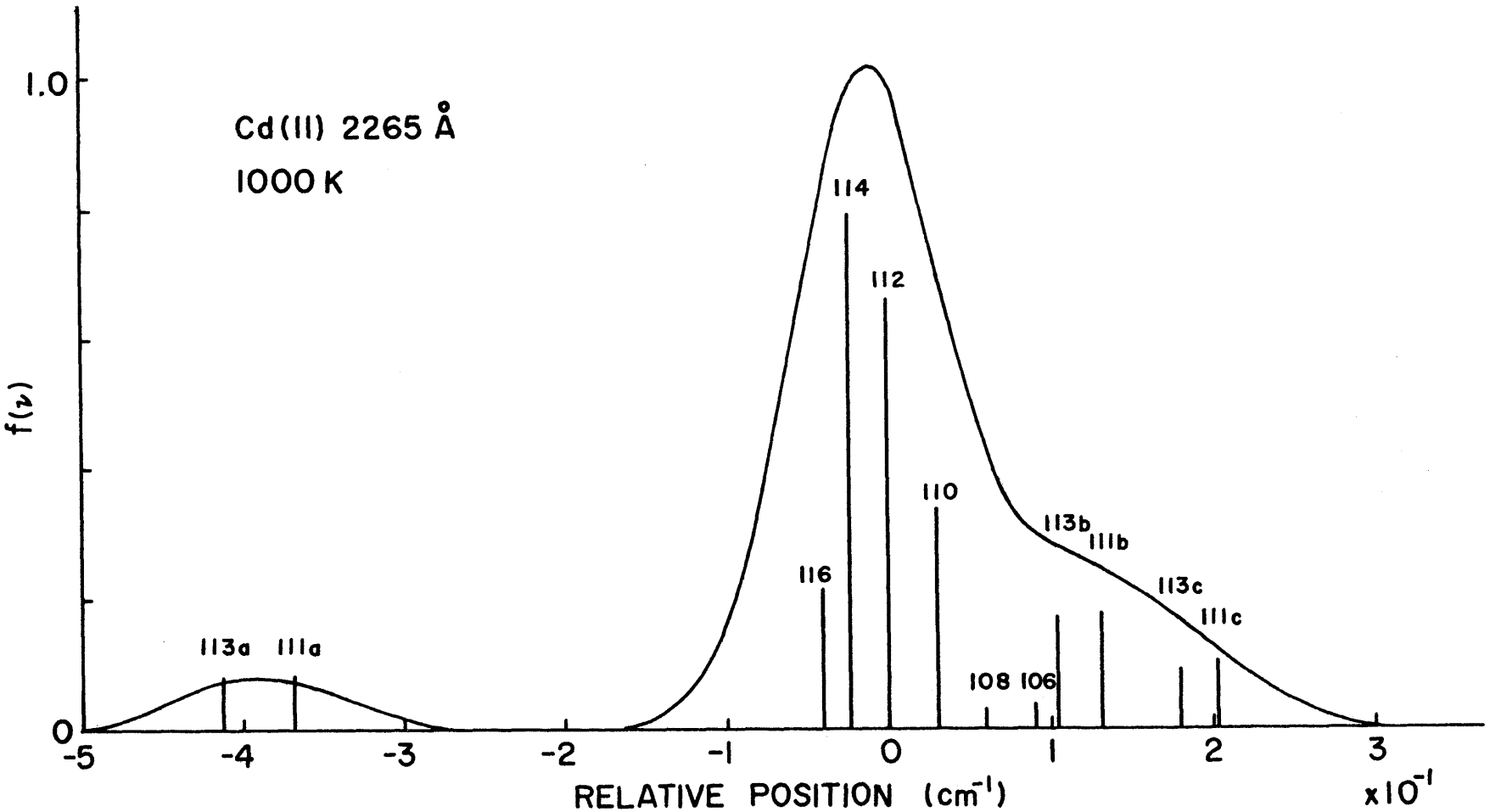

Fig.2-5(a). Line profile of the Cd(II) 2265 Å line. The number adjacent to each component is the mass number. The components due to the odd isotopes are labelled by a, b, and c.

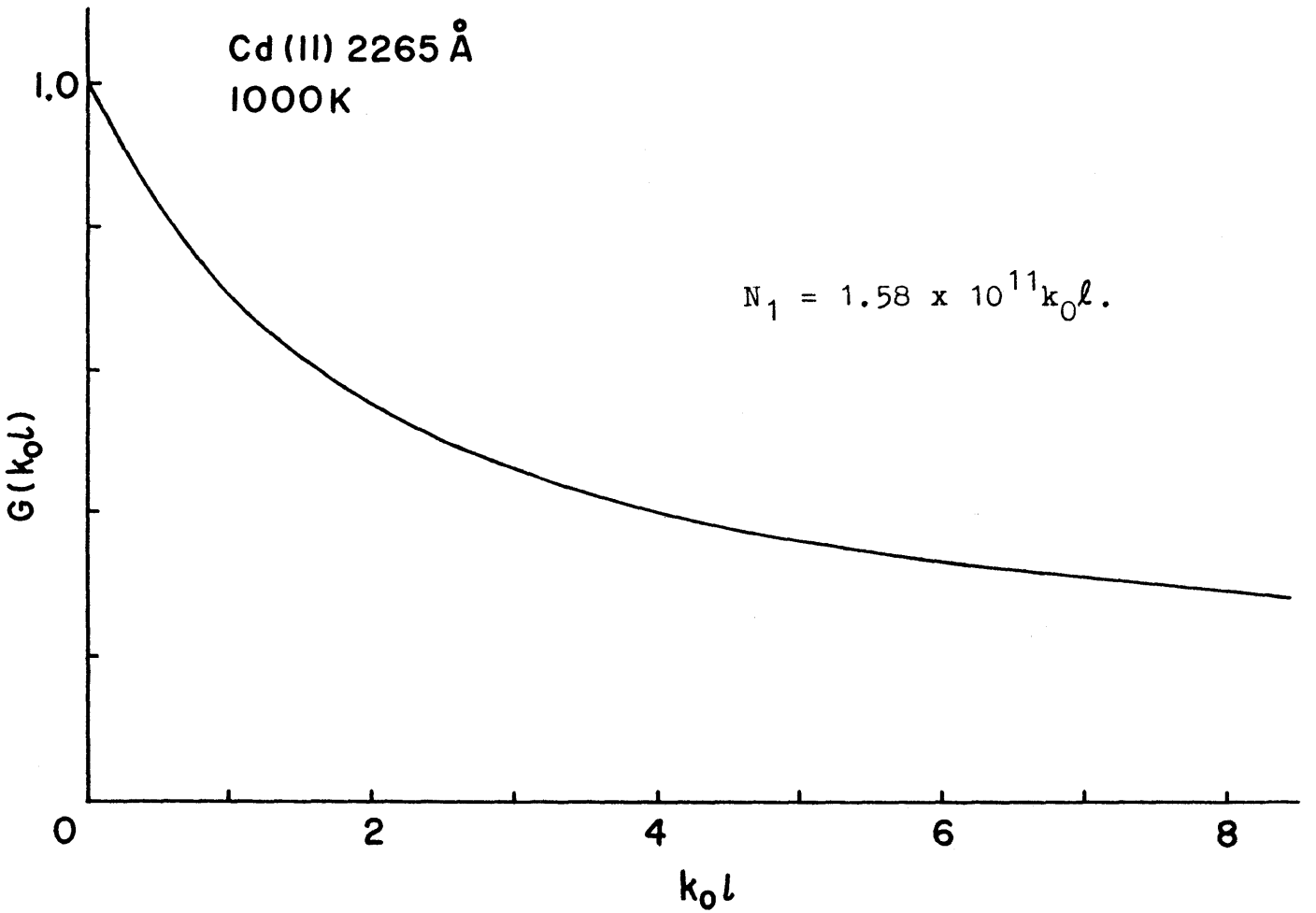

Fig.2-5(b). $G(k_0 \ell)$ of the Cd(II) 2265 Å line as a function of $k_0 \ell$.

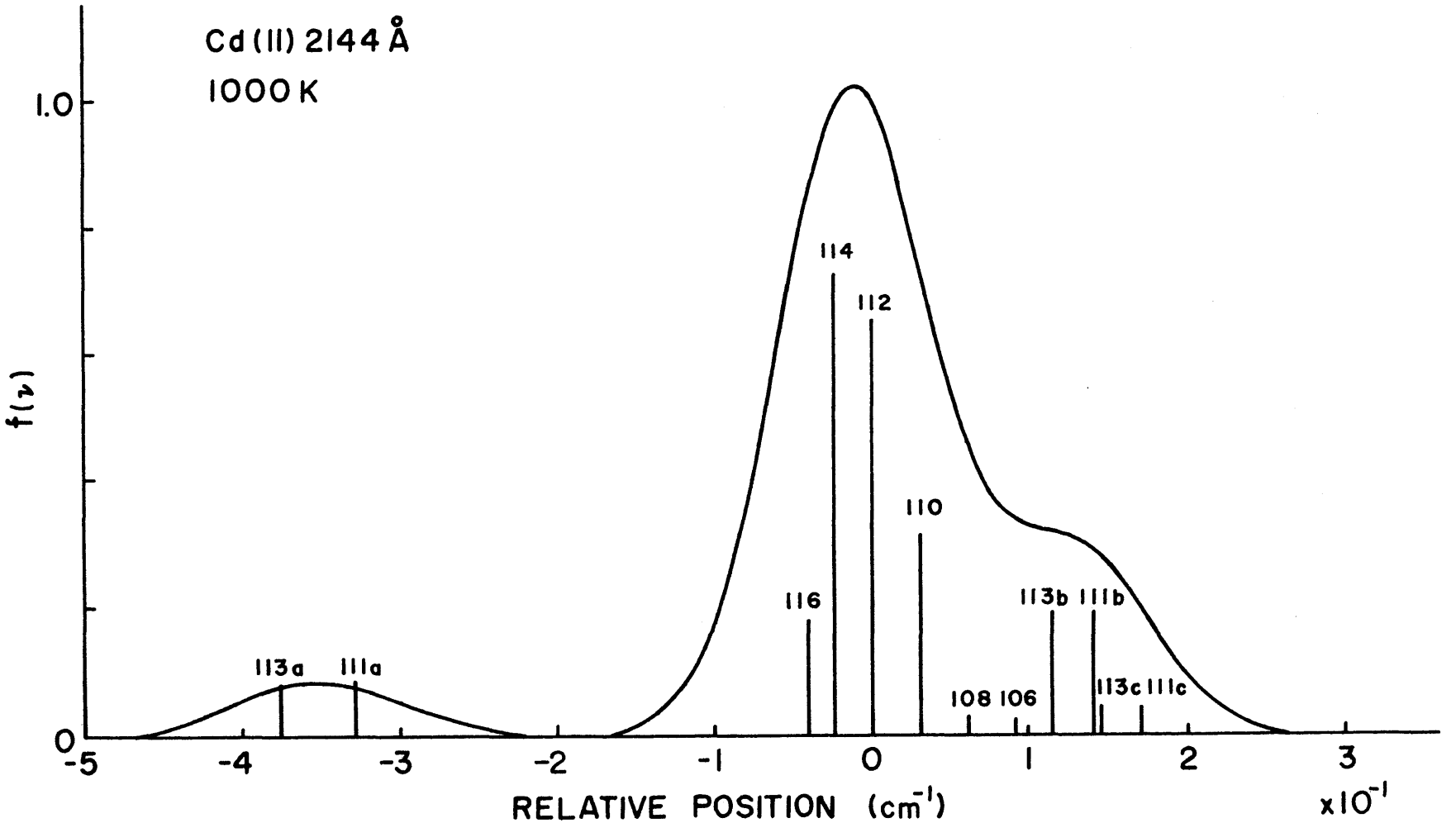

Fig.2-6(a). Line profile of the Cd(II) 2144 Å line. The number adjacent to each component is the mass number. The components due to the odd isotopes are labelled by a, b, and c.

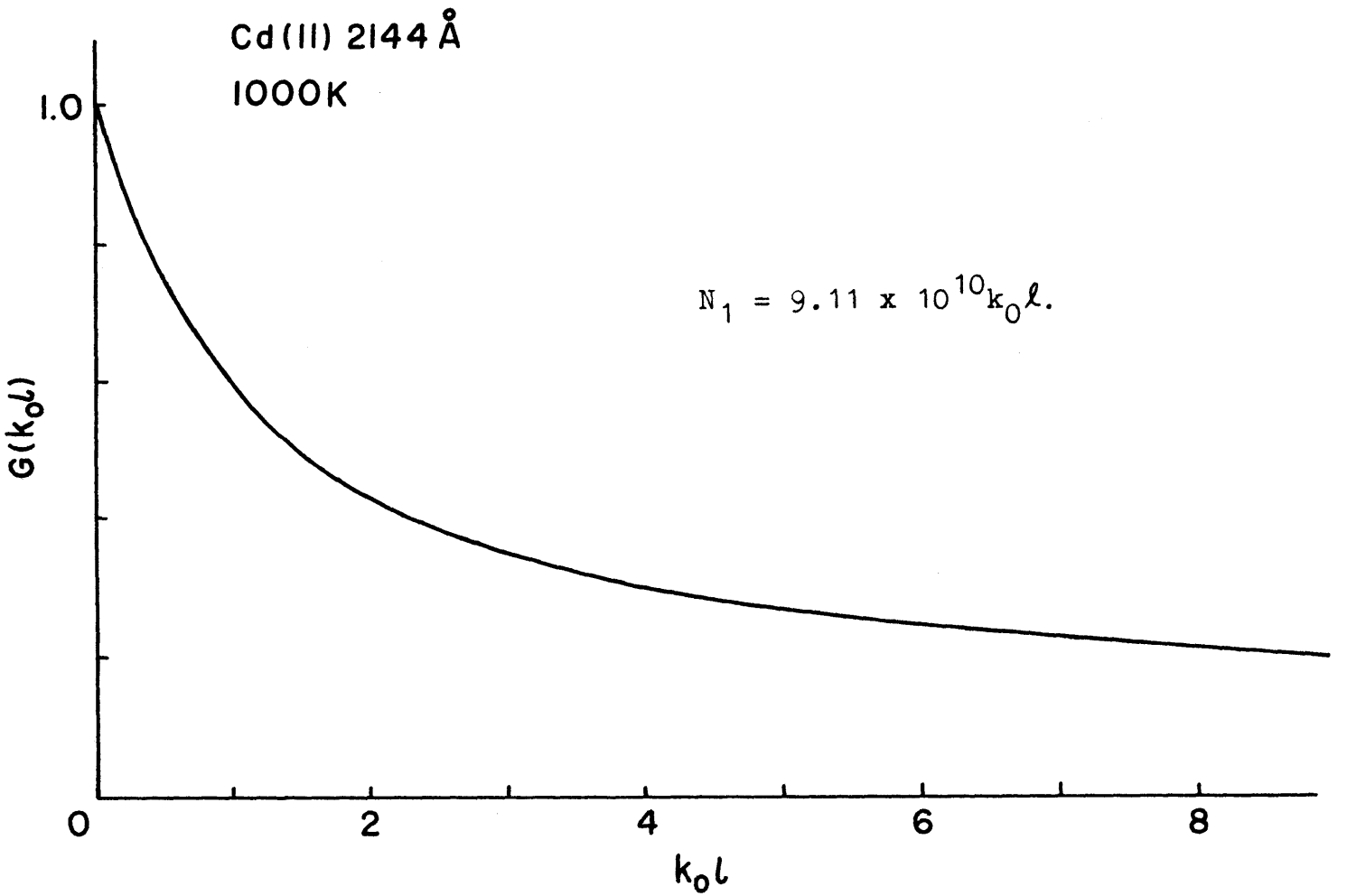

Fig.2-6(b). $G(k_0\ell)$ of the Cd(II) 2144 Å line as a function of $k_0\ell$.

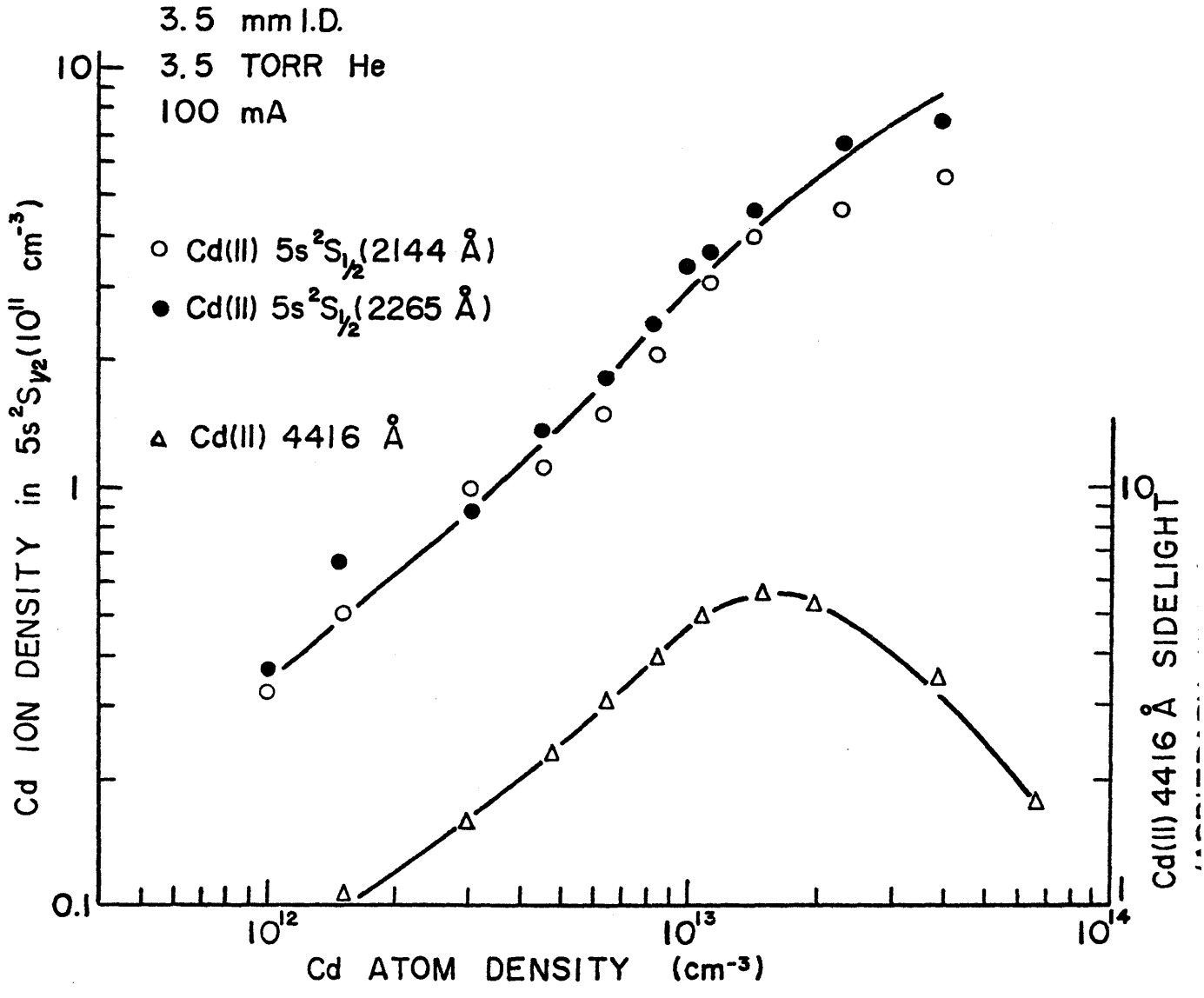

Fig.2-7. Cd atom density dependence of the population density of the Cd(II) ground state.

○ ; determined with the Cd(II) 2144 Å line,

● ; determined with the Cd(II) 2265 Å line.

△ represents the Cd(II) 4416 Å sidelight intensity.

as a function of the Cd atom density together with the Cd(II) 4416 Å sidelight intensity. The discharge current was 100 mA and the initial He pressure was 3.5 Torr, which were close to the optimum condition for the laser action. The actual He atom density in the capillary part was about 6.2×10^{16} cm^{-3} in the present experimental system. The Cd atom density shown in a horizontal axis was determined with the Cd(I) 3261 Å line. Figures 2-8(a) and 2-8(b) show the line profile and $G(k_0\ell)$ of the Cd(I) 3261 Å line, respectively.

§2.5. Reliability of the Method

The present method is superior to the self-absorption method (SAM) in three points: (1) The measurable quantity $I_{A-K2}/I_{A-K1} - 1$ in eq.(2.2) is connected directly with $G(k_0\ell)$ in the present method while it is given by $FF_q^2G(k_0\ell)$ in SAM, where F is the reflectivity of the mirror. As no information about F or F_q is needed, accurate measurement of the absorption coefficient can be made even in the ultraviolet region, and even if the contamination on the window increases. (2) It has been reported that the ion drift velocity is rather large in the He-metal discharge.[15] Doppler shifts due to it cause no difference of the frequencies between the line profile of the lights I_{A-K1} and I_{A-K2}, because both of them propagate from the plasmas to the monochoramator in the same direction, while in SAM, the two profiles shift in frequency oppositely. (3) The alignment of the optical system is easier than that

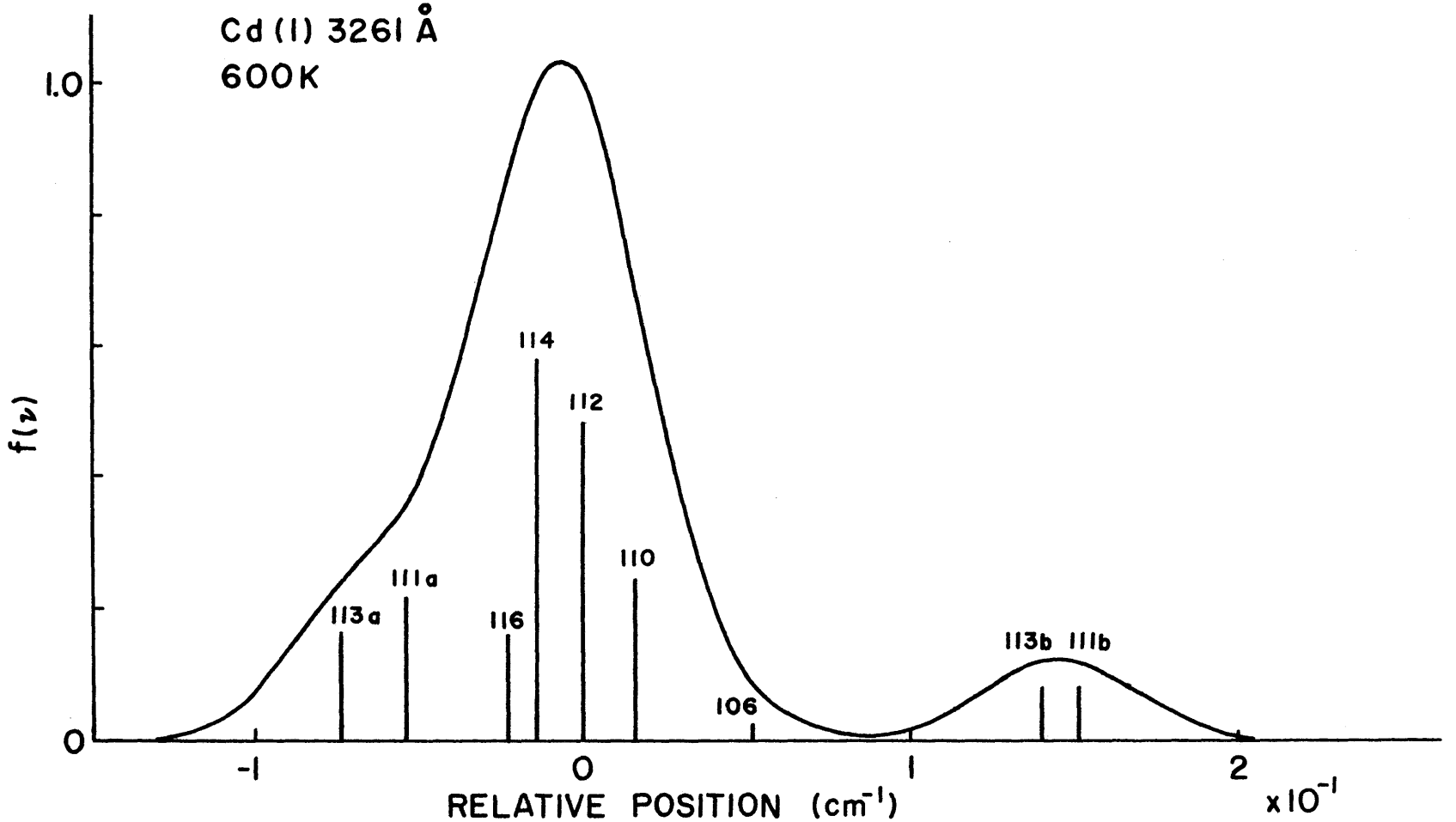

Fig.2-8(a). Line profile of the Cd(I) 3261 Å line. The number adjacent to each component is the mass number. The components due to the odd isotopes are labelled by a and b.

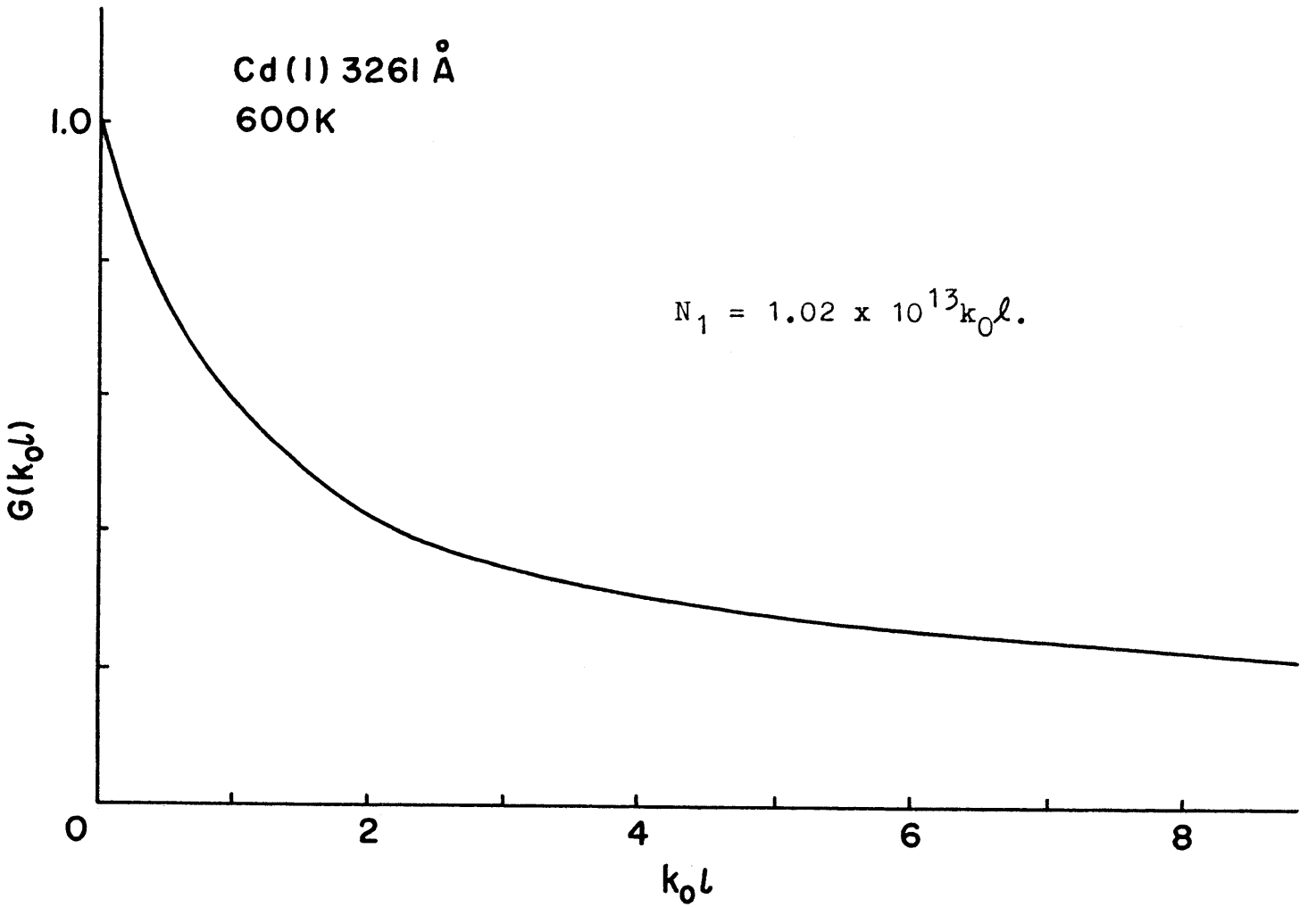

Fig.2-8(b). $G(k_0 \ell)$ of the Cd(I) 3261 Å line as a function of $k_0 \ell$.

in SAM, because only one discharge tube is used in the present method while the discharge tube and the mirror are used in SAM.

As shown in Fig.2-7, the agreement of the two results obtained with the Cd(II) 2265 and 2144 Å lines is quite well. Moreover, the Cd atom density measured with the Cd(I) 3261 Å line coincided with the value obtained from the temperature of the Cd source and a diffusion equation quite well. These facts show that the present method is very reliable and useful, particularly at the absorption measurements in the ultraviolet region. The errors of the absorption coefficients and relative population densities are small although the absolute values of them depend on the errors of the measured transition probabilities.

The hook method described in ref.16 also can be applied to determine the population densities of various excited states. In this method, although we need not know the line profiles, it is not possible to obtain the population density of the Cd(II) ground state in the laser action region as long as an extremely long tube is not used. Moreover, the alignment of the optical system is rather difficult, and the spacial resolving power is not good.

§ 2.6. Conclsion

A method was described with which we could easily obtain exact absorption coefficients not only of visible lines but also of ultraviolet lines to determine population densities of various excited states in a cataphoresis type of positive

column gas discharges. The favorable points of the modified absorption method are that only one discharge tube is used, that a mirror is not necessary, and that we need not know the transmissivity of the window. These enable us to obtain very reliable results even in the ultraviolet region. This method has been applied to the PC He-Cd^+ laser discharge, and it has been confirmed that the method gives an accurate value of the population density of the Cd(II) ground state.

In the visible region, naturally, the modified absorption method gives more reliable results than SAM. Therefore, we can determine the population densities of the He(I) first excited states (2^3S, 2^1S, 2^3P, 2^1P) and those of the low lying Cd(I) excited states with this method accurately.

The modified absorption method will be used to determine various parameters of the PC He-Cd^+ laser discharge in the following chapters.

References in Chapter 2.

1) T.Goto, M.Mori, and S.Hattori,"Modified absorption method to determine level population densities in a cataphoresis type of He-metal laser discharge,"Appl.Phys.Lett.,vol.29, pp.358-360,Sep.1976.

2) P.G.Browne and M.H.Dunn,"Metastable densities and excitation processes in the He-Cd laser discharge,"J.Phys.B:Atom.Molec. Phys.,vol.6,pp.1103-1117,June 1973.

3) K.Miyazaki, Y.Ogata, T.Fujimoto, and K.Fukuda,"Excitation mechanism of 3250 and 4416 Å laser lines in the cataphoretic He-Cd laser discharge,"Japan.J.Appl.Phys.,vol.13,pp.1866-1874,Nov.1974.

4) W.T.Silfvast,"Penning ionization in a He-Cd dc discharge," Phys.Rev.Lett.,vol.27,pp.1489-1492,Nov.1971.

5) R.Ladenburg und F.Reiche,"Über selektive Absorption," Ann.der Physik,vol.42,pp.181-209,1913.

6) J.K.Mizeraczyk, Z.Zakrzewski, T.Goto, and S.Hattori, "Ionization mechanisms in positive-column He-Cd^+ laser discharge,"Proc.Twelfth Int.Conf.Phen.Ion.Gases,Eindhoven, (North-Holland, Amsterdam, 1975),p.224.

7) A.C.G.Mitchell and M.W.Zemansky, Resonance Radiation and Excited Atoms (Cambridge U.P., Cambridge, England, 1934).Chat.III.

8) R.D.Cowan and G.H.Dieke,"Self-absorption of spectrum lines," Rev.Mod.Phys.,vol.20,pp.418-455,April 1948.

9) A.M.Bruneteau, A.M.Icole, C.Rouillé, A.Poquérusse, et H.J.Doucet,"Mésure de la densite ionique par absorption optique dans une décharge au mercure,"Phys.Lett.,vol.46A, pp.309-310,Jan.1974.

10) J.A.Harrison,"Self-absorption in an electrodeless discharge in hydrogen and helium,"Proc.Phys.Soc.,vol.73,pp.841-848, 1959.

11) W.T.Silfvast and P.W.Smith,"Mode locking of the He-Cd laser at 4416 and 3250 Å,"Appl.Phys.Lett.,vol.17,pp.70-73,July 1970.

12) J.P.Goldsborough, Laser Handbook, edited by F.T.Arecchi and E.O.Schulz-DuBois (North-Holland, Amsterdam, 1972),vol.1, p.620.

13) R.H.Contreras and F.M.Kelly,"Isotope shift in the second spectrum of cadmium,"Can.J.Phys.,vol.47,pp.1979-1982,1969.

14) T.Andersen and G.Sørensen,"Systematic trends in atomic transition probabilities in neutral and singly-ionized zinc, cadmium and mercury,"J.Quant.Spectrosc.Radiat.Transfer., vol.13,pp.369-376,1973.

15) G.N.Tolmachev, E.L.Latush, and V.S.Mikhalovichi,"Effect of the radiation density on ion drift velocity in a cadmium-helium laser,"Sov.Phys.-Tech.Phys.,vol.19,pp.1120-1121, Feb.1975.

16) D.Roschdestwensky,"Anomale Dispersion im Natriumdampf," Ann.der Physik,vol.39,pp.307-345,1912.
(The reader can find the general theory of the hook method in the English literatures; A.C.G.Mitchell and M.W.Zemansky, in ref.7,pp.139-145, and W.C.Marlow,"Hakenmethode,"Appl. Optics,vol.6,pp.1715-1724,Oct.1967.)

Chapter 3. Determination Method of Population Densities of Highly Excited States

§ 3.1. Introduction

In the quantitative study of the PC He-Cd^+ laser, it is necessary to determine the population densities of the laser upper and lower states and those of excited states of He(I), Cd(I), and Cd(II) relating to the laser states. The population densities of the He(I) first excited states or those of the Cd(I) and Cd(II) ground states can be determined with the modified absorption method described in the preceding chapter. However, it is difficult to measure the population densities of the laser upper states or those of highly excited states of He(I), Cd(I), and Cd(II) directly with this method, because the absorption coefficients of the optical transitions terminating in those states are very small and the fractions of the light intensities absorbed in the short discharge length ℓ are hardly detected.

In principle, the population densities of excited states, from which optical transitions to lower states are allowed, can be determined by measuring the absolute intensities of the spontaneous emissions when the transition probabilities are known. To this end, the absolute sensitivity of the optical detection system must be calibrated. One of the most simple methods of the calibration is to use the standard lamp such as the tungsten-iodine lamp.[1)] This method of calibration, however, has the following three problems:(1) The tungsten-iodine lamp has the continuous spectra while the spontaneous emissions

from the PC He-metal discharges have line spectra. (2) The geometrical shape of the tungsten-iodine lamp is different from that of the discharge tube. (3) It is difficult to estimate the solid angle subtended at the light source by the monochoromator.

In this chapter, the population densities of the highly excited states of He(I), Cd(I), and Cd(II) are determined by combining the modified absorption method with the sidelight intensity measurements.

§3.2. Principle of the Method

The energy level diagram of Cd(I) is shown in Fig.3-1. We consider here a pair of the optical transitions; the Cd(I) 4800 Å ($6s^3S_1 - 5p^3P_1$) and 3261 Å ($5p^3P_1 - 5s^{21}S_0$) lines. The population densities of the upper and lower states of the Cd(I) 4800 Å line, N_2 and N_1, respectively, are related to the absorption coefficient of the Cd(I) 4800 Å line by

$$N_1 - \frac{g_1 N_2}{g_2} = \frac{8\pi g_1 k_0 \ell \int_0^\infty f(\nu')\,d\nu'}{\lambda_{21}^2 g_2 A_{21} \ell} . \qquad (3.1)$$

Here, λ_{21} is the wavelength (4800 Å), A_{21} is the transition probability, and other symbols are the same as those used in eq.(2.3). The line profile $f(\nu)$ and the function $G(k_0\ell)$ for the Cd(I) 4800 Å line are shown in Figs.3-2(a) and 3-2(b), respectively. By measuring $k_0\ell$ with the modified absorption method, we can obtain $N_1-(g_1/g_2)N_2$ from eq.(3.1).

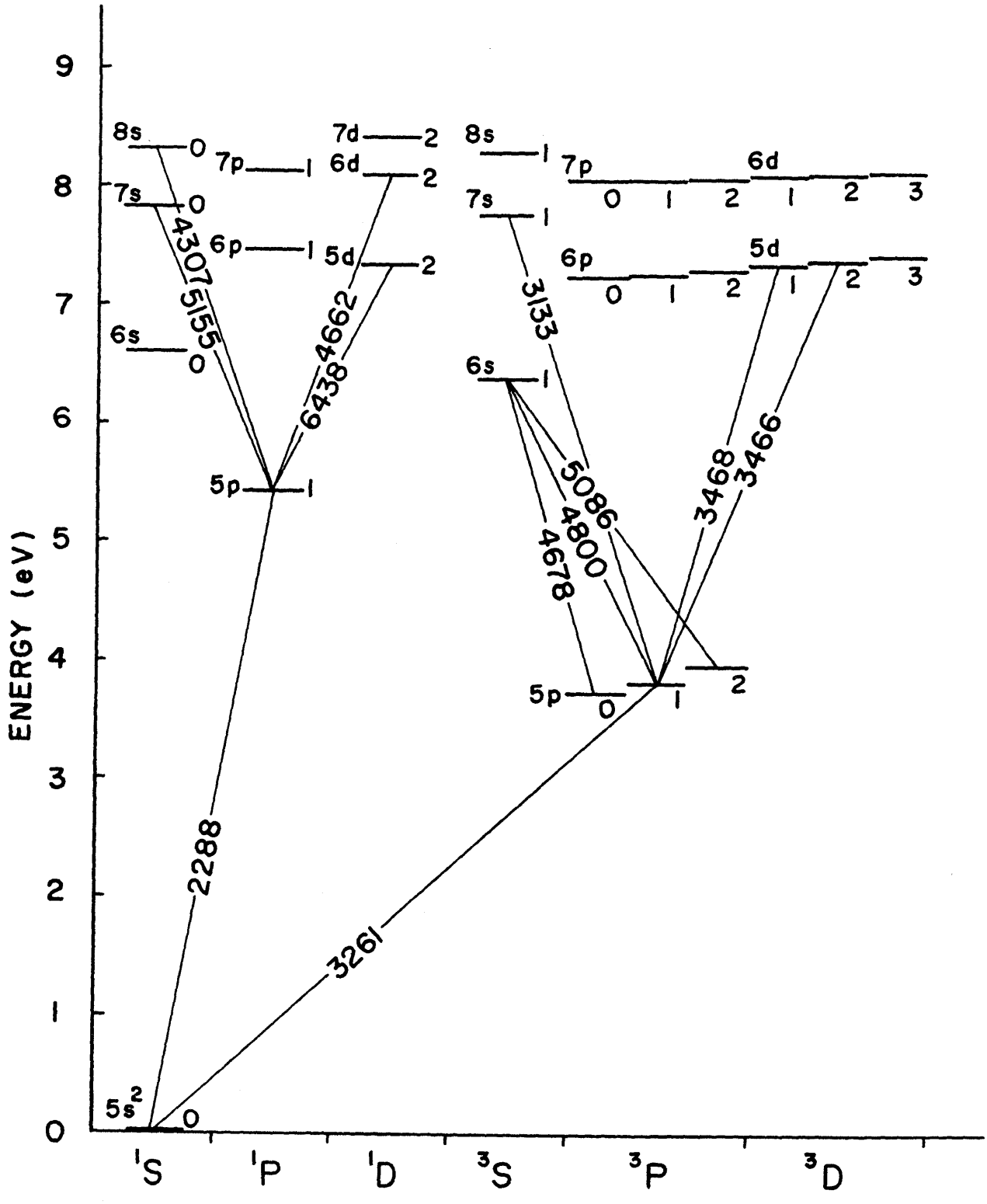

Fig.3-1. Energy level diagram of Cd(I).

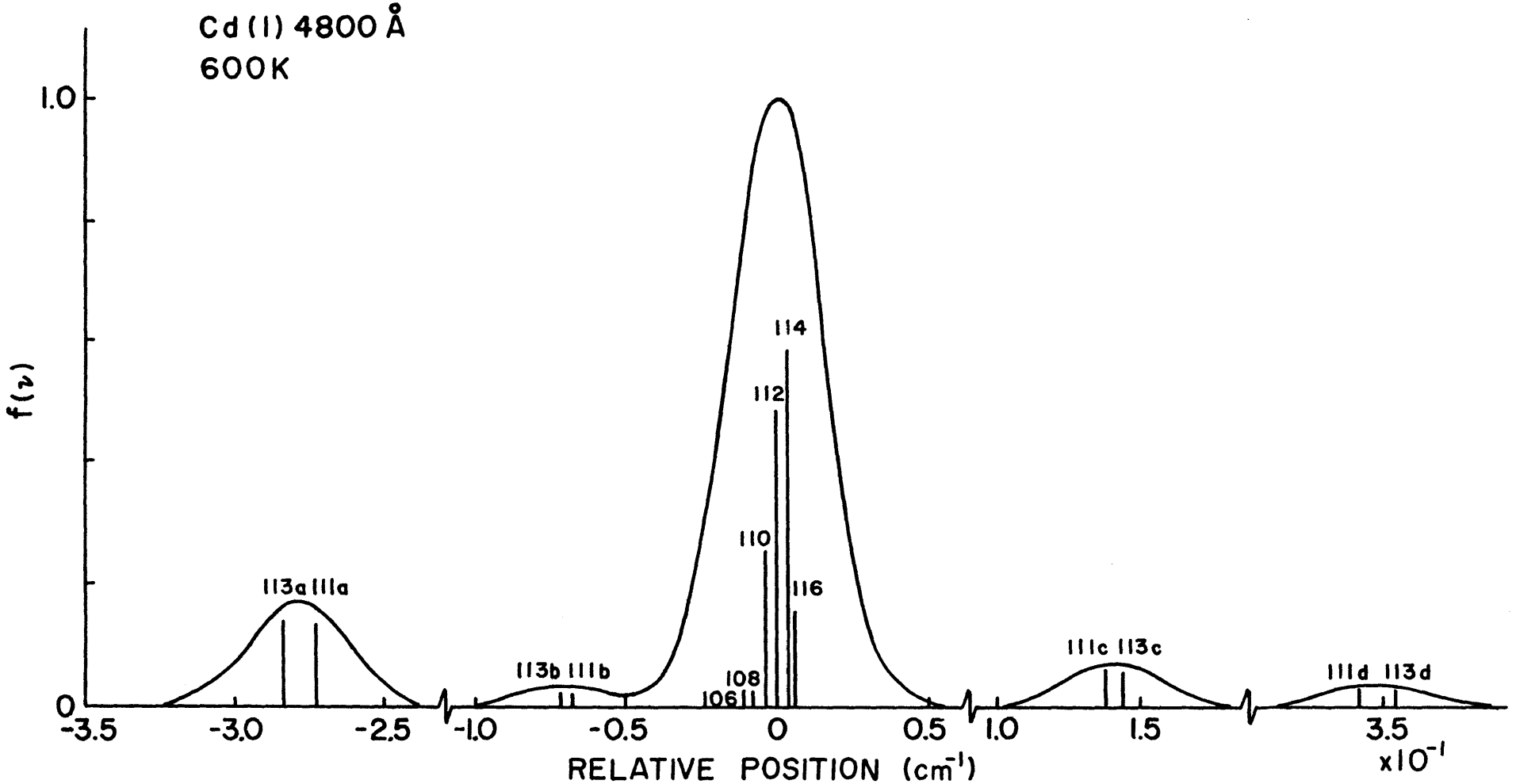

Fig.3-2(a). Line profile of the Cd(I) 4800 Å line. The number adjacent to each component is the mass number. The components due to the odd isotopes are labelled by a, b, c, and d.

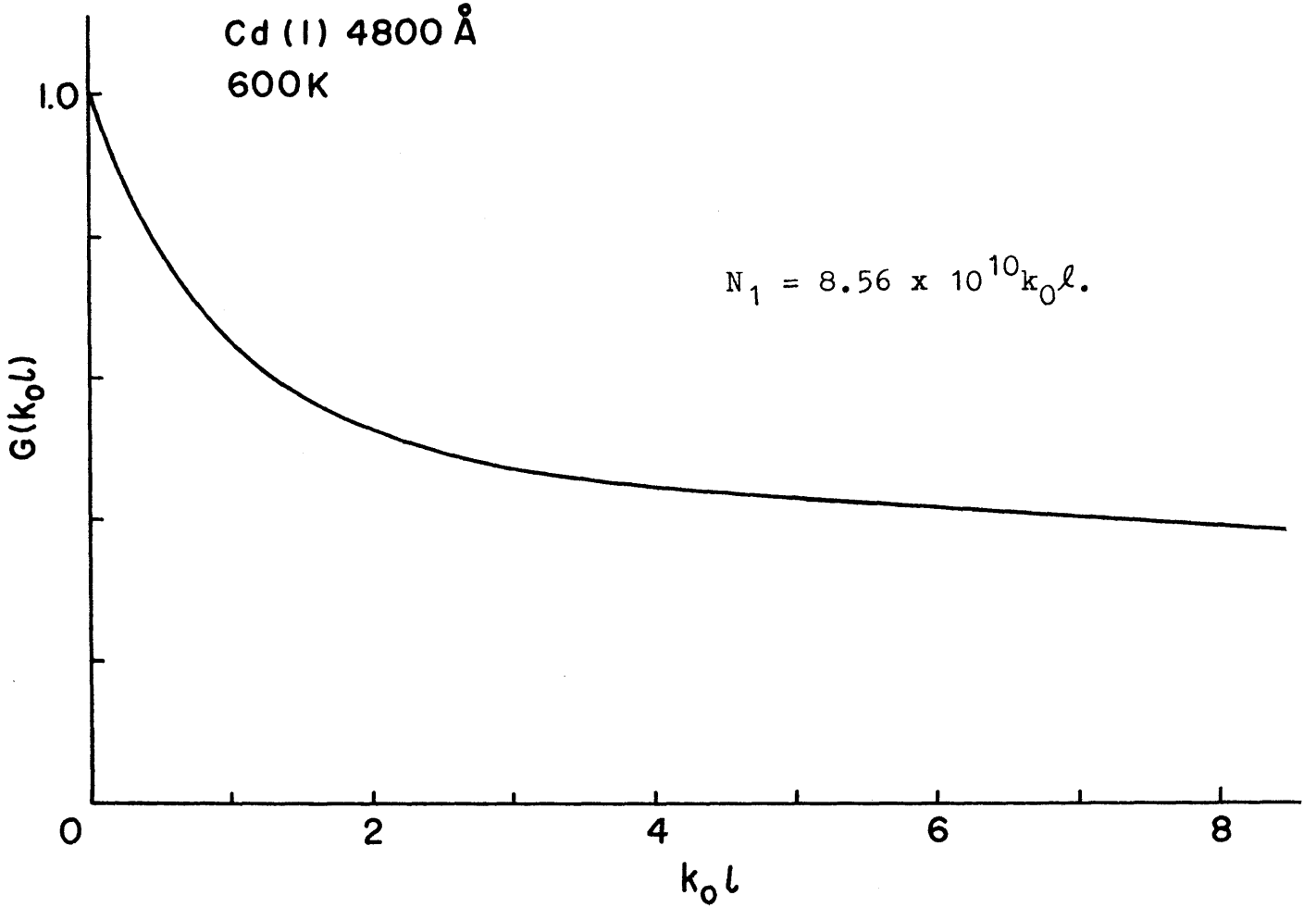

Fig.3-2(b). $G(k_0 \ell)$ of the Cd(I) 4800 Å line as a function of $k_0 \ell$.

On the other hand, the absolute intensities of the spontaneous emissions of the Cd(I) 3261 Å and 4800 Å lines per unit volume, I_1 and I_2, respectively, are given by

$$I_1 = \eta N_1 A_{10} hc/\lambda_{10}, \tag{3.2}$$

and

$$I_2 = N_2 A_{21} hc/\lambda_{21}, \tag{3.3}$$

where A_{10} and λ_{10} are the transition probability and the wavelength of the Cd(I) 3261 Å line, respectively, c is the light velocity, and h is the Planck constant. η is a factor relating to the imprisonment of the Cd(I) 3261 Å line, which can be calculated from the population density of the Cd(I) ground state.[4-6]

Actually, N_1 and N_2 have radial distributions. It may be assumed, however, that the radial distributions of N_1 and N_2 do not differ considerably from each other, and the ratio of the Cd(I) 3261 and 4800 Å sidelight intensities is nearly equal to I_1/I_2. This means that the ratio N_1/N_2 can be determined by measuring the Cd(I) 3261 and 4800 Å sidelight intensities with the optical detection system whose relative energy sensitivity as a function of the wavelength is known. Then N_1 can be obtained by combining eq.(3.1) with the ratio. The absolute intensity of the spontaneous emission I_1 is determined from eq.(3.2).

Once I_1 is determined, the absolute intensity I of any spontaneous emission per unit volume in the pure He or He-metal discharge also can be determined by measuring the ratio of the

sidelight intensities provided that the radial distribution of each spontaneous emission is the same. The population density of the upper state of each spectral line can be determined by knowing the transition probability.

In determining the absolute intensity of the Cd(I) 3261 Å line, the trapping coefficient η in eq.(3.2) must be evaluated. Assuming that the optical depth k_0R is small compared with unity, where R is the tube radius, we see that the radial distribution of the population density $N_1(r)$ of the upper state of the Cd(I) 3261 Å line is scarcely affected by the effect of the imprisonment of the radiation. Therefore, it may be assumed that $N_1(r)$ is given by $N_1(r) = N_1 J_0(r/\Lambda)$, where $J_0(x)$ is the Bessel function of the zeroth order and $\Lambda = R/2.41$. Assuming that the population density of the Cd(I) ground state is uniform over the discharge tube, the trapping coefficient η is calculated in a manner similar to that in ref.4, and it is given by

$$\eta = 1 - \{\Lambda^2 \xi \pi \sum_{m=0}^{\infty} G_{2m} F_{2m} / R^2 J_1(R/\Lambda)\} k_0 R, \tag{3.4}$$

where

$$\left.\begin{aligned} \xi &= \int_0^{\infty} f_1^2(\nu')\,d\nu' \Big/ \int_0^{\infty} f_1(\nu'')\,d\nu'', \\ G_{2m} &= \Lambda^{-3} \int_0^R dr \int_r^R dr'\; r^{2m+1} J_0(r/\Lambda)/r'^{2m}, \\ \text{and} \quad F_{2m} &= (2\pi)^{-1} \int_0^{2\pi} P_{2m}(\cos\theta)\,d\theta. \end{aligned}\right\} \tag{3.5}$$

In eqs.(3.4) and (3.5), k_0 is the absorption coefficient of the Cd(I) 3261 Å line at the center frequency of the isotope Cd^{112} component, $f_1(\nu)$ is the line profile, and $P_n(x)$ is the Legendre polynomial of the n-th order. Figure 3-3 shows η as a function of k_0R.

§3.3. Experimental and Results

The experiments were carried out with two discharge tubes made of quartz which had the structures similar to those used in the preceding chapter. The sidelight intensities were measured with the type 139 Hitachi UV-VIS spectrophotometer (Hitachi Ltd.) and the R-106 photomultiplier tube (Hamamatsu TV Ltd.). The relative energy sensitivity $G(\lambda)$ of the optical detection system was calibrated as a function of the wavelength λ with an Optronic Laboratories model 220 A standard lamp. It is shown in Fig.3-4.

At a low Cd atom density, where the trapping coefficient η of the Cd(I) 3261 Å line is nearly equal to 1, the population density N_1 of the upper state and the sidelight intensity I_1 of the Cd(I) 3261 Å line were measured in a manner described above. The measurements were repeated about 30 ~ 60 times, and the average values of N_1 and I_1 were calculated. Using the measured sidelight intensity I_λ of a spectral line (wavelength λ, transition probability A_λ), the population density N_λ of the upper state was calculated from

$$N_\lambda = N_1 \frac{G(\lambda_{10}) I_\lambda \lambda A_{10}}{G(\lambda) I_1 \lambda_{10} A_\lambda} . \qquad (3.6)$$

These measurements were carried out under various experimental conditions. The measured results in the discharge tube of 3.5 mm I.D. are summarized in Tables 3-1 and 3-2. The spectral lines of the He(I) used in the measurements are shown in Fig.3-5 together with other He(I) lines. In determining the population density of each excited state, the trapping coefficient was calculated in a manner similar to that in eq.(3.4) assuming that the radial distributions of the population densities of the upper and lower states were of the Bessel function of zero order.

The population density of the upper state of the Cd(II) 4416 Å line determined with the method will be used in Chapter 7 to obtain the population density of the lower state of the Cd(II) 4416 Å line, and in Chapter 8 to discuss the excitation mechanism quantitatively.

A more detailed discussion about the reliabilities of the measured results will be given in Chapter 6 by comparing them with the theoretical results calculated from the rate equations.

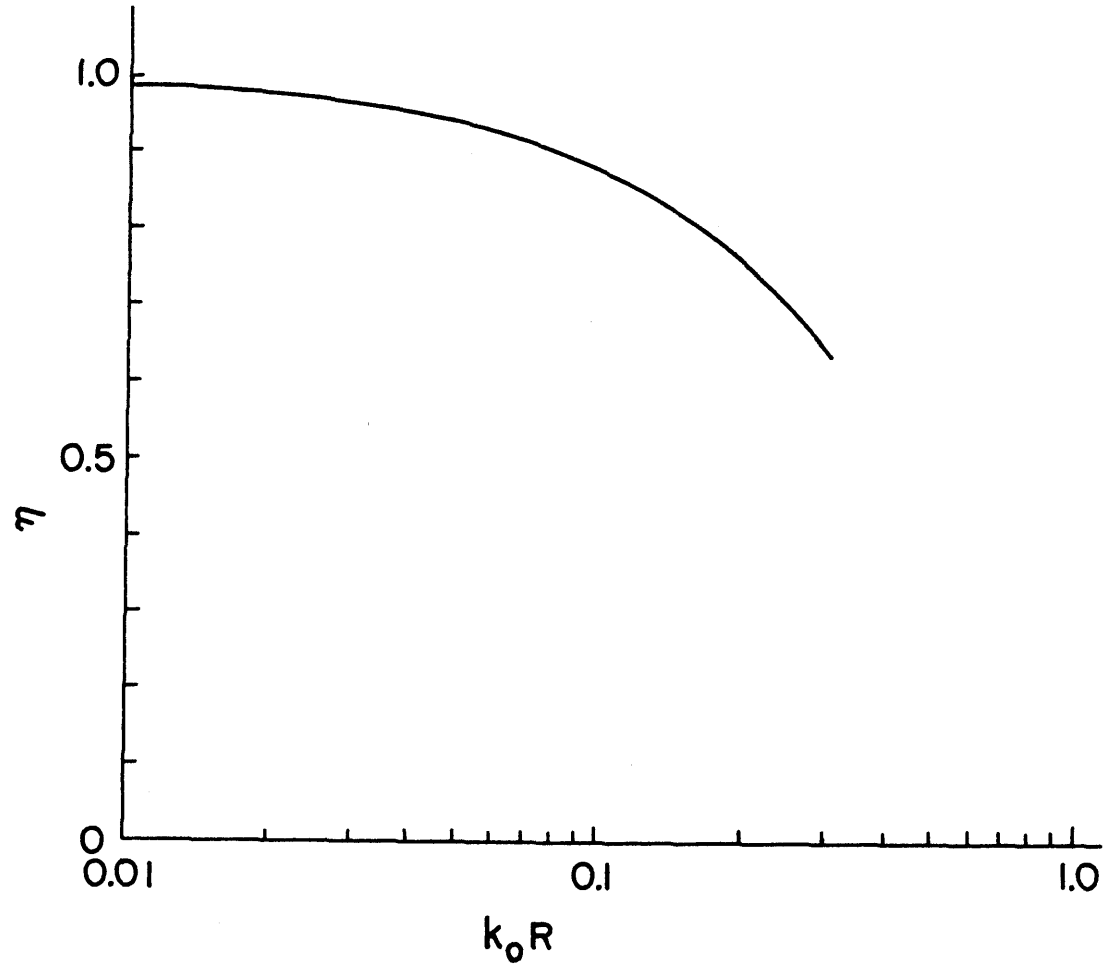

Fig.3-3. Trapping coefficient η of the Cd(I) 3261 Å line as a function of k_0R.

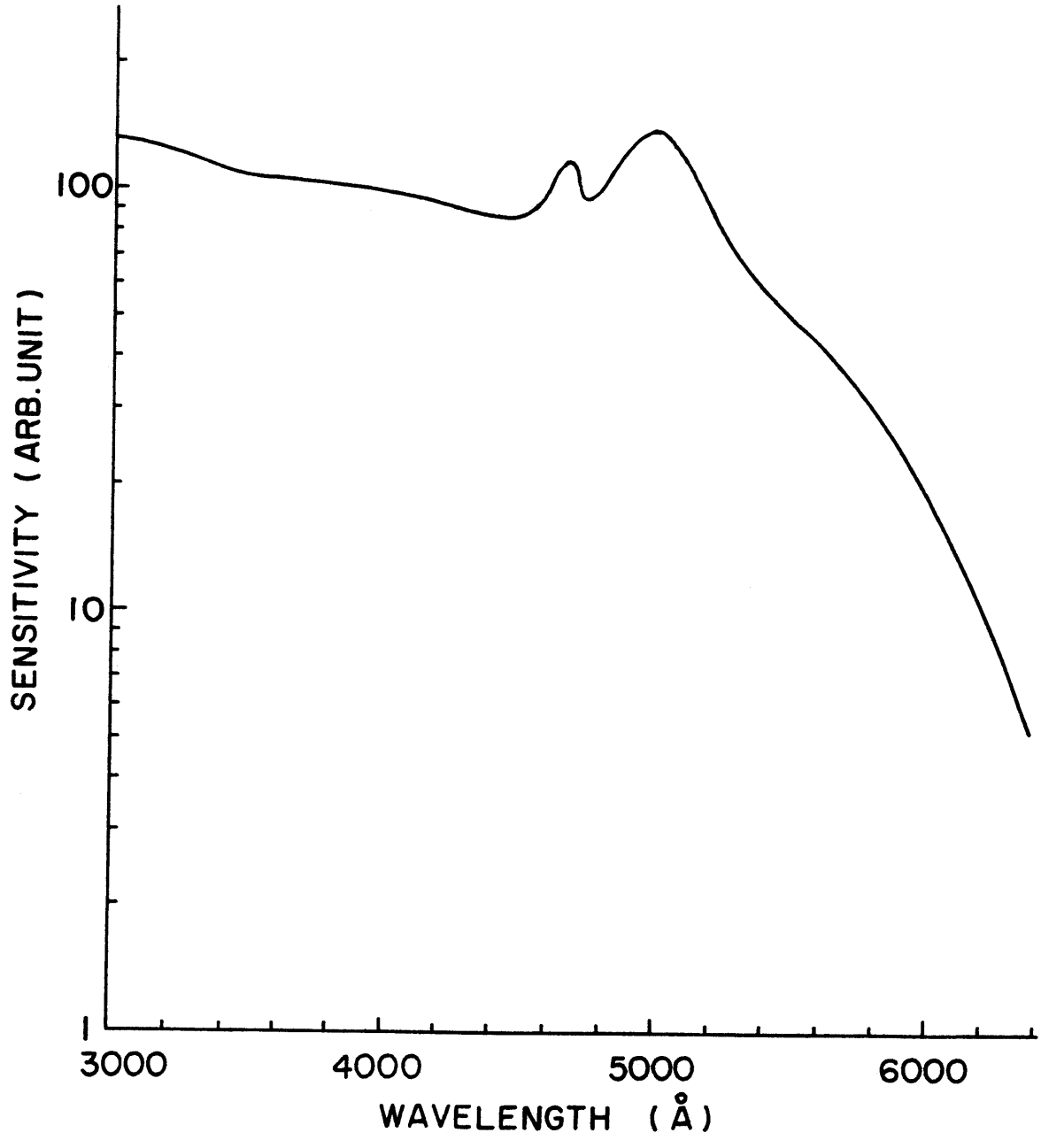

Fig.3-4. Relative energy sensitivity of optical detection system as a function of wavelength.

Table 3-1. Population densities of He(I) excited states in the pure He discharge; 3.5 mm I.D., discharge current of 100 mA, initial He pressure of 3.5 Torr.

State	Wave-length (Å)	Trapping Coefficient	N (cm^{-3})
He(I) 3^1P	5016	0.93	3.7^{10}
4^1P	3965	0.98	3.1^{9}
3^3P	3889	0.91	7.9^{10}
4^3P	3188	0.95	4.7^{9}
4^1D	4922	0.96	7.4^{9}
5^1D	4388	0.99	1.4^{9}
3^3D	5876	0.51	1.7^{11}
4^3D	4472	0.87	1.8^{10}
5^3D	4026	0.96	4.0^{9}
6^3D	3820	0.98	1.2^{9}
4^1S	5048	1.00	3.5^{9}
4^3S	4713	0.99	7.4^{9}
5^3S	4121	1.00	1.6^{9}

Table 3-2. Population densities of excited states of He(I) Cd(I), and Cd(II) in the He-Cd discharge; 3.5 mm I.D., discharge current of 100 mA, initial He pressure of 3.5 Torr, Cd atom density of 1.5×10^{13} cm^{-3}.

State		Wavelength (Å)	Trapping Coefficient	N (cm^{-3})
He(I)	3^1P	5016	0.96	1.5^{10}
	3^3P	3889	0.94	2.7^{10}
	3^3D	5876	0.68	6.4^{10}
	4^1D	4922	0.98	3.1^{9}
	4^3S	4713	1.00	3.0^{9}
Cd(I)	$5p^3P_1$	3261	0.94	6.7^{11}
	$6s^3S_1$	4800	0.87	1.4^{10}
Cd(II)	$5s^{22}D_{5/2}$	4416	1.00	7.7^{10}
	$5s^{22}D_{3/2}$	3250	1.00	9.6^{9}
	$4f^2F_{5/2}$	5337	1.00	9.6^{7}
	$4f^2F_{7/2}$	5378	1.00	1.7^{8}

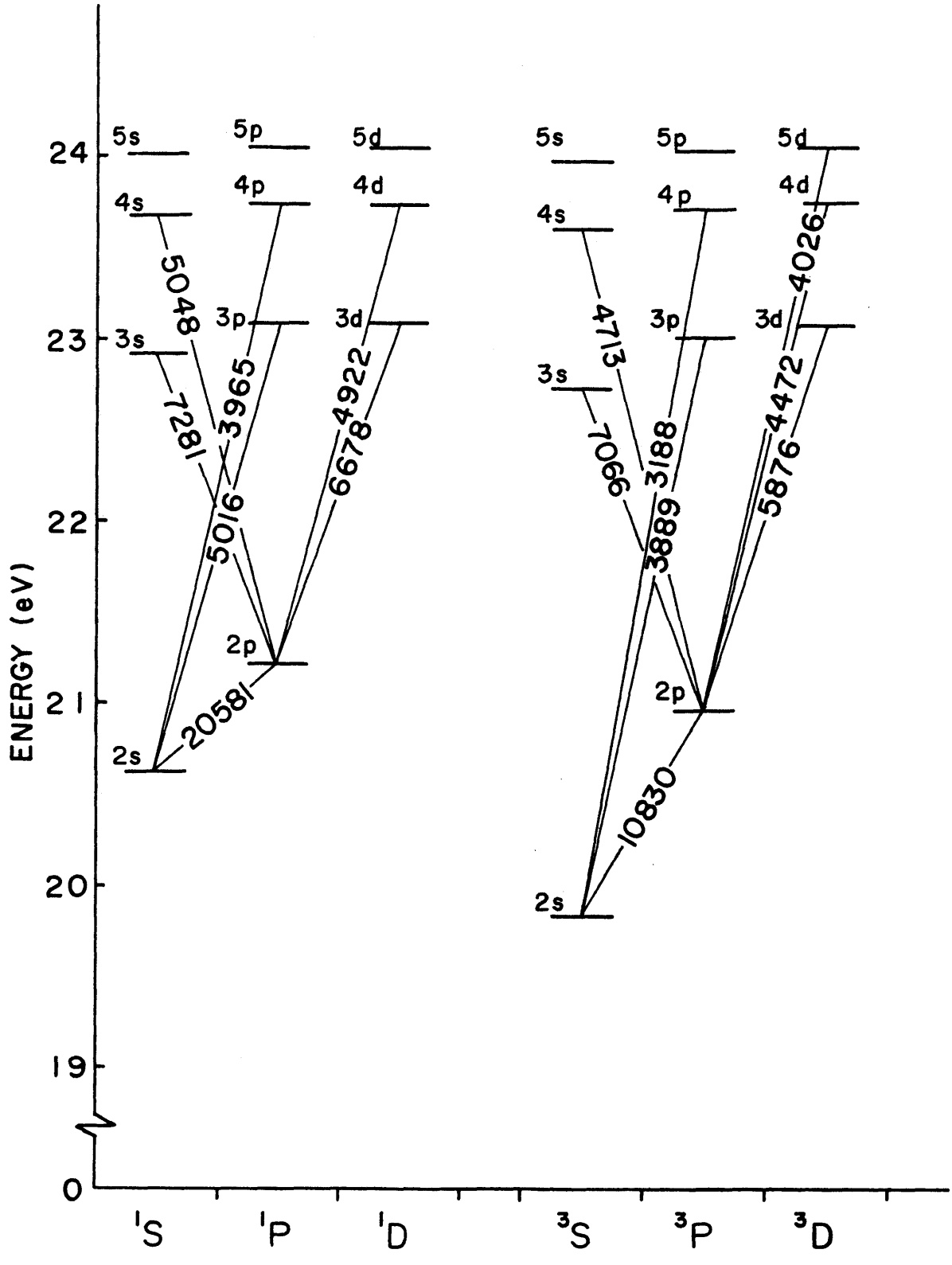

Fig.3-5. Energy level diagram of He(I).

References in Chapter 3.

1) R.Stair, W.E.Schneider, and J.K.Jackson,"A new standard of spectral irradiance,"Appl.Optics,vol.2,pp.1151-1154,Nov.1963.

2) F.M.Kelly and E.Tomchuk,"Isotope shift in the Cd(I) intercombination resonance line λ3261 Å,"Proc.Roy.Soc. (London),vol.74,pp.689-692,1959.

3) H.G.Kuhn, Atomic Spectra (Longmans, London, 1962).

4) T.Holstein,"Imprisonment of resonance radiation in gases," Phys.Rev.,vol.15,pp.1212-1233,Dec.1947.

5) T.Holstein,"Imprisonment of resonance radiation in gases.II," Phys.Rev.,vol.15,pp.1159-1168,Sep.1951.

6) A.V.Phelps,"Effect of the imprisonment of resonance radiation on excitation experiments,"Phys.Rev.,vol.15,pp.1362-1368, June 1958.

Chapter 4. Determination of the Electron Density in a PC He-Cd Discharge Having the Non-Maxwellian Electron Energy Distribution

§4.1. Introduction

The electron density in the PC He-Cd^+ laser discharge is necessary to calculate electronic collisional rates. The electron density in PC He-metal discharges have been measured with the double probe method[1-3] because of its simplicity and good spacial resolving power. In the method, one had to use ambiguous values of the mobilities of ions in gas mixtures, and the uncertainties of the results were large. Moreover, the knowledge about the electron energy distribution function (EDF) is needed.

If EDF is Maxwellian in a pure He discharge at a medium pressure, the electron density in it can be determined from Dote's formula with the conventional double probe method.[4] In a He-metal discharge, Mizeraczyk proposed the modified double probe method[5] in which one need not use ambiguous values of the mobilities of ions in a two-component gas discharge. EDF was assumed to be Maxwellian in this case also.

It has been pointed out from the experimental results and also from the theoretical analyses that EDF is non-Maxwellian in some discharges at medium pressures which are used in PC He-metal lasers.[6-12] The situation is the same also in the pure He discharges at medium pressures. In the discharge, high energy electrons which can excite atoms to excited states are significantly few in comparison with those in the case of

the Maxwellian EDF of the same average energy. Therefore, it is questionable whether the electron density determined with the conventional or modified double probe method is correct or not in some He and He-metal discharges.

In this chapter, it is shown that the electron density in the PC He-Cd^+ laser discharge, where EDF is non-Maxwellian, can be determined conveniently with the same modified double probe method as used in the case of the Maxwellian EDF.[13] This method can be applied to other PC He-metal laser discharges at medium pressures generally.

§4.2. Fundamental Considerations

4.2.1. Principle of the modified double probe method

The principle of the modified double probe method proposed by Mizeraczyk[5] is illustrated in Fig.4-1. Two pairs of probes 1 and 2 are placed as shown in Fig.4-1. Because of the cataphoresis effect, the He-metal discharge is confined in the region between the metal source and the cathode, and the pure He discharge is obtained in the region between the metal source and the anode. A calculation shows that the addition of the low pressure metal vapor ($\lesssim 10^{-3}$ Torr) to the discharge region has little effect on the mobility of electrons.[5] The following equation is obtained from the continuity of the discharge current by assuming that the radial distributions of the electron densities are the same in the two discharge regions.

$$n^e_{\text{He-metal}} = n^e_{\text{He}} \cdot E_{\text{He}}/E_{\text{He-metal}}, \qquad (4.1)$$

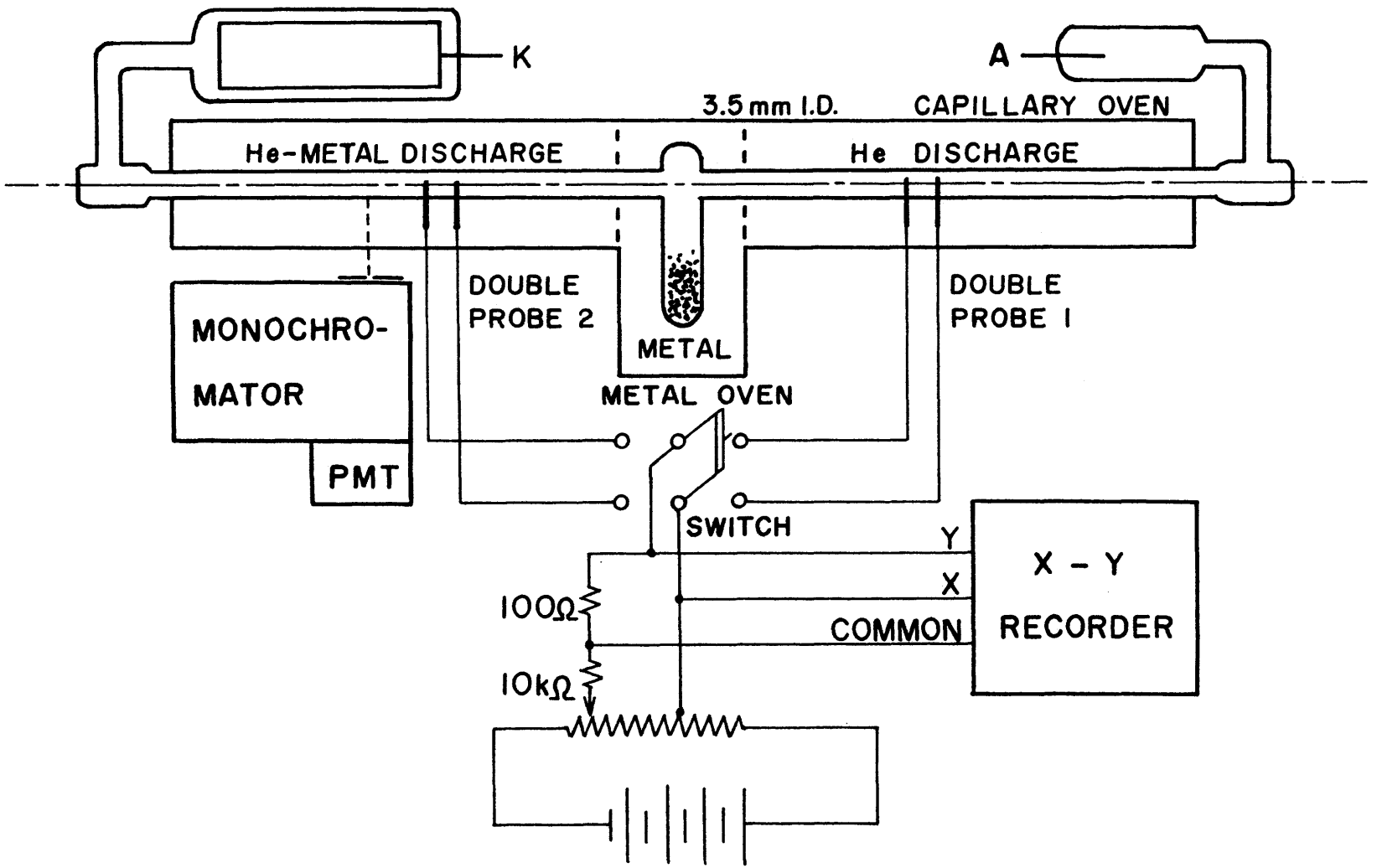

Fig.4-1. Schematic diagram of the modified double probe method.

where n^e and E are the electron density and the electric field strength, respectively. The subscripts in eq.(4.1) denote the pure He and He-metal discharge regions. Here, n^e_{He} and E_{He} are determined with the double probe 1, and $E_{He\text{-}metal}$ is measured with the double probe 2. If n^e_{He} is obtained, we can determine $n^e_{He\text{-}metal}$ whatever EDF in the He-metal discharge is, because E_{He} and $E_{He\text{-}metal}$ can be measured directly and accurately regardless of EDF. Therefore, we must know how n^e_{He} can be determined with the double probe method in the case of the non-Maxwellian EDF.

4.2.2. Electron density and characteristic energy of electrons in the pure He discharge

To obtain the electron density in the pure He discharge, our group has used Dote's formula[4] before. It has been assumed in the formula that EDF is Maxwellian, and therefore, the Einstein relation applies both to electrons and to ions. However, it has been reported from the theoretical calculations that EDF in the pure He discharge is far from the Maxwellian EDF in the region $E/p > 2$ V/cmTorr.[10,11] In our present discharge, as E/p is larger than 5 V/cmTorr, we must regard EDF as non-Maxwellian and introduce the characteristic energies,[10,14]

$$D_e/\mu_e = \mathcal{E}_{ke}, \tag{4.2}$$

and

$$D_i/\mu_i = \mathcal{E}_{ki}, \tag{4.3}$$

where D and μ are the diffusion coefficient and mobility of electrons (subscript e) or ions (subscript i), respectively. Then the electron and ion current densities, J_e and J_i, respectively, are given by

$$J_e = D_e e\nabla n^e + en^e\mu_e E$$

$$= D_e e\nabla n^e - (D_e en^e/\mathcal{E}_{ke})\nabla V, \tag{4.4}$$

and

$$J_i = -D_i e\nabla n^i + en^i\mu_i E$$

$$= -D_i e\nabla n^i - (D_i en^i/\mathcal{E}_{ki})\nabla V, \tag{4.5}$$

where n^e and n^i are the electron and ion densities, respectively, V is the electric potential, E is the electric field strength, -e is the charge of the electron.

Solving eqs.(4.4) and (4.5) simultaneously in the same manner as ref.4 for a cylindrical probe of R_p in radius and ℓ in length under the condition that the plasma is quasi-neutral, we obtain that

$$n^e = \frac{1}{2\pi}\cdot\frac{1}{(1+\mathcal{E}')}\cdot\frac{p_0}{e\mathcal{E}_{ke}}\cdot\frac{i_i}{\mu_{i0}}\cdot\ln\left(\frac{\ell}{R_p q_0}\right), \tag{4.6}$$

where

$$\mathcal{E}' = \mathcal{E}_{ki}/\mathcal{E}_{ke}, \tag{4.7}$$

and p_0 is the gas pressure in Torr, i_i is the probe current per unit length in A/cm, and μ_{i0} is the mobility of He^+ ions at 1 Torr in cm^2/Vsec. $\mathcal{E}'$ is the ratio of the characteristic energy of ions to that of electrons, and usually $\mathcal{E}' \ll 1$.

$R_p q_0$ is the singular point of the quasi-neutral solution, and q_0 is determined in a manner similar to that in ref.4. Here, ε_{ke} is given by

$$\varepsilon_{ke} = D_e/\mu_e = \int_0^\infty \frac{xf(x)}{Q_M(x)}\,dx \Big/ \left\{-\int_0^\infty x\frac{df(x)}{dx}\frac{}{Q_M(x)}\,dx\right\}, \tag{4.8}$$

where, x is the energy in eV, $\sqrt{x}f(x)$ is EDF, and $Q_M(x)$ is the momentum transfer cross section for electrons in He. This EDF can be calculated from the Boltzmann transport equation given by the following equation,[9,11,12] which includes the following processes for electrons; (1) the elastic collisions with He atoms in the neutral ground state, (2) the inelastic collisions exciting He atoms from the neutral ground state to the first excited states, (3) the direct ionizations of He atoms from the neutral ground state, (4) the Coulomb collisions between electrons, (5) the stepwise ionizations of He atoms from the He(I) first excited states:

$$\begin{aligned}
&\left\{E_{He}^2 u/3N_0 Q_M(u) + (2mkT/eM)N_0 Q_M(u)u^2\right\}\cdot\frac{df(u)}{du} \\
&+ (2m/M)N_0 Q_M(u)u^2 f(u) \\
&+ N_0\sum_g \int_u^{u+u_{0g}} xQ_{0g}(x)f(x)\,dx + \sum_{h=1}^{4} N_h \int_u^{u+u_h} xQ_h(x)f(x)\,dx \\
&+ Ym^2/2e^2\cdot\left[I_0^0(u)f(u) + 2u/3\cdot\left\{I_2^0(u) + J_{-1}^0(u)\right\}\cdot\frac{df(u)}{du}\right] \\
&= 0.
\end{aligned} \tag{4.9}$$

Here, u is the electron energy in eV, and

$$\int_0^\infty \sqrt{x} f(x)\,dx = 1,$$

$$Y = 4\pi(e^2/4\pi\varepsilon_0 m)^2(\ln\lambda)n_{He}^e,$$

$$I_0^0(u) = \int_0^u \sqrt{x} f(x)\,dx,$$

$$I_2^0(u) = \left\{\int_0^u x^{3/2} f(x)\,dx\right\}/u,$$

$$J_{-1}^0(u) = \sqrt{u}\cdot\int_u^\infty f(x)\,dx, \qquad (4.10)$$

In eqs.(4.9) and (4.10), N_0 and N_h are the population density of the He(I) ground state and those of the He(I) first excited states, respectively. The latter were determined experimentally with the modified absorption method described in Chapter 2.[15] u_{0g} and $Q_{0g}(u)$ are the threshold energy and the cross section for inelastic collisions exciting He atoms from the neutral ground state to the g-th excited states, respectively. u_h and $Q_h(u)$ are those for the stepwise ionizations of He atoms from the He(I) first excited states. E_{He} is the electric field strength, which is determined with the double probe. T is the gas temperature (= 600 K), k is the Boltzmann constant. n_{He}^e, m, and -e are the density, mass, and charge of the electron, respectively. M is the mass of the He atom, and $\ln\lambda$ is the Coulomb logarithm.

The fifth term in eq.(4.9) which came from the stepwise ionizations of He atoms, was estimated here for the first time under the actual discharge condition with the use of the measured

population densities of the He(I) first excited states. The effect of the Coulomb collision term on EDF was estimated by solving eq.(4.9) with and without the the term. The change in $\mathcal{E}_{ke}$ by this term was less than 1 %. Therefore, although $\mathcal{E}_{ke}$ depends on n_{He}^{e} in principle, we need not solve eqs.(4.6) and (4.9) simultaneously in calculating $\mathcal{E}_{ke}$ in the first approximation.

Here, we refer to EDF in a He-metal discharge in brief. Inelastic collisions of electrons with metal atoms begin to occur in the low energy region, and even the low energy part of EDF is influenced by those inelastic collisions. Therefore, EDF in the He-metal discharge deviates from the Maxwellian EDF of the same average energy more considerably.[8,12)]

4.2.3. Definition of the nominal electron temperature V_e

When EDF is Maxwellian, the electron temperature can be determined with the double probe method from Dote's formula,[16)]

$$\frac{kT_e}{e} = \frac{\sum I_{p0}}{4(1/R_0 - 0.82S)}, \qquad (4.11)$$

where $\sum I_{p0}$ is the probe current, R_0 is the derivative of the probe current with respect to the probe voltage at the point of reflection of the double probe characteristic, S is the slope of the ion saturation current to the probe. When EDF is non-Maxwellian, eq.(4.11) does not give the electron temperature any longer but should give a certain value V_e nominally. Moreover, even if EDF is Maxwellian, it is not known whether eq.(4.11) gives

the actual electron temperature in the discharges at medium pressures or not, where collisions of electrons with neutral atoms cannot be neglected. We call V_e "nominal electron temperature for convenience in this chapter.

§4.3. Experimental Procedures

The experiments were made on the He-Cd^+ laser discharge, which is the typical He-metal laser discharge. The arrangement of them is shown schematically in Fig.4-1. The discharge tube of 3.5 mm in diameter was used mainly, but the electron density was measured also with the tube of 3 mm in diameter. The double probe consisted of two tungsten wires of 0.1 mm in diameter and 1 mm in length, which were separated by 2 cm along the axis of the discharge tube. The discharge tube was connected to a flask of large volume, and the capillary part of the tube was put in an oven of 600 K.

The nominal electron temperature V_e and the electric field strength E_{He} in the pure He discharge region were measured with the double probe 1. The electric field strength E_{He-Cd} in the He-Cd discharge region was measured with the double probe 2.

The population densities of the He(I) first excited states, which were necessary in calculating EDF in the pure He discharge, were determined with the discharge tubes of 3.5 and 3 mm in diameter using the modified absorption method described in Chapter 2. The capillary part of each discharge tube was put in an oven of 600 K.

The relative changes of the He(I), Cd(I), and Cd(II) sidelight intensities were measured with a monochromator and a photomultiplier tube.

§4.4. Results

4.4.1. ε_{ke}, ε_{av}, and V_e in the pure He discharge

Figure 4-2 shows EDF necessary for the calculation of the characteristic energy and average energy of electrons, ε_{ke} and ε_{av}. This EDF was calculated from eq.(4.9) with the values of E_{He} and the population densities of the He(I) first excited states measured with the 3.5 mm bore tube. Figure 4-3 shows ε_{ke} and ε_{av} calculated with EDF in Fig.4-2, and the nominal electron temperature V_e measured with the double probe 1. The discharge current was 100 mA. In the discharge current region from 50 to 150 mA, ε_{ke}, ε_{av}, and V_e hardly changed. The scatter of the measured values of V_e was less than $\pm$10 % at each He pressure. As can be seen from Fig.4-3, ε_{ke}, $2\varepsilon_{av}/3$, and V_e are nearly equal to one another.

4.4.2. Electron density in the He-Cd discharge

If we allow for the fact that $\varepsilon_{ke} \approx V_e$ in the pure He discharge together with eqs.(4.1) and (4.2), we can get a practically useful conclusion: the electron density in the He-metal discharge can be determined simply with the modified double probe method by using V_e in place of ε_{ke} in eq.(4.6) even if EDF in the discharge is non-Maxwellian. Figure 4-4 shows n^e_{He-Cd} determined with V_e as a function of the Cd atom density. The Cd atom density was determined from the absorption coefficient of the Cd(I) 3261 Å line measured with the modified absorption method, and also from the variation of the sidelight intensity of the Cd(II) 4416 Å line with the Cd oven temperature.[17] A more

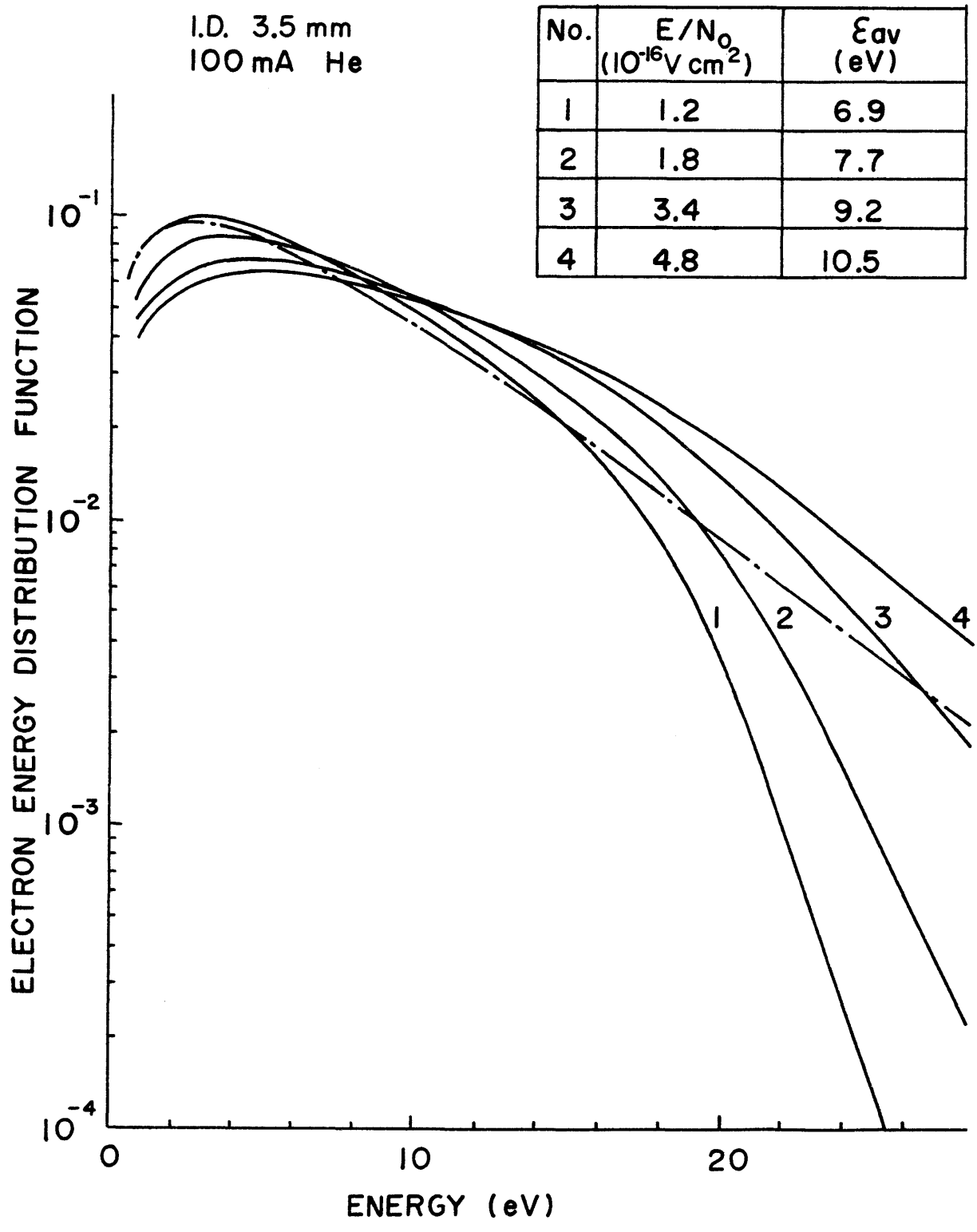

Fig.4-2. EDF in the pure He discharge as a function of electron energy. Maxwellian EDF of the average energy of 7.7 eV is also shown by the dash-dot line for the comparison.

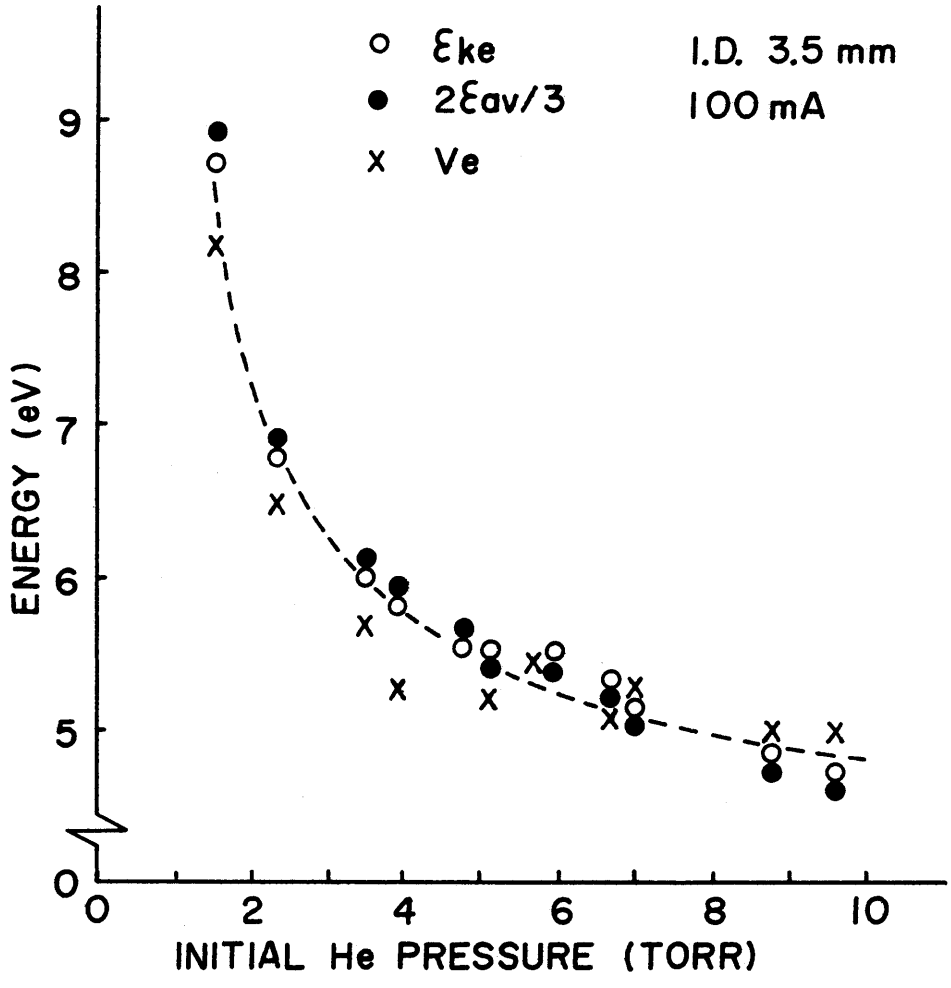

Fig.4-3. $\mathcal{E}_{ke}$, $2\mathcal{E}_{av}/3$, and V_e in the pure He discharge.

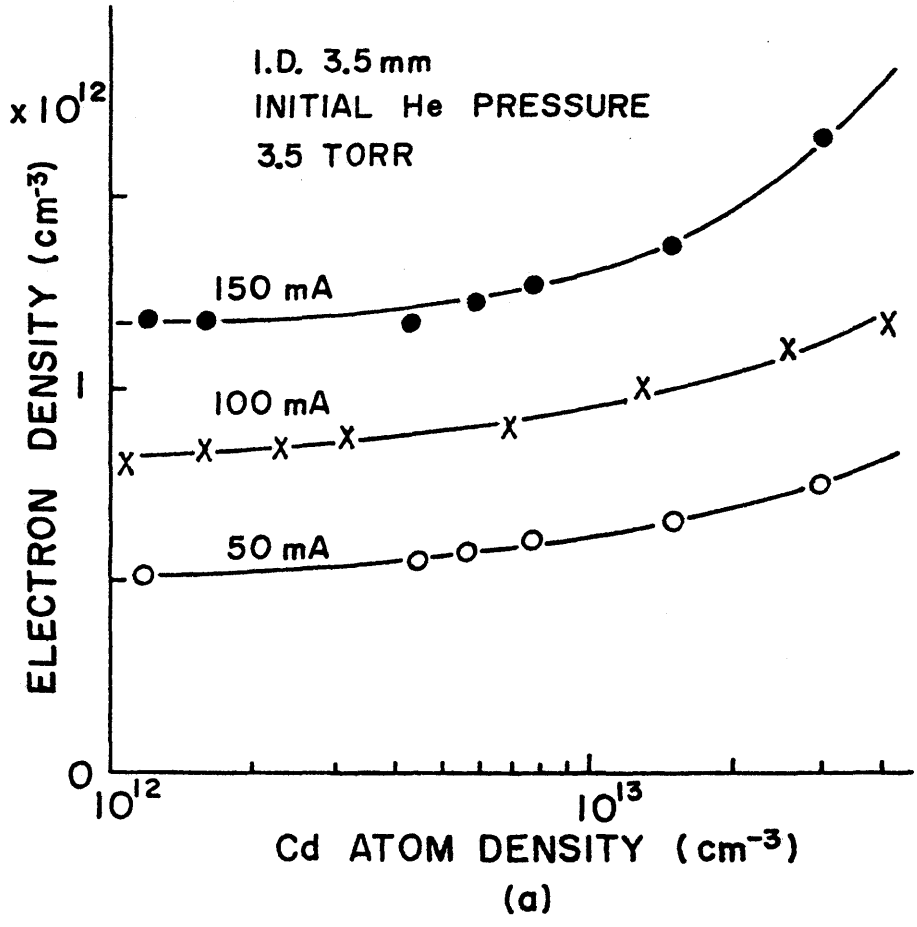

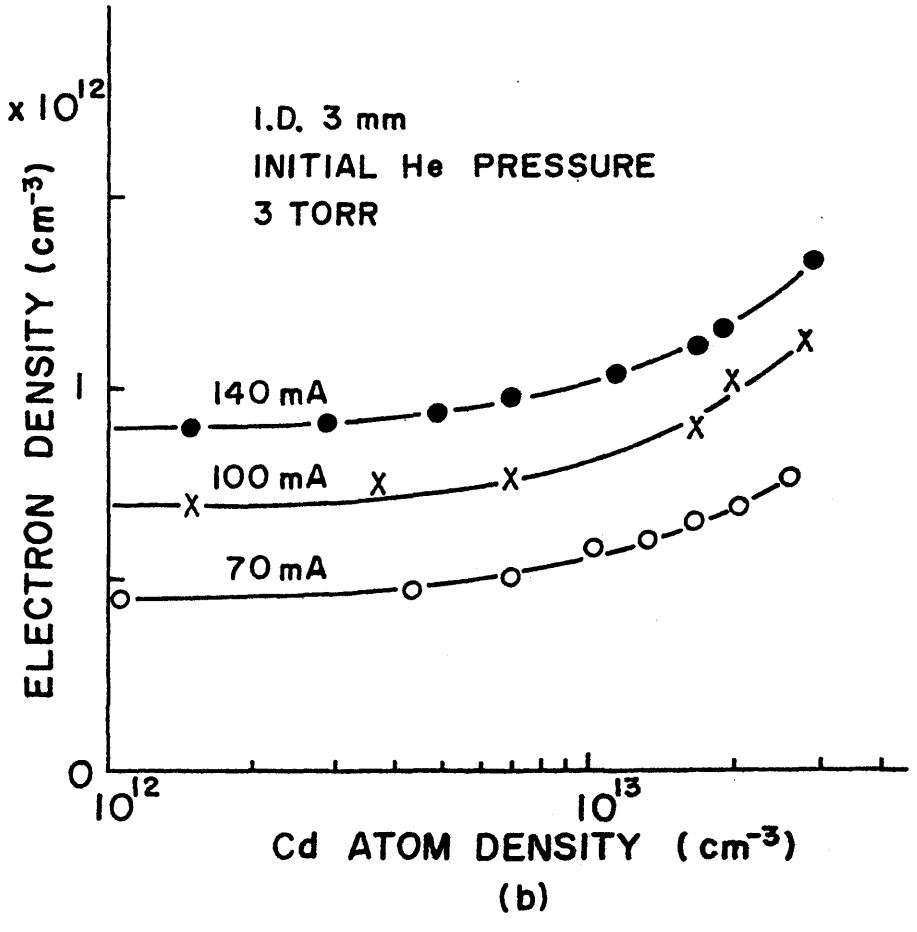

Fig.4-4. Electron density as a function of Cd atom density.

detailed description of the procedure is given in Chapter 5. As shown in Fig.4-4, when the discharge current and the initial He pressure are kept constant, n^e_{He-Cd} increases monotonically with the Cd atom density.

§4.5. Discussion

4.5.1. $\mathcal{E}_{ke}$, $\mathcal{E}_{av}$, and V_e in the pure He discharge

As the reliabilities of the calculated $\mathcal{E}_{ke}$ and $\mathcal{E}_{av}$ depend mainly on that of EDF, it has been examined in the following way whether EDF shown in Fig.4-2 is close to the actual EDF or not. The influence of EDF on the population densities should appear in the He(I) 3^3P and 3^1P states more distinctly than in the He(I) first excited states, because the former relate closely to the higher energy part of EDF and the destruction processes are not so complicated as those of the He(I) first excited states. Therefore, we calculated those population densities with rate equations for the non-Maxwellian EDF and the Maxwellian EDF of the electron temperature V_e. As the excitation processes to the He(I) 3^3P and 3^1P states, the direct excitation from the neutral ground state and the stepwise excitation from the He(I) 2^3S state were taken into account. The collision cross sections of these processes were taken from refs.18 and 19. The radiative cascadings from the higher lying excited states were neglected because the contribution of the process was small. As the destruction process of the He(I) 3^3P and 3^1P states, only the radiative transitions from these states to lower states were assumed. The results were compared with the relative changes of

the measured sidelight intensities of the He(I) 3889 Å (3^3P - 2^3S) and 5016 Å (3^1P - 2^1S) lines. They are shown in Fig.4-5. The effect of the imprisonment of the radiation on the sidelight intensities[20] were very slight and the sidelight intensities were almost proportional to the population densities of the He(I) 3^3P and 3^1P states in the present case.

As shown in Fig.4-5, the initial He pressure dependences of the population densities calculated with the Maxwellian EDF are quite different from those of the sidelight intensities. This difference exceeds the range of the resultant error caused by the uncertainties involved in the rate equations and the collision cross sections. The unified theory by Dote and Ichikawa[21] gives a lower electron temperature than V_e. The population densities calculated with the unified theory, however, also increase monotonically up to the initial He pressure of 9 Torr. On the contrary, the results calculated with the non-Maxwellian EDF account for the variations of the sidelight intensities very well. This shows that the higher energy part of EDF can be approximated by the present non-Maxwellian EDF in the region of the typical initial He pressures or E/N_0 ($1 \times 10^{-16} \lesssim E/N_0 \lesssim 8 \times 10^{-16}$ Vcm^2) used in the He-metal laser. On the other hand, Postma calculated the mobility of electrons in He with EDF derived from the Boltzmann transport equation similar to eq.(4.9), and obtained a good agreement with the experimental results over a wide range of the reduced electric field strength E/p.[11] This means that the lower energy part of the actual EDF in the pure He discharge also can be well approximated by EDF calculated here. Therefore, $\mathcal{E}_{ke}$ and $\mathcal{E}_{av}$

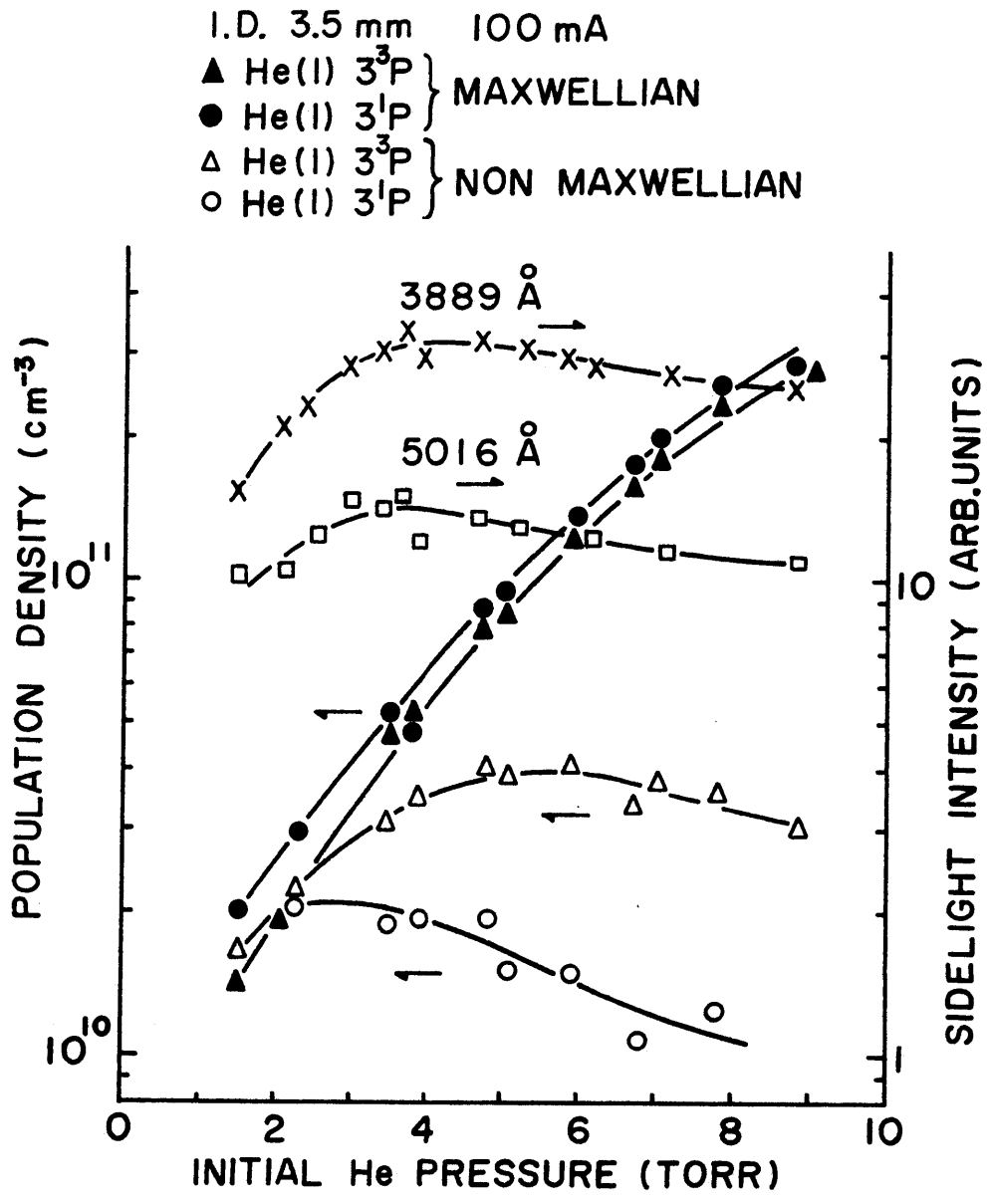

Fig.4-5. Population densities of the He(I) 3^3P and 3^1P states as a function of initial He pressure.

calculated with the present EDF can be reliable.

As can be seen from Fig.4-3, $\mathcal{E}_{ke}$ is very close to $2\mathcal{E}_{av}/3$ in the pure He discharge. This can be understood as follows. They are dominantly determined by the low energy part of EDF (< 20 eV). In this low energy region, the inelastic and Coulomb collision terms in eq.(4.9) can be neglected because the lowest threshold energies of inelastic collisions which are significant in determining EDF are very large (~ 20 eV) compared with the average energy of electrons, and the ionization degree is rather low ($\sim 10^{-5}$). Moreover, the momentum transfer cross section for electrons in He is approximately proportional to $1/\sqrt{u}$ for $u \gtrsim 5$ eV.[22] In this case, we see from eq.(4.9) that EDF has an energy dependence similar to the Maxwellian EDF in the low energy region. Therefore, $\mathcal{E}_{ke}$ is very close to $2\mathcal{E}_{av}/3$.

The reason why $\mathcal{E}_{ke}$ is close to V_e in the pure He discharge is not known at present because there is no probe theory based on the non-Maxwellian EDF and the calculation of the floating potential is rather difficult on account of collisions of electrons with He atoms in the probe sheath.[23] Whatever the reason may be, as V_e is almost equal to $\mathcal{E}_{ke}$ in the pure He discharge by chance, the electron density can be determined with the conventional double probe method though EDF is non-Maxwellian. But this cannot be always applied to other rare gas discharges. In the Ar discharge, for instance, the energy dependence of the momentum transfer cross section for electrons in Ar is completely different from that in He. Inelastic collisions of electrons with Ar atoms begin to occur at relatively low energies. Therefore, EDF deviates from the

Maxwellian EDF in the entire energy region.[11]

4.5.2. Electron density in the He-Cd discharge

The accuracy of the electron density in the He-Cd discharge n^e_{He-Cd} obtained here is determined primarily by the validity of eq.(4.1) and the accuracy of the measured electron density n^e_{He} in the pure He discharge. In deriving eq.(4.1), it has been assumed that the mobility of electrons in the He-metal discharge is almost equal to that in the pure He discharge. For the He-Cd discharge, the validity of this assumption was assured from a calculation based on the Boltzmann transport equation,[17] and also from the measurement of the electron drift velocity in ref.24. On the other hand, the accuracy of n^e_{He} is determined dominantly by the scatter of the measured values of the nominal electron temperature V_e and the probe current i_i. The values of the mobility of He^+ ions in He which have been reported after 1965 agree within ± 2 % with one another.[25] Hence, the uncertainty involved in the electron density in the He-Cd discharge is estimated to be less than ± 15 %.

We compare the present results with those obtained with the microwave cavity technique in ref.24. The technique need not any knowledge about EDF in determining the electron density. In this comparison, we must take into account the following facts; (1) our n^e_{He-Cd} are values on the tube axis, while those in ref.24 are values averaged over the radial direction, (2) the He atom density in the capillary part of the discharge tube is the half of the He atom density filled initially at

room temperature in our experimental system, while in ref.24, it is given directly by the He atom density filled initially at room temperature. If the facts mentioned above are brought into consideration, the two results at the equal current density and equal reduced tube radius pR agree within 20 %. This good agreement will show that the convenient determination method of the electron density with the modified double probe method can be used when the reduced electric field strength E/N_0 in the pure He discharge region ranges from 1×10^{-16} to 8×10^{-16} Vcm^2.

§4.6. Conclusion

It has been shown that the electron density in the He-metal discharge at medium pressures, where EDF is non-Maxwellian, can be determined simply with the modified double probe method by using the nominal electron temperature V_e in the pure He discharge. Although this convenient method is useful, the meaning of the nominal electron temperature V_e is not known at present. Therefore, we should regard this convenient method as a temporary one.

Also it has been assured from the calculations based on the rate equations that EDF in the pure He discharge at medium pressures has to be treated as non-Maxwellian. The situation is the same in the He-metal laser discharges. Therefore, the calculations of rate coefficients of electronic collisions will be made on the basis of the non-Maxwellian EDF hereafter.

The electron density determined here will be used in Chapter 5 to obtain the He^+ ion density, and in Chapters 6-8 to calculate the population densities of the He(I), Cd(I), and Cd(II) excited states in the PC He-Cd^+ laser discharge.

References in Chapter 4.

1) T.Goto, A.Kawahara, G.J.Collins, and S.Hattori,"Electron temperature and density in positive column He-Cd^+ lasers," J.Appl.Phys.,vol.42,pp.3816-3818,Sep.1971.

2) T.Goto, H.Kano, and S.Hattori,"Plasma parameters in gas discharges for positive-Column He-Se^+ lasers,"J.Appl.Phys., vol.43,pp.5064-5068,Dec.1972.

3) H.Kano, T.Goto, and S.Hattori,"Electron temperature and density in the He-CdI_2 positive column used for an I^+ laser," IEEE J.Quantum Electron.,vol.QE-9,pp.776-778,July 1973.

4) T.Dote,"A method for determining the plasma density by a cylindrical probe at medium pressures,"Reports of the Institute of Physical and Chemical Research,vol.46,pp.122-130,1970.

5) J.K.Mizeraczyk,"A simple method of determination of electron density in positive-column He-metal laser discharges," J.Appl.Phys.,vol.46,pp.1847-1848,1975.

6) J.Y.Wada and H.Heil,"Electron energy spectra in neon, xenon, and helium-neon laser discharges,"IEEE J.Quantum Electron., vol.QE-1,pp.327-335,Nov.1965.

7) E.E.Mainwaring and J.D.Swift,"Determination of the average electron energy in the positive column of an He-Ne glow discharge,"J.Phys.D:Appl.Phys.,vol.5,pp.1433-1437,1972.

8) M.I.Ciobanu, A.I.Ciura, Eva Cojocaru, and I.M.Popescu, "Electron energy distribution function in the positive column of a helium-cadmium laser,"Rev.Roum.Phys.,vol.20, pp.29-41,1975.

9) H.Margenau,"Theory of high frequency gas discharges. I.

Methods for calculating electron distribution functions," Phys.Rev.,vol.73,pp.297-308,Feb.1948.

10) L.S.Frost and A.V.Phelps,"Momentum-transfer cross sections for slow electrons in He, Ar, Kr, and Xe from transport coefficients,"Phys.Rev.,vol.136,pp.1538-1545,Dec.1964.

11) A.J.Postma,"Calculated electron energy disribution functions for discharges in helium and helium-argon mixtures,"Physica, vol.43,pp.581-595,1969.

12) E.Vokatý and K.Mašek,"Glow discharge in rare-gas and metal vapour mixture I.Distribution functions and kinetic coefficients in He-Cd mixture discharge,"Czech.J.Phys.,vol.B22,pp.776-789,1972.

13) M.Mori, T.Goto, and S.Hattori,"On the determination of the electron density in a positive column He-metal laser discharge having a non-Maxwellian electron energy distribution," J.Phys.Soc.Japan,vol.43,pp.662-668,Aug.1977.

14) L.S.Frost and A.V.Phelps,"Rotational excitation and momentum transfer cross sections for electrons in H_2 and N_2 from transport coefficients,"Phys.Rev.,vol.127,pp.1621-1633, Sep.1962.

15) T.Goto, M.Mori, and S.Hattori,"Modified absorption method to determine level population densities in a cataphoresis type of He-metal laser discharge,"Appl.Phys.Lett.,vol.29, pp.358-360,Sep.1976.

16) T.Dote,"A new method for determination of plasma electron temperature from the current-voltage characteristic of a floating double probe,"Reports of the Institute of Physical and Chemical Research,vol.44,pp.119-127,1968.

17) M.Mori, K.Takasu, T.Goto, and S.Hattori,"Ion densities in a positive column He-Cd^+ laser discharge,"J.Appl.Phys., vol.48,pp.2226-2230,June 1977.

18) B.L.Moiseiwitsch and S.J.Smith,"Electron impact excitation of atoms,"Rev.Mod.Phys.,vol.40,pp.238-353,April 1968.

19) J.G.Showalter and R.B.Kay,"Absolute measurement of total electron-impact cross sections to singlet and triplet levels in helium,"Phys.Rev.,vol.A11,pp.1899-1910,June 1975.

20) T.Holstein,"Imprisonment of resonance radiation in gases," Phys.Rev.,vol.72,pp.1212-1233,Dec.1947.

21) T.Dote and Y.Ichikawa,"Unified theory of the electron temperature in positive columns,"J.Phys.Soc.Japan,vol.40, pp.1217-1218,April 1976.

22) S.G.Elkomoss,"Energy distribution function for helium," Phys.Rev.,vol.172,pp.153-162,1968.

23) J.S.Chang and J.G.Laframboise,"Probe theory for arbitrary shape in a large Debye length, stationary plasma,"Phys. of Fluids,vol.19,pp.25-31,Jan.1976.

24) M.H.Dunn,"Electron densities and drift velocities in a positive column He-Cd laser discharge,"J.Phys.B:Atom.Molec. Phys.,vol.5,pp.665-672,March 1972.

25) E.W.McDaniel and E.A.Mason, The Mobility and Diffusion of Ions in Gases(Wiley,New York,1973),p.266.

Chapter 5. Separate Determination of He^+ and Cd^+ Ion Densities[1)]

§5.1. Introduction

The excitation mechanisms or saturation phenomena in the PC He-Cd^+ laser have been investigated with the spectroscopic methods,[2-4)] with the double probe method,[5,6)] and with the after-glow methods.[7,8)] It has been pointed out that the dominant excitation process to the laser upper state is the Penning collision process between He atoms in the metastable states and Cd atoms in the ground state. But other excitation processes to the laser states, such as the excitation process by collisions between electrons and Cd^+ ions in the ground state, or the thermal energy charge transfer collisions between He^+ ions in the ground state and Cd atoms in the ground state, have not been investigated in detail. The He^+ and Cd^+ ion densities have to be determined to estimate the contributions of those processes to the laser states.

Ivanov and Sém proposed a method to separate ion densities in a PC He-Cd discharge from the double probe and microwave measurements by using the mobilities of He^+ and Cd^+ ions.[9)] Mizeraczyk et al. obtained the ion densities in the PC He-Cd^+ laser discharge in the similar way.[10)] But the results contain a quite large uncertainty, because there are no reliable data concerning the dependences of the mobilities of He^+ and Cd^+ ions on the Cd partial pressure, temperature, or electric field strength in the He-Cd discharge. Therefore, they cannot be used in the quantitative study of the PC He-Cd^+ laser discharge.

In Chapter 2, the modified absorption method[11)] was

described, with which absorption coefficients not only of visible lines but also of ultraviolet lines could be determined accurately and simply. It was shown that the population density of the Cd(II) ground state could be determined accurately with the method. On the other hand, in Chapter 4, it was shown that the electron density in the He-metal discharge at medium pressures could be determined with the modified double probe method although the electron energy distribution function (EDF) in it was non-Maxwellian.

In this chapter, by combining the modified absorption method with the modified double probe method, the He^+ and Cd^+ ion densities in the PC He-Cd^+ laser discharge are determined separately without using the Cd^+ ion mobility. Also the He^+ and Cd^+ ion densities are calculated on the basis of the non-Maxwellian EDF in the He-Cd discharge, and the ionization mechanisms are discussed.

§5.2. Principle of the Determination Method

The population density of the Cd(II) ground state was determined with the modified absorption method described in Chapter 2, and those of the various Cd(II) excited states were determined from the sidelight intensities as described in Chapter 3. The total Cd^+ ion density n_{Cd^+} was obtained by adding the population densities of the Cd(II) excited states to that of the Cd(II) ground state. Here, the Cd^+ ion temperature was assumed to be 1000 K taking into account that the Cd^+ ion temperature calculated from the Doppler widths of the Cd(II)

lines reported previously scattered from 600 K to 1400 K.[12,13] However, according to the calculation of the absorption coefficient of the Cd(II) 2265 Å line, even if the actual Cd^+ ion temperature is different by ± 400 K from 1000 K, the error of the population density of the Cd(II) ground state determined from the absorption coefficient of the Cd(II) 2265 Å line is only ±3 % under the optimum condition for the laser action and the same order in the other Cd atom density region.

The electron density n^e_{He-Cd} in the He-Cd discharge was determined with the modified double probe method[6] and the revised probe theory for the pure He discharge as described in Chapter 4.

The population density of the He(II) ground state, which is nearly equal to the total He^+ ion density, can be determined from the absorption coefficient of the He(II) 304 Å line with the modified absorption method. But additional vacuum system and the modification of the window of the discharge tube are needed. In this chapter, therefore, the He^+ ion density n_{He^+} was obtained from

$$n_{He^+} = n^e_{He-Cd} - n_{Cd^+} , \qquad (5.1)$$

assuming that all of the ions were singly ionized.

§5.3. Experimental Procedure

The absorption measurement and the double probe measurement

were carried out in two cataphoresis type discharge tubes of the same inner diameter 3.5 mm separately. The capillary of each discharge tube was put in an oven of 600 K. Each tube was connected to a flask of large volume at room temperature to keep the He atom density N_0 in the capillary constant at any discharge current.

The discharge tube used for the absorption measurement was the same as that used in Chapter 2.

The population densities of the Cd(II) excited states were estimated from the measurements of the sidelight intensities with a quartz discharge tube of 3.5 mm in diameter in a manner described in Chapter 3. However, the sidelight intensity measurements were restricted to those lines which originated from the low lying Cd(II) excited states, because the population densities of the high lying Cd(II) excited states were generally very small in comparison with that of the Cd(II) ground state. Their transition probabilities were taken from refs.14 and 15.

The population densities of the upper states of the Cd(II) 2144 and 2265 Å lines, n_{2144} and n_{2265}, could not be determined with the method mentioned above because the relative spectral sensitivity of the optical detection system could not be calibrated with the ordinary standard lamp in the wavelength region shorter than 3000 Å. n_{2144} was determined by combining the laser gain measurement with the modified absorption method as described in Chapter 7. n_{2265} was determined from the ratio of the Cd(II) 2265 Å and the Cd(I) 2288 Å sidelight intensities as described in p.140 in Chapter 7. The trapping coefficients of the Cd(II) 2144 and 2265 Å lines were estimated by using

the population density of the Cd(II) ground state obtained in Chapter 2.

The discharge tube used for the double probe measurement was the same as that used in Chapter 4. The He^+ ion mobility at 600 K was taken from ref.16.

Although the Cd atom density could be determined directly from the absorption coefficient of the Cd(I) 3261 Å line in the discharge tube used for the absorption measurement, it could not be determined directly in the discharge tube used for the double probe measurement. Usually, the Cd atom density is determined from the Cd oven temperature. However, even if the same discharge tube is used, the optimum Cd oven temperature is different generally. This means that the Cd atom density derived from the Cd oven temperature includes a large uncertainty.

In order to estimate the reliable Cd atom density in the discharge tube used for the double probe measurement, the following experiment was carried out. In the discharge tube used for the absorption measurement, the Cd atom density was determined as a function of the Cd oven temperature at a constant discharge current. The relative intensity of the Cd(II) 4416 Å sidelight was also measured at the same time. These measurements were carried out with three Cd ovens, whose heater positions and temperature distributions are different from one another. Next, the normalized Cd(II) 4416 Å sidelight intensity I_{4416} was plotted as a function of the measured Cd atom density as shown in Fig.5-1. Figure 5-1 shows that the Cd atom density at which I_{4416} shows a maximum is the same with using any Cd oven, although the apparent Cd oven temperature is different

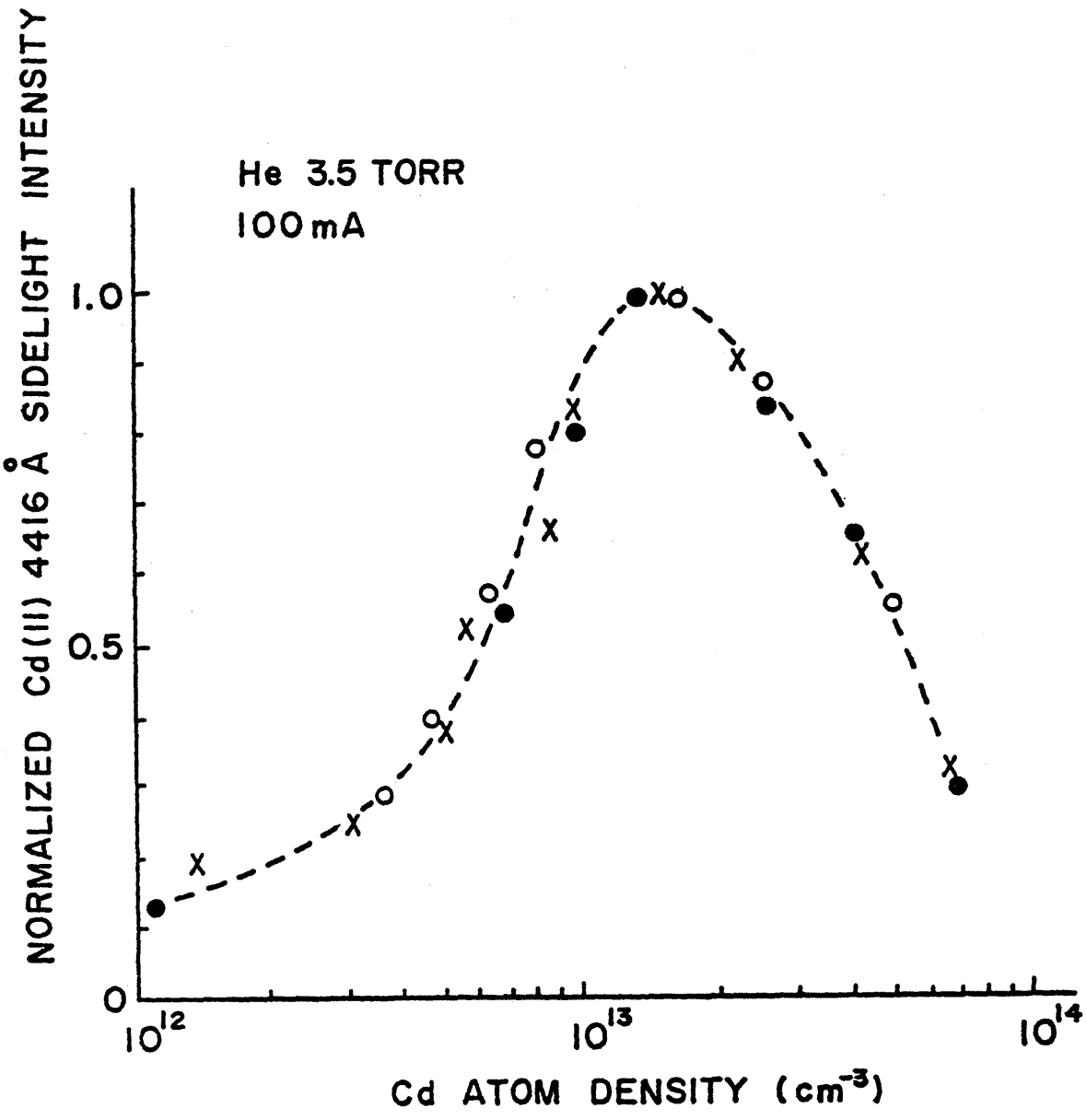

Fig.5-1. Normalized Cd(II) 4416 Å sidelight intensity as a function of Cd atom density with Cd ovens of three different structures.

from one another. The same holds true about any other value of I_{4416}. This means that the Cd atom density can be determined from I_{4416} conversely. The Cd atom density in the discharge tube used for the double probe measurement was determined by comparing I_{4416} obtained as a function of the Cd oven temperature with that in Fig.5-1. The determination of the Cd atom density in any discharge tube of the same inner diameter also can be done with this method.

§5.4. He^+ and Cd^+ Ion Densities

Figure 5-2(a) presents the electron density, He^+ ion density, and Cd^+ ion density as a function of the Cd atom density, and Fig.5-2(b) presents the population densities of the He(I) first excited states (2^3S, 2^1S, 2^3P, 2^1P) as a function of the Cd atom density. Here, the population densities of the He(I) first excited states 2^3S, 2^1S, 2^3P, and 2^1P were determined from the absorption coefficients of the He(I) 3188 Å, 3965 Å, 4026 Å, and 4922 Å lines, respectively. The initial He pressure was 3.5 Torr and the discharge current was 100 mA.

In Fig.5-2, as the Cd atom density increases, the He^+ ion density and the population densities of the He(I) first excited states decrease, and the Cd^+ ion density increases nearly in proportion to the Cd atom density. This is due to the facts that inelastic collisions of electrons with Cd atoms of the low ionization energy occur more frequently and, consequently, the average electron energy decreases. Note that, in the curve of the Cd^+ ion density, a very low hump appears around the Cd atom density which corresponds to the maximum of the Cd(II)

4416 Å sidelight intensity, while a rather high hump did in the curve obtained by Silfvast.[17] The He^+ ion density shows a behavior similar to those of the population densities of the He(I) first excited states.

It is very interesting to see that the Cd(II) 5337 Å sidelight intensity follows a behavior similar to that of the Cd(II) 4416 Å sidelight intensity in Fig.5-2. The upper state of the Cd(II) 5337 Å line is said to be excited dominantly by the thermal energy charge transfer collisions of He^+ ions in the ground state and Cd atoms in the ground state.[7]

Figure 5-3 shows the electron density, He^+ ion density, and Cd^+ ion density as a function of the discharge current at the near optimum condition for the Cd(II) 4416 Å laser operation. The He^+ and Cd^+ ion densities increase in proportion to the discharge current. The Cd(II) 4416 Å sidelight intensity is saturated at high discharge currents while the Cd(II) 5337 Å sidelight intensity increases almost linearly with the discharge current.

The electron density, He^+ ion density, and Cd^+ ion density were also measured as a function of the initial He pressure p_0. The discharge current was 100 mA and the Cd atom density was 1.1×10^{13} cm^{-3}. The Cd^+ ion density is nearly constant over the initial He pressures investigated, while the He^+ ion density increases with the initial He pressure. The electron density is roughly proportional to $p_0^{1.5}$. The Cd(II) 4416 Å sidelight intensity is saturated at high initial He pressures while the Cd(II) 5337 Å sidelight intensity increases monotonically.

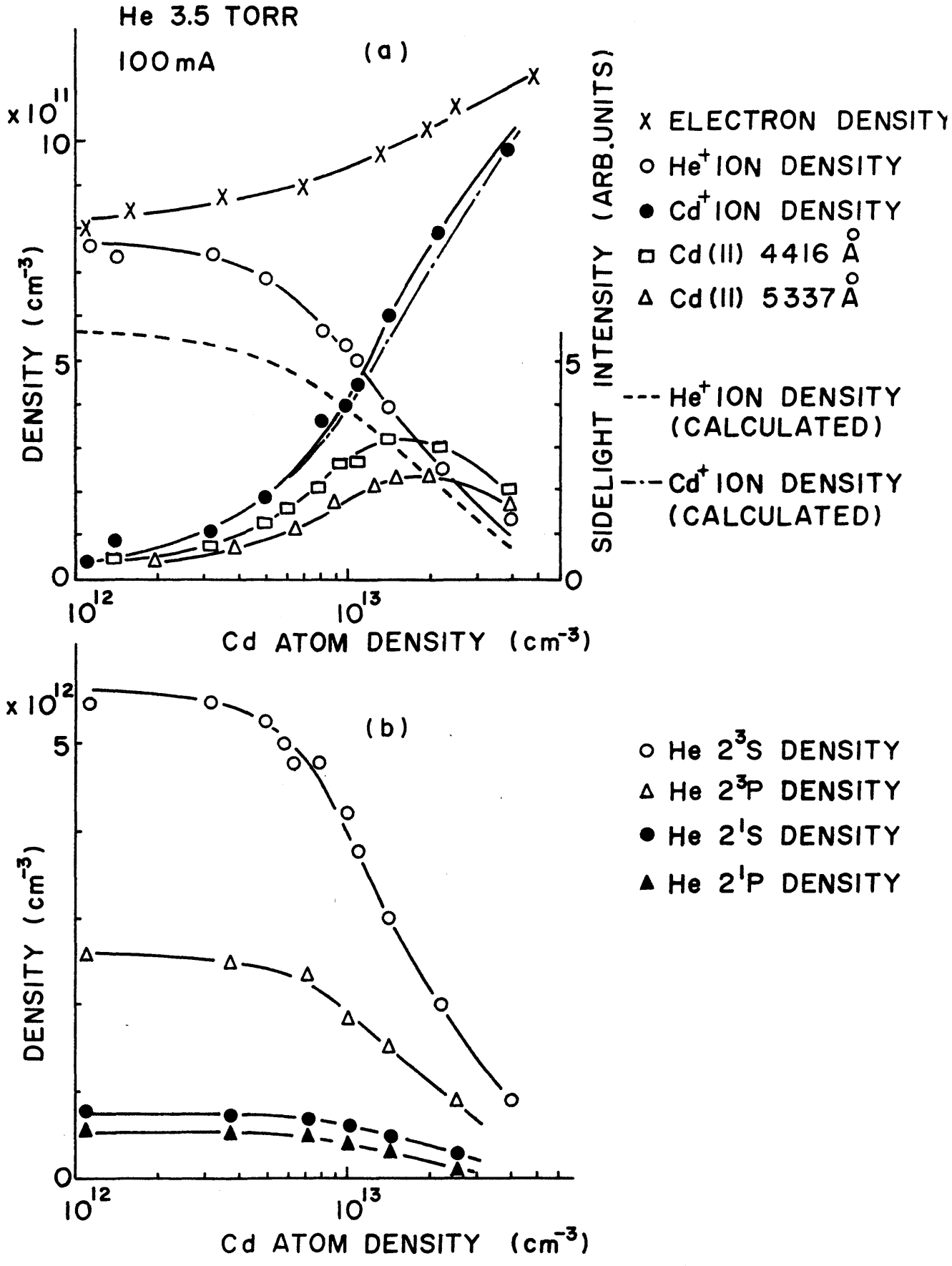

Fig.5-2. Electron, He^+ ion, Cd^+ ion densities, Cd(II) sidelight intensities, and population densities of He(I) first excited states as a function of Cd atom density.

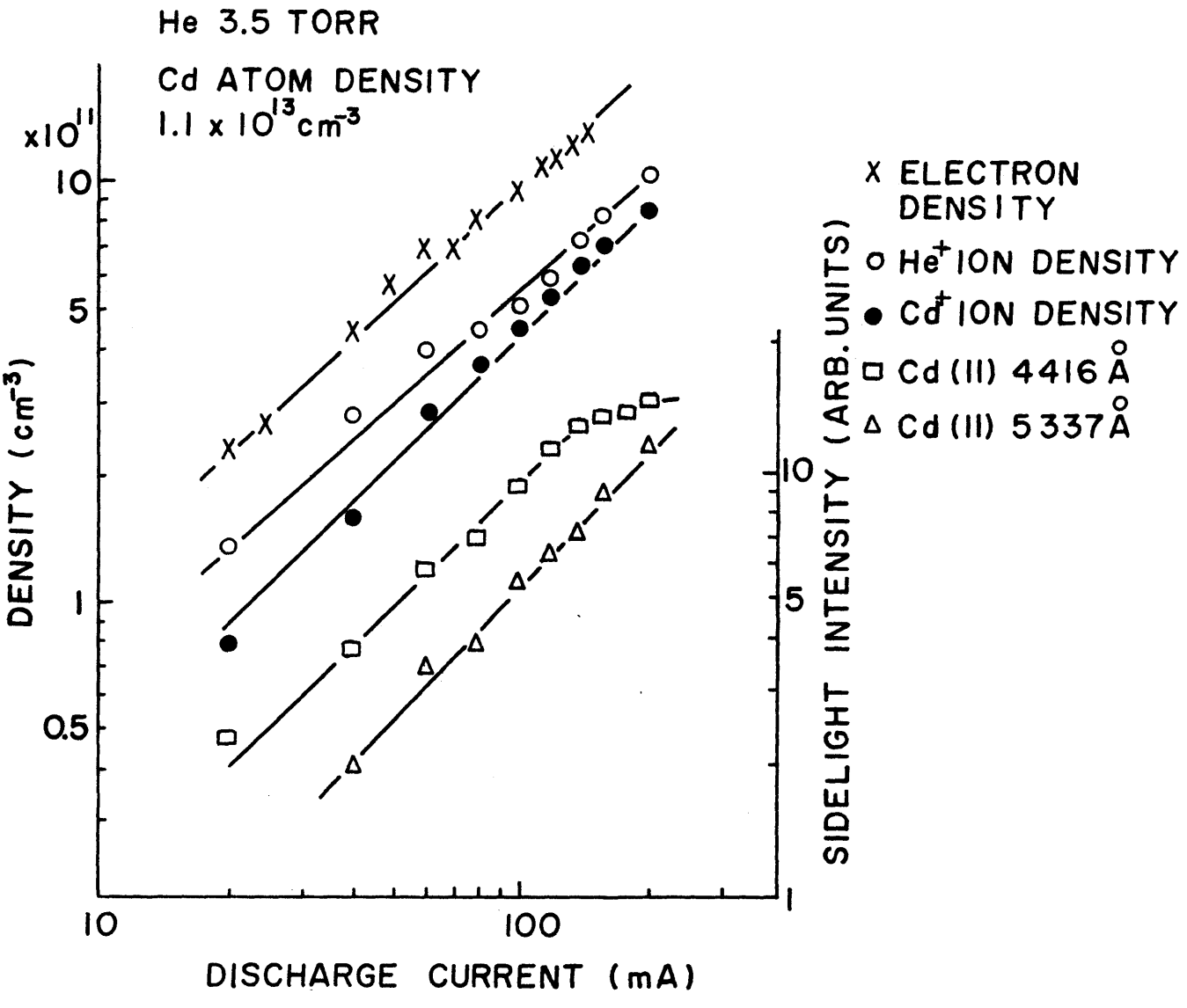

Fig.5-3. Electron, He^+ ion, Cd^+ ion densities, and Cd(II) sidelight intensities as a function of discharge current.

§5.5. Accuracy of the Experimental Results

The accuracy of the population density of the Cd(II) ground state obtained with the modified absorption method is determined dominantly by the accuracy of the transition probability of the Cd(II) 2265 Å line and the scatter of the measured values of the absorption coefficient. The transition probability of the Cd(II) 2265 Å line has been measured recently with the beam-foil technique,[14] with the electron-photon delayed coincidence,[15] and with the Hanle effect.[18] The results agree within ± 5 %. The scatter of the measured values of the absorption coefficient was less than ± 10 %. Then the uncertainty involved in the population density of the Cd(II) ground state is estimated to be less than ± 15 %.

The sum of the population densities of the Cd(II) excited states amounted to 10 ~ 20 % of that of the Cd(II) ground state. Therefore, the uncertainty which arises from the sidelight intensity measurements is negligibly small in comparison with that involved in the population density of the Cd(II) ground state.

The accuracy of the electron density in the He-Cd discharge obtained with the modified double probe method was discussed in Chapter 4, and the resultant uncertainty of the electron density was estimated to be less than ± 15 %.

From those of the electron and Cd^+ ion densities, the uncertainty involved in the obtained He^+ ion density can be estimated with the aid of eq.(5.1). At the Cd atom density below 1.5×10^{13} cm^{-3}, which is the optimum Cd atom density for

the Cd(II) 4416 Å laser operation, the estimated uncertainty is less than ± 30 %, and it increases at higher Cd atom densities.

In Figs.5-2 and 5-3, the product $n_{He^+}N_{Cd}$ of the He^+ ion density and the Cd atom density shows a behavior similar to that of the Cd(II) 5337 Å sidelight intensity. This agrees with the result obtained from the after-glow study in ref.7 that the dominant excitation process to the upper state of the Cd(II) 5337 Å line is the thermal energy charge transfer collision process of He^+ ions in the ground state with Cd atoms in the ground state followed by the radiative cascadings.

The results about the ion densities obtained with the previous methods,[9,10] agree with the present one qualitatively. That is, the He^+ ion density decreases and the Cd^+ ion density increases monotonically with the increase of the Cd atom density at the constant discharge current and initial He pressure. But the values of the ion densities obtained with the application of the method described in ref.10 to our data were considerably different from those shown in Fig.5-2 except for the very narrow Cd atom density region. As the previous methods strongly depend on the mobilities of the ions in the He-Cd discharge, which are not known exactly at present, probably the discrepancies come from the large uncertainties involved in the mobilities of the ions.

§5.6. Comparison with Theoretical Calculations

EDF in the He-Cd discharge was calculated with substituting the measured values of the electric field strength and the population densities of the He(I) first excited states into the Boltzmann equation and solving it numerically in a manner as described in Chapter 4. In the Boltzmann equation, the following collision processes between electrons and Cd atoms were included in addition to those between electrons and He atoms; (1) the elastic collisions with Cd atoms in the ground state, (2) the inelastic collisions exciting Cd atoms from the neutral ground state to the first excited states ($5p\,^1P_1$, $5p\,^3P_{0,1,2}$), (3) the direct ionizations of Cd atoms from the neutral ground state. The collision cross sections used in the calculation were taken from refs. 19-23, and are shown in Fig.5-4 as a function of the electron energy. Calculated EDF in the He-Cd discharge is shown in Fig.5-5. The initial He pressure was 3.5 Torr and the discharge current was 100 mA.

The He^+ and Cd^+ ion densities were calculated on the basis of the following equations and EDF shown in Fig.5-5:

$$n_{He^+} = \frac{\Lambda^2}{D_{He^+}}\left(n^e_{He\text{-}Cd} N_0 S^H + n^e_{He\text{-}Cd} \sum_{i=1}^{4} N_i M_i^H + N_3^2 \langle 6v \rangle_{He\text{-}He}\right), \tag{5.2}$$

and

$$n_{Cd^+} = \frac{\Lambda^2}{D_{Cd^+}}\left(n^e_{He\text{-}Cd} N_{Cd} S^C + N_3 N_{Cd} \langle 6v \rangle_{He\text{-}Cd}\right). \tag{5.3}$$

Here, $\Lambda = R/2.41$, and R is the radius of the discharge tube. The subscripts H and C denote that the quantities are concerned with helium and cadmium, respectively. The subscripts 1, 2, 3, and 4 (= i) are defined to represent the He(I) first excited states 2^1S, 2^1P, 2^3S, and 2^3P, respectively. N_0 is the He atom density and N_{Cd} is the Cd atom density. S denotes the collisional rate for the direct ionizations of atoms from the neutral ground state, and M_i denotes the collisional rate for the stepwise ionizations of He atoms from the He(I) first excited state i. D_{He^+} and D_{Cd^+} denote the ambipolar diffusion coefficients of helium and cadmium ions, respectively. The last term in eq.(5.2) represents the ionization rate by collisions between two He atoms in the He(I) 2^3S state. The last term in eq.(5.3) represents the Penning collisional rate between He atoms in the He(I) 2^3S state and Cd atoms in the ground state. The cross sections were taken from refs.24-27. The calculated results are presented in Fig.5-2.

As there are no reliable data on the Cd^+ ion mobility in a He-Cd discharge, the value was so chosen that the calculated Cd^+ ion density agreed with the experimentally determined one in the low Cd atom density region. The quite good agreement between the measured and calculated relative changes of the Cd^+ ion density over the wide Cd atom density region shows that the results are correct. The relative change of the calculated He^+ ion density agrees with that of the measured one completely. The absolute values are different by about 20 % from each other. This difference is small inspite of the relatively low reliability

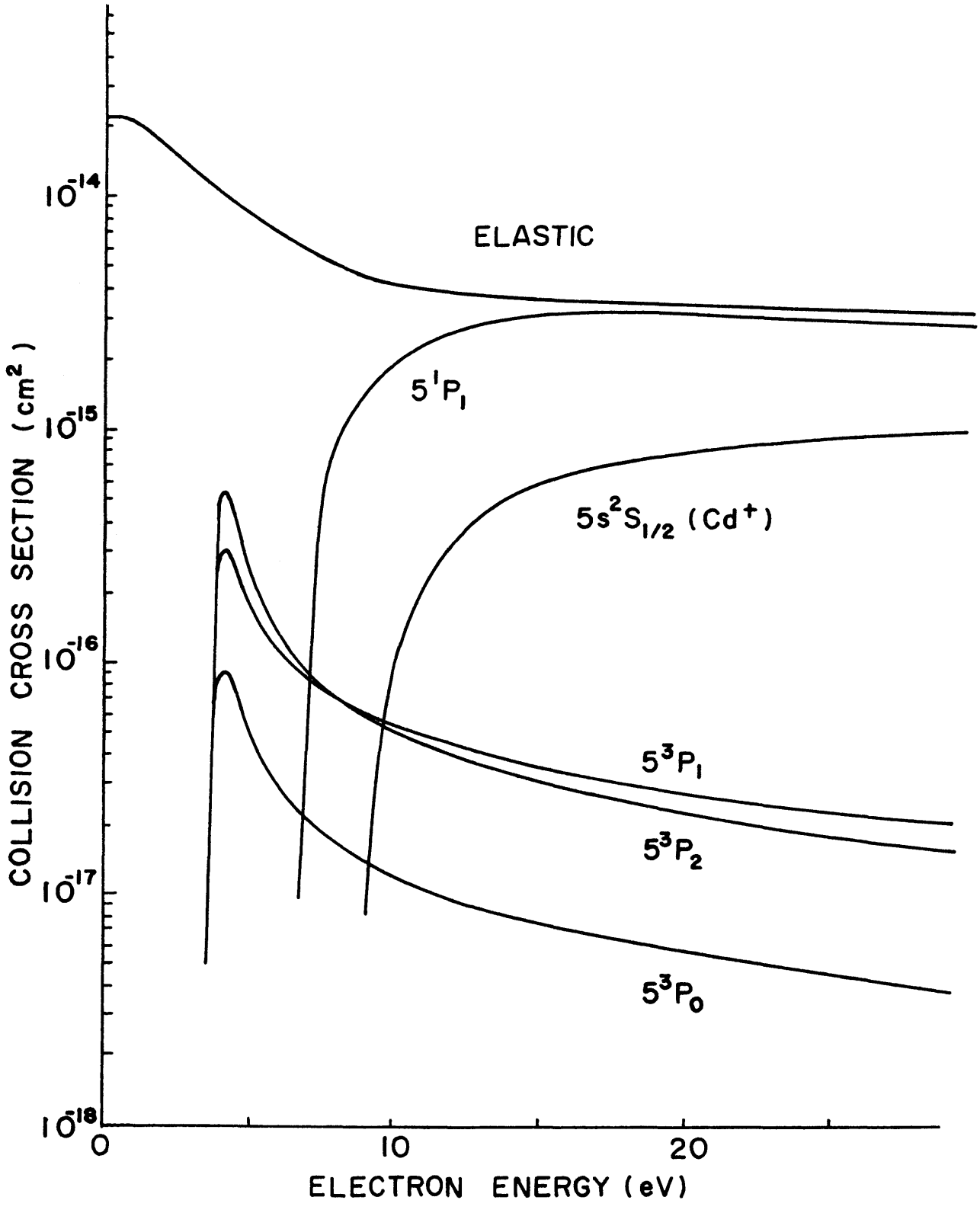

Fig.5-4. Elastic and inelastic collision cross sections for electron impacts with Cd atoms as a function of electron energy.

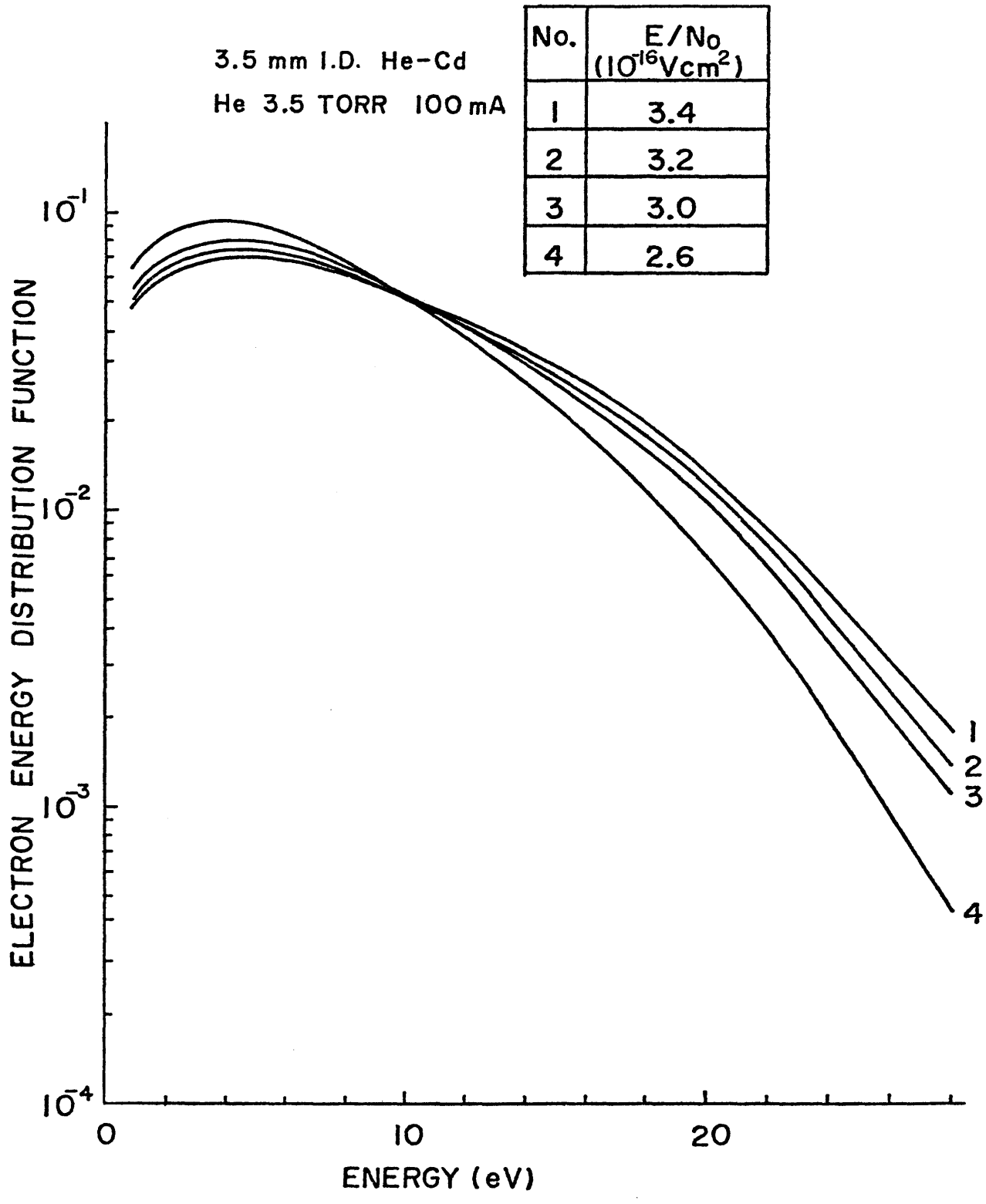

Fig.5-5. EDF in the He-Cd discharge as a function of electron energy.

of several collision cross sections.

Calculation shows that the Cd^+ ions are formed mainly by the direct ionizations of Cd atoms in the ground state. The ionization rate by the Penning collisions between He atoms in the He(I) 2^3S state and Cd atoms in the ground state is not more than 10 % of the total ionization rate of Cd atoms in the Cd atom density region in Fig.5-2. Therefore, there appears only a very low hump in the Cd^+ ion density as shown in Fig.5-2. Moreover, the Cd^+ ion density increases nearly in proportion to the discharge current as shown in Fig.5-3, and it is not saturated. On the contrary, Jánossy et al. supposed that the Cd(II) ground state was excited most dominantly by the Penning collision process.[28] As the population density of the He(I) 2^3S state was saturated in the low discharge current region of $I \ll 100$ mA,[3,4] they concluded that the population density of the Cd(II) ground state was also saturated in the low discharge current region. This contradicts the experimental results obtained here entirely.

§ 5.7. Conclusion

By combining the modified absorption method with the modified double probe method, the He^+ and Cd^+ ion densities in the PC He-Cd^+ laser discharge could be determined experimentally without using the Cd^+ ion mobility.

The ionization mechanisms in the PC He-Cd^+ laser discharge was investigated on the basis of the theoretical calculations using EDF in the He-Cd discharge. It has been shown that the dominant ionization process of Cd atoms is the direct ionization

process, not the Penning collision process.

The He^+ and Cd^+ ion densities obtained here will be used in Chapter 8 to calculate the excitation rates to the laser upper and lower states by the stepwise excitations from the Cd(II) ground state and thermal energy charge transfer excitation process followed by the radiative cascadings.

References in Chapter 5.

1) M.Mori, M.Takasu, T.Goto, and S.Hattori,"Ion densities in a positive column He-Cd^+ laser discharge,"J.Appl.Phys.,vol.48, pp.2226-2230,June 1977.

2) W.T.Silfvast,"Efficient CW laser oscillation at 4416 Å in Cd(II),"Appl.Phys.Lett.,vol.13,pp.169-171,Sep.1968.

3) P.G.Browne and M.H.Dunn,"Metastable densities and excitation processes in the He-Cd laser discharge,"J.Phys.B:Atom.Mole. Phys.,vol.6,pp.1103-1117,1973.

4) K.Miyazaki, Y.Ogata, T.Fujimoto, and K.Fukuda,"Excitation mechanism of 3250 and 4416 Å laser lines in the cataphoretic He-Cd laser discharge,"Japan.J.Appl.Phys.,vol.13,pp.1866-1874, Nov.1974.

5) T.Goto, A.Kawahara, G.J.Collins, and S.Hattori,"Electron temperature and density in positive column He-Cd^+ lasers," J.Appl.Phys.,vol.42,pp.3816-3818,Sep.1971.

6) J.K.Mizeraczyk,"A simple method of determination of electron density in positive-column He-metal laser discharge,"J.Appl. Phys.,vol.46,pp.1847-1848,April 1975.

7) G.J.Collins, R.C.Jensen, and W.R.Bennett,Jr.,"Charge-exchange excitation in the He-Cd laser,"Appl.Phys.Lett.,vol.19,pp.125-128,Sep.1971.

8) A.R.Turner-Smith, J.M.Green, and C.E.Webb,"Charge transfer into excited states in thermal energy collisions,"J.Phys. B:Atom.Molec.Phys.,vol.6,pp.114-130,Jan.1973.

9) I.G.Ivanov and M.F.Sém,"Determination of charged-particle density in the plasma of a cadmium-helium cataphoresis laser," Sov.Phys.-Tech.Phys.,vol.17,pp.1234-1235,Jan.1973.

10) J.K.Mizeraczyk, Z.Zakrzewski, T.Goto, and S.Hattori, "Ionization mechanisms in positive-column He-Cd^+ laser discharge,"Proc.Twelfth Int.Conf.Phen.Ion.Gases,Eindhoven, (North-Holland, Amsterdam, 1975).

11) T.Goto, M.Mori, and S.Hattori,"Modified absorption method to determine level population densities in a cataphoresis type of He-metal laser discharge,"Appl.Phys.Lett.,vol.29, pp.358-360,Sep.1976.

12) W.T.Silfvast and P.W.Smith,"Mode locking of the He-Cd laser at 4416 and 3250 Å,"Appl.Phys.Lett.,vol.17,pp.70-73,July 1970.

13) J.P.Goldsborough, Laser Handbook, edited by F.T.Arecchi and E.O.Schulz-DuBois (North-Holland, Amsterdam, 1972), vol.1, p.620.

14) T.Andersen and G.Sørensen,"Systematic trends in atomic transition probabilities in neutral and singly-ionized zinc, cadmium and mercury,"J.Quant.Spectrosc.Radiat.Transfer., vol.13,pp.369-376,1973.

15) D.A.Shaw, A.Adams, and G.C.King,"Lifetime measurements in cadmium II using the electron-photon delayed coincidence technique,"J.Phys.B:Atom.Molec.Phys.,vol.8,pp.2456-2460,1975.

16) E.W.McDaniel and E.A.Mason, The Mobility and Diffusion of Ions in Gases (Wiley, New York, 1973),p.266.

17) W.T.Silfvast,"Penning ionization in a He-Cd dc discharge," Phys.Rev.Lett.,vol.27,pp.1489-1492,Nov.1971.

18) J.Hamel and J.P.Barrat,"Durée de vie et dépolarisation par collisions avec l'helium des niveaux $5^2P_{3/2}$ et $5^2P_{1/2}$ de l'ion Cd^+,"Opt.Commun.,vol.10,pp.331-336,April 1974.

19) R.B.Brode,"The absorption coefficient for slow electrons in cadmium and zinc vapors,"Phys.Rev.,vol.35,pp.504-508, March 1930.

20) N.P.Penkin and T.P.Redko,"Effective cross sections for excitation of the $5^3P_{0,1,2}$ levels Cd I by electron impact," Opt.Spectrosc.,vol.22,pp.252-253,Sep.1967.

21) V.N.Gavchenko,"Calculation of effective cross sections for electron collision excitation of the fine structure components $^1P_1$ and $^3P_{0,1,2}$ of mercury, cadmium, and zinc atoms," Opt.Spectrosc.,vol.30,pp.6-9,Jan.1970.

22) J.W.Otvos and D.P.Stevenson,"Cross-sections of molecules for ionization by electrons,"J.Am.Chem.Soc.,vol.78,pp.546-551,Feb.1956.

23) R.F.Pottie,"Cross sections for ionization by electrons.I. Absolute ionization cross sections of Zn, Cd, and Te_2. II. Comparison of theoretical with experimental values for atoms and molecules,"J.Chem.Phys.,vol.44,pp.916-922,1966.

24) D.R.Long and R.Geballe,"Electron-impact ionization of $He(2s^3S)$,"Phys.Rev.,vol.A1,pp.260-265,Feb.1970.

25) L.Vriens,"Calculation of absolute ionization cross sections of He, He^*, He^+, Ne, Ne^*, Ne^+, Ar, Ar^*, Hg and Hg^*," Phys.Lett.,vol.8,pp.260-261,Feb.1964.

26) V.Čermák,"Penning ionization electron spectroscopy.III. Ionization of cadmium,"Collec.Czech.Chem.Commun.,vol.36, pp.948-950,1971.

27) A.V.Phelps and J.P.Molnar,"Lifetimes of metastable states of noble gases,"Phys.Rev.,vol.89,pp.1202-1208,March 1953.

28) M.Jánossy, V.V.Itagi, and L.Csillag,"On the excitation mechanism and operation parameters of the 4416 Å He-Cd laser," Acta Phys.Hungar.,vol.32,pp.149-163,Jan.1972.

Chapter 6. Population Densities of He(I) Excited States in the PC He-Cd^+ Laser Discharge[1)]

§6.1. Introduction

In the PC He-Cd^+ laser discharge, it has been proposed that the dominant excitation process to the laser upper states is the Penning collision process between He atoms in the He(I) 2^3S state and Cd atoms in the ground state.[2,3)] The population densities of the He(I) excited states in the PC He-Cd^+ laser discharge, especially that of the He(I) 2^3S state, have been measured[4,5)] or examined theoretically using the Maxwellian electron energy distribution function (EDF).[6,7)] It has been observed experimentally that the population density of the He(I) 2^3S state is saturated at a considerably lower discharge current than 100 mA [4,5)] while the laser output powers and the sidelight intensities of the Cd(II) 4416 and 3250 Å lines increase monotonically with the discharge current up to about 140 mA. This contradicts the assumption that the laser upper states are excited dominantly by the Penning collision process.

On the other hand, the calculated population density of the He(I) 2^3S state in refs.6 and 7 increased linearly up to a discharge current around 100 mA. Therefore, a significant discrepancy was found between the discharge current dependence of the measured population density of the He(I) 2^3S state and that of the calculated one.

These discrepancies may come from defects in the measurements and theoretical calculations, or it may be caused by neglecting excitation processes other than the Penning excitation process.

In order to make the above and finally the excitation mechanisms in the PC He-Cd^+ laser clear, first of all, it is necessary to measure the population densities of the He(I) excited states including the metastable states carefully and explain their dependences on various experimental parameters theoretically. In the theoretical calculations, it has to be taken into account that EDF in the discharge is non-Maxwellian, although the analysis has been done generally assuming the Maxwellian EDF up to the present. Because it has been shown from experimental and also theoretical results that EDF is non-Maxwellian in He and He-metal discharges at medium pressures.[8-10] Although Mewe carried out the extensive study of the pure He discharge using the non-Maxwellian EDF,[12,13] in the PC He-metal discharges, there has been reported no quantitative analysis of the population densities using the non-Maxwellian EDF.

In this chapter, the population densities of the He(I) excited states in the PC He-Cd^+ laser discharge have been measured carefully and accurately, and it is shown that the results calculated using the non-Maxwellian EDF coincide with the experimental ones well. Especially, a theoretical explanation is given in detail as to the discharge current dependences of the population densities of the He(I) metastable states.[1]

§6.2. Experimental Procedure

A discharge tube of 3.5 mm in diameter made of Pyrex glass was used mainly in this experiment, but also a tube of 3 mm in diameter was used. Each discharge tube was connected to a flask of large volume and the capillary part of the tube was put in an oven of 600 K to maintain the profiles of the spectral lines and the He atom density N_0 in the capillary part constant irrespective of the discharge current. Therefore, each spectral line of He(I), or each component in the case of the triplet, has a Doppler broadened profile corresponding to the gas temperature of 600 K.

The population densities of the He(I) 2^3S, 2^1S, 2^3P, and 2^1P states, and that of the Cd(I) ground state were determined from the absorption coefficients of the He(I) 3188 Å, 3965 Å, 4026 Å, and 4922 Å lines,and the Cd(I) 3261 Å line, respectively, which were measured with the modified absorption method.[14] These lines were used because the population densities of the upper states of the lines were negligibly small compared with those of the lower states.

Population densities of other He(I) excited states were determined from the absolute intensities of the spontaneous emissions in a manner described in Chapter 3. The ratio of the sidelight intensities were measured with the quartz discharge tube of the same inner diameter. We can see from the relative changes of the sidelight intensities whether the experimental conditions in the two discharge tubes are identical or not.[15]

In calculating the population densities of the He(I)

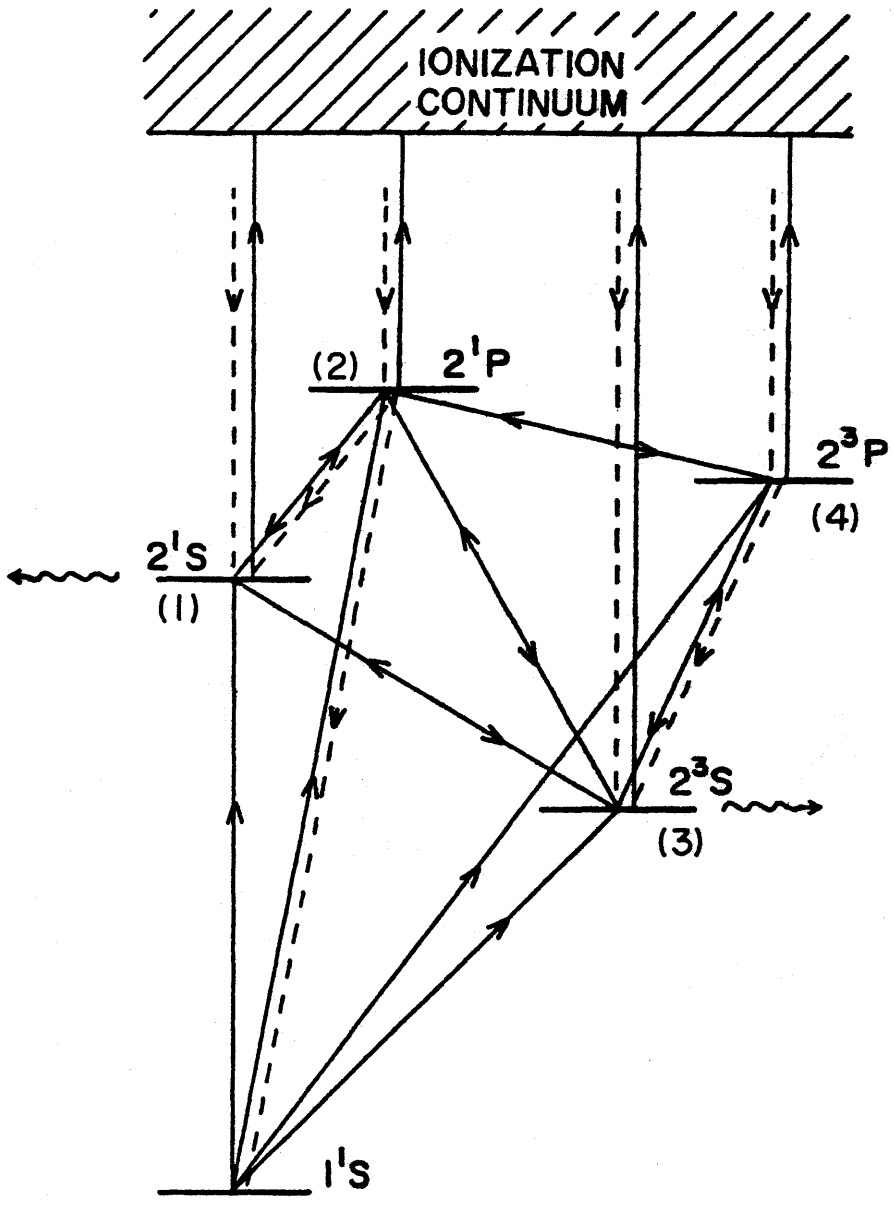

Fig.6-1. Collision, radiation, and diffusion processes for He(I) first excited states. Straight arrows; electronic collisions, dotted arrows; radiative transitions, wavy arrows; diffusion to the wall.

excited states using the rate equations, it is necessary to measure the electric field strength and the electron density in the He-Cd discharge, where EDF is non-Maxwellian. The values of them obtained in Chapter 4 were used here.

§6.3. Theoretical Calculations

A simple collisional-radiative model similar to that in ref.12 has been applied to the pure He and He-Cd discharges. In order to take into account the influence of the radiative cascadings, the He(I) excited states of the principal quantum number n = 3 and 4 as well as the He(I) first excited states of n = 2 were included in the rate equations. The radiative cascadings from the states of $n \geq 5$ were neglected because it was assured from the sidelight intensity measurements that the contribution of the process to the population densities never exceeded 10 % under the present experimental conditions.

For the He(I) first excited states, the following processes were included in the calculation; the direct excitation, de-excitation and stepwise excitation (also ionization) by electron impacts, radiative decay, radiative cascadings from the higher lying excited states of n = 3 and 4, Penning collisions of He atoms in the He(I) 2^3S state with Cd atoms in the ground state, ionization due to the collisions between He atoms in the He(I) 2^3S state, and the diffusion to the wall. The collision, radiation, and diffusion processes for the He(I) first excited states are shown schematically in Fig.6-1. The rate equations are given by

$$2^1S;\quad -\left\{n^e(S_{1-2}+S_{1-3}+S_{1-c})+D_1\Lambda^{-2}\right\}N_1 + (n^eS_{2-1}+T_{2-1}A_{2-1})N_2$$
$$+ n^eS_{3-1}N_3 + \sum_j T_{j-1}A_{j-1}N_j + N_0n^eS_{0-1} = 0,$$

$$2^1P;\quad n^eS_{1-2}N_1 - \left\{n^e(S_{2-1}+S_{2-3}+S_{2-4}+S_{2-c})+T_{2-0}A_{2-0}+T_{2-1}A_{2-1}\right\}N_2$$
$$+ n^eS_{3-2}N_3 + n^eS_{4-2}N_4 + \sum_j T_{j-2}A_{j-2}N_j + N_0n^eS_{0-2} = 0,$$

$$2^3S;\quad n^eS_{1-3}N_1 + n^eS_{2-3}N_2 - \left\{n^e(S_{3-1}+S_{3-2}+S_{3-4}+S_{3-c}+\sum_{j\geq 5} S_{3-j})+\right.$$
$$\left.+D_3\Lambda^{-2}+N_{Cd}\langle\sigma v\rangle_{He-Cd}+N_3\langle\sigma v\rangle_{He-He}\right\}N_3 + (n^eS_{4-3}+T_{4-3}A_{4-3})N_4$$
$$+ \sum_j T_{j-3}A_{j-3}N_j + N_0n^eS_{0-3} = 0,$$

$$2^3P;\quad n^eS_{2-4}N_2 + n^eS_{3-4}N_3 - \left\{n^e(S_{4-2}+S_{4-3}+S_{4-c})+T_{4-3}A_{4-3}\right\}N_4$$
$$+ \sum_j T_{j-4}A_{j-4}N_j + N_0n^eS_{0-4} = 0.$$

(6.1)

In the rate equations for the He(I) 2^1S and 2^3S states, the diffusion terms $D_i\nabla^2N_i$ (i = 1 and 3) were estimated by assuming that the radial distributions of those excited states could be approximated by the Bessel function of the zeroth order.

We obtain that $D_i\nabla^2 N_i = -D_i N_i/\Lambda^2$ in this case. Here Λ is the diffusion length and $\Lambda = R/2.41$. In eq.(6.1), the subscripts c, 0, 1, 2, 3, and 4 denote the ionization continuum[12], the ground state, 2^1S, 2^1P, 2^3S, and 2^3P states of He, respectively. N_0 is the He atom density, N_j is the population density of the excited state j, n^e is the electron density, and N_{Cd} is the Cd atom density. D_i is the diffusion coefficient of He atoms in the state i. $\langle 6v\rangle_{He\text{-}Cd}$ and $\langle 6v\rangle_{He\text{-}He}$ are the rate coefficient for the Penning collisions of He atoms in the He(I) 2^3S state with Cd atoms in the ground state and that for the ionizations due to the collisions between two He atoms in the He(I) 2^3S state, respectively. A_{i-j} and T_{i-j} are the transition probability and the trapping coefficient[16] for the radiative transition $i \rightarrow j$. S_{i-j} is the rate coefficient for the transition $i \rightarrow j$ induced by electron impacts, and is given by

$$S_{i-j} = \sqrt{\frac{2e}{m}} \int_{V_{th}}^{\infty} Q_{i-j}(x)\sqrt{x}\, F(x)\,dx, \qquad (6.2)$$

where x is the energy in eV, $Q_{i-j}(x)$ is the corresponding cross section, V_{th} is the threshold energy, and F(x) is EDF.

For the excited states of n = 3 and 4, the following processes were included in the rate equations; the direct excitation, stepwise excitation from the He(I) 2^3S state, radiative cascadings (only for those states of n = 3), and radiative decay.

EDF in the pure He and He-Cd discharges obtained in Chapters 4 and 5 were used in the calculation. The cross

sections were taken from experimental and theoretical data in refs.3, 12, and 17-22. The diffusion coefficient at 600 K were quoted from ref.23, taking into account that they were linearly dependent on the gas temperature.[24] A simple calculation shows that the trapping coefficients of the radiative transitions except for the transitions $2^1P \rightarrow 0$, $2^1P \rightarrow 2^1S$, $2^3P \rightarrow 2^3S$, $3^1P \rightarrow 0$, $3^3D \rightarrow 2^3P$, and $4^1P \rightarrow 0$ are nearly equal to 1.

With the measured electron and Cd atom densities and the calculated EDF, eq.(6.1) was solved numerically. Some iterative method was employed to solve eq.(6.1) because the trapping coefficient of each radiative transition had the complicated dependence on the population densities of the upper and lower states of it generally.

6.4. Experimental and Theoretical Results

6.4.1. He discharge

First the experiments and calculations were performed about the pure He discharge. The measured and calculated population densities of the He(I) first excited states and those of the He(I) 3^3P and 3^1P states are shown in Fig.6-2 as a function of the initial He pressure. The calculated rate coefficients S_{i-j} are listed in Table 6-1. The tube diameter was 3.5 mm and the discharge current was 100 mA. Calculations were also done using the Maxwellian EDF of the electron temperature determined with the conventional double probe method[25] for the comparison. The results are denoted by dotted lines in Fig.6-2, which deviate very much from the measured values. On the contrary,

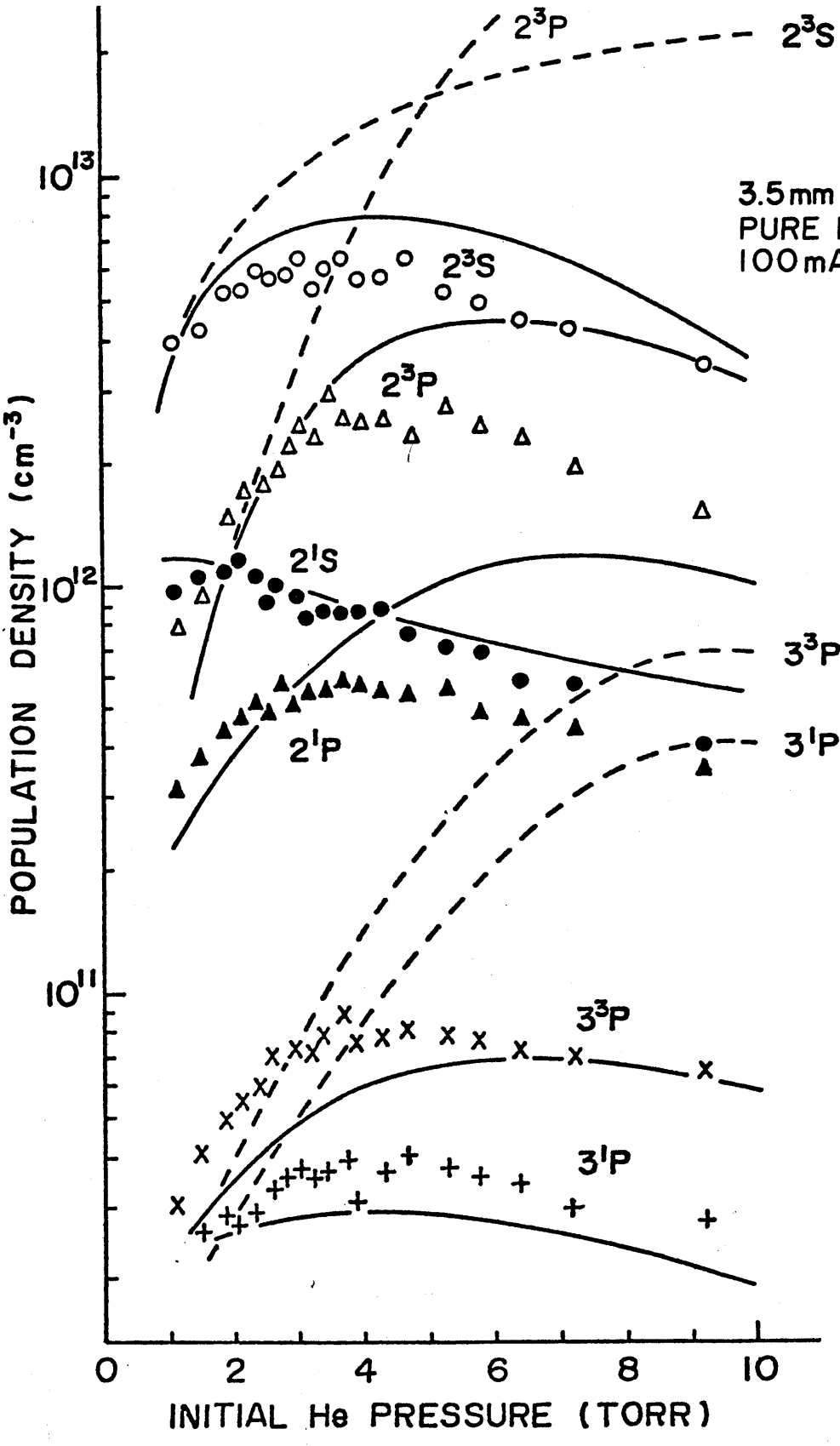

Fig.6-2. Population densities of He(I) excited states in the pure He discharge as a function of initial He pressure. The solid lines and the dotted lines represent the results calculated with non-Maxwellian EDF and Maxwellian EDF, respectively.

Table 6-1. Rate coefficients in the pure He discharge as a function of initial He pressure; 3.5 mm I.D., discharge current of 100 mA.

p_0 (Torr)		0.8	1.4	2.1	3.5	5.4	8.9	11.2
n^e (cm^{-3})		1.1^{11}	2.2^{11}	4.0^{11}	8.1^{11}	1.5^{12}	2.9^{12}	4.0^{12}
Population Density (cm^{-3})	N_1	1.2^{12}	1.3^{12}	1.2^{12}	8.8^{11}	8.0^{11}	5.7^{11}	3.9^{11}
	N_2	1.8^{11}	2.8^{11}	4.4^{11}	6.6^{11}	1.0^{12}	1.1^{12}	9.0^{11}
	N_3	2.2^{12}	5.2^{12}	2.6^{12}	7.6^{12}	6.6^{12}	4.6^{12}	3.0^{12}
	N_4	1.2^{11}	5.3^{11}	1.5^{12}	2.6^{12}	3.6^{12}	3.5^{12}	2.6^{12}
Rate Coefficient (cm^3/sec)	S_{0-1}	2.2^{-10}	7.4^{-11}	3.3^{-11}	8.2^{-12}	4.1^{-12}	1.0^{-12}	4.3^{-13}
	S_{1-2}	3.4^{-6}	3.2^{-6}	3.2^{-6}	3.2^{-6}	3.2^{-6}	3.2^{-6}	3.2^{-6}
	S_{1-3}	3.0^{-7}	3.2^{-7}	3.5^{-7}	3.9^{-7}	4.0^{-7}	4.3^{-7}	4.4^{-7}
	S_{1-C}	1.5^{-7}	1.2^{-7}	1.0^{-7}	8.6^{-8}	7.9^{-8}	6.9^{-8}	6.3^{-8}
	S_{0-2}	7.4^{-10}	1.9^{-10}	7.2^{-11}	1.5^{-11}	6.6^{-12}	1.3^{-12}	5.1^{-13}
	S_{2-1}	6.6^{-7}	6.4^{-7}	6.5^{-7}	6.6^{-7}	6.6^{-7}	6.7^{-7}	6.7^{-7}
	S_{2-3}	5.5^{-8}	7.5^{-8}	9.4^{-8}	1.3^{-7}	1.4^{-7}	1.6^{-7}	1.7^{-7}
	S_{2-4}	5.1^{-7}	5.5^{-7}	5.9^{-7}	6.6^{-7}	6.9^{-7}	7.3^{-7}	7.6^{-7}
	S_{2-C}	2.1^{-7}	1.7^{-7}	1.5^{-7}	1.3^{-7}	1.2^{-7}	1.0^{-7}	9.6^{-8}
	S_{0-3}	2.0^{-10}	1.0^{-10}	6.1^{-11}	2.4^{-11}	1.3^{-11}	4.4^{-12}	2.2^{-12}
	S_{3-1}	8.2^{-8}	8.5^{-8}	8.8^{-8}	9.3^{-8}	9.4^{-8}	9.7^{-8}	9.8^{-8}
	S_{3-2}	5.3^{-8}	7.1^{-8}	8.7^{-8}	1.1^{-7}	1.2^{-7}	1.4^{-7}	1.5^{-7}
	S_{3-4}	2.0^{-6}	1.8^{-6}	1.8^{-6}	1.7^{-6}	1.7^{-6}	1.6^{-6}	1.6^{-6}
	S_{3-C}	1.1^{-7}	7.8^{-8}	6.7^{-8}	5.3^{-8}	4.8^{-8}	4.1^{-8}	3.6^{-8}
	S_{0-4}	2.1^{-10}	9.6^{-11}	5.2^{-11}	1.8^{-11}	9.4^{-12}	2.7^{-12}	1.3^{-12}
	S_{4-2}	1.5^{-7}	1.6^{-7}	1.7^{-7}	1.9^{-7}	1.9^{-7}	2.0^{-7}	2.1^{-7}
	S_{4-3}	4.0^{-7}	3.7^{-7}	3.7^{-7}	3.7^{-7}	3.7^{-7}	3.7^{-7}	3.7^{-7}
	S_{4-C}	1.8^{-7}	1.4^{-7}	1.3^{-7}	1.1^{-7}	1.0^{-7}	8.8^{-8}	8.1^{-8}

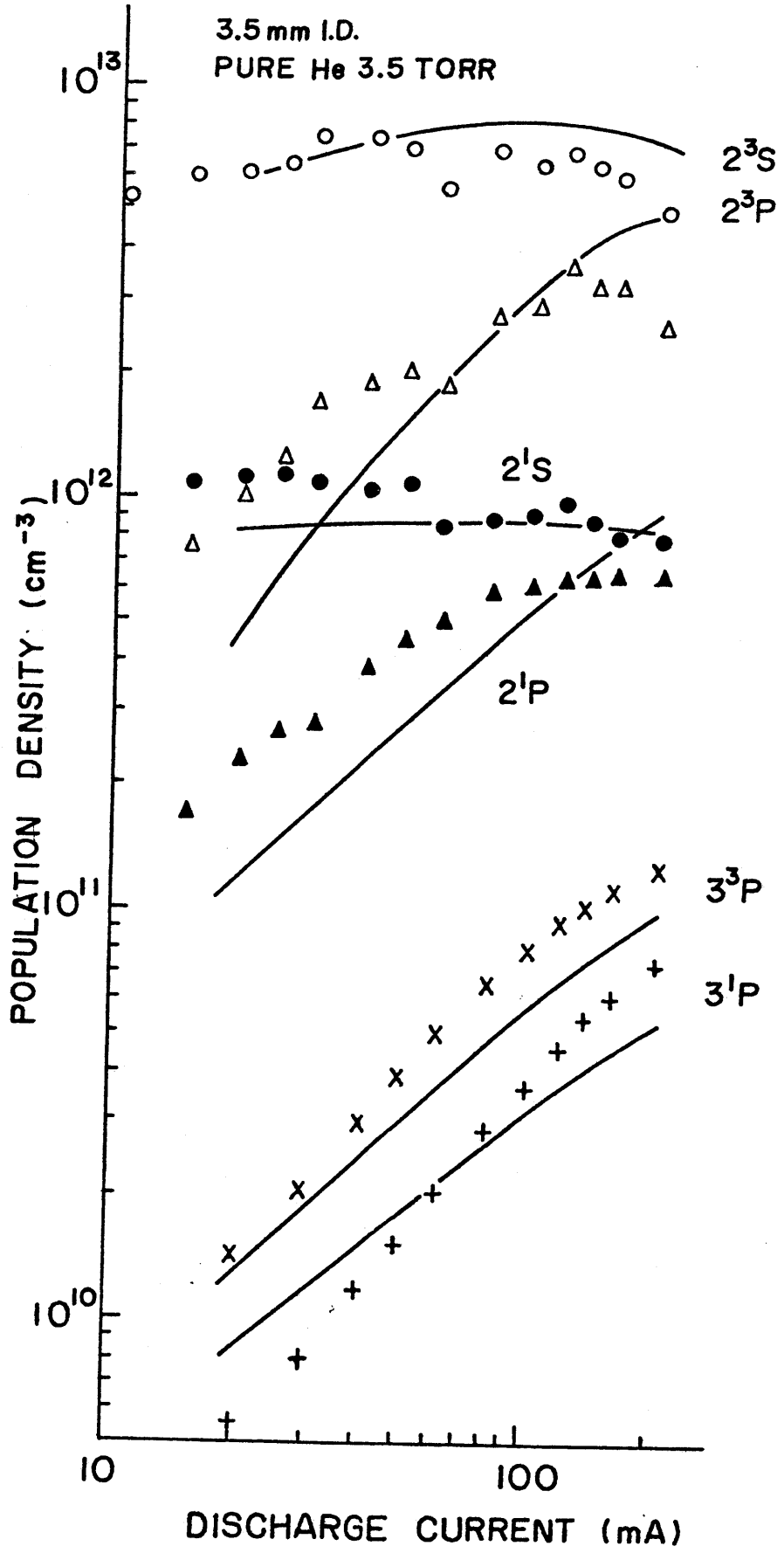

Fig.6-3. Population densities of He(I) excited states in the pure He discharge as a function of discharge current. The solid lines represent the results calculated with non-Maxwellian EDF.

the results calculated using the non-Maxwellian EDF explain the experimental results well for all the states.

Figure 6-3 shows the discharge current dependences of the population densities in the pure He discharge. The experimentally determined population densities of the He(I) 2^3S and 2^1S states remain almost constant over the discharge current region investigated.

6.4.2. He-Cd discharge

Figure 6-4 shows the Cd atom density dependences of the population densities of the He(I) excited states in the discharge tube of 3.5 mm in diameter. The initial He pressure was 3.5 Torr and the discharge current was 100 mA. As the Cd atom density increases, the population densities of the He(I) excited states of n = 2, 3, and 4 decrease monotonically, because the higher energy part of EDF decreases rapidly on account of the inelastic collisions of electrons with Cd atoms of the low ionization energy. The calculated results agree with the experimental data well. The calculated rate coefficients S_{i-j} are listed in Table 6-2.

Figure 6-5 shows the discharge current dependences of the population densities of the He(I) excited states at the constant Cd atom density of 1.1×10^{13} cm^{-3} in the He-Cd discharge. The initial He pressure was 3.5 Torr. The scatter of the measured values was somewhat large at the discharge current of 10 mA. The Cd atom density N_{Cd} was monitored by measuring the absorption coefficient of the Cd(I) 3261 Å line, and was kept constant at any discharge current by controlling the Cd oven temperature.

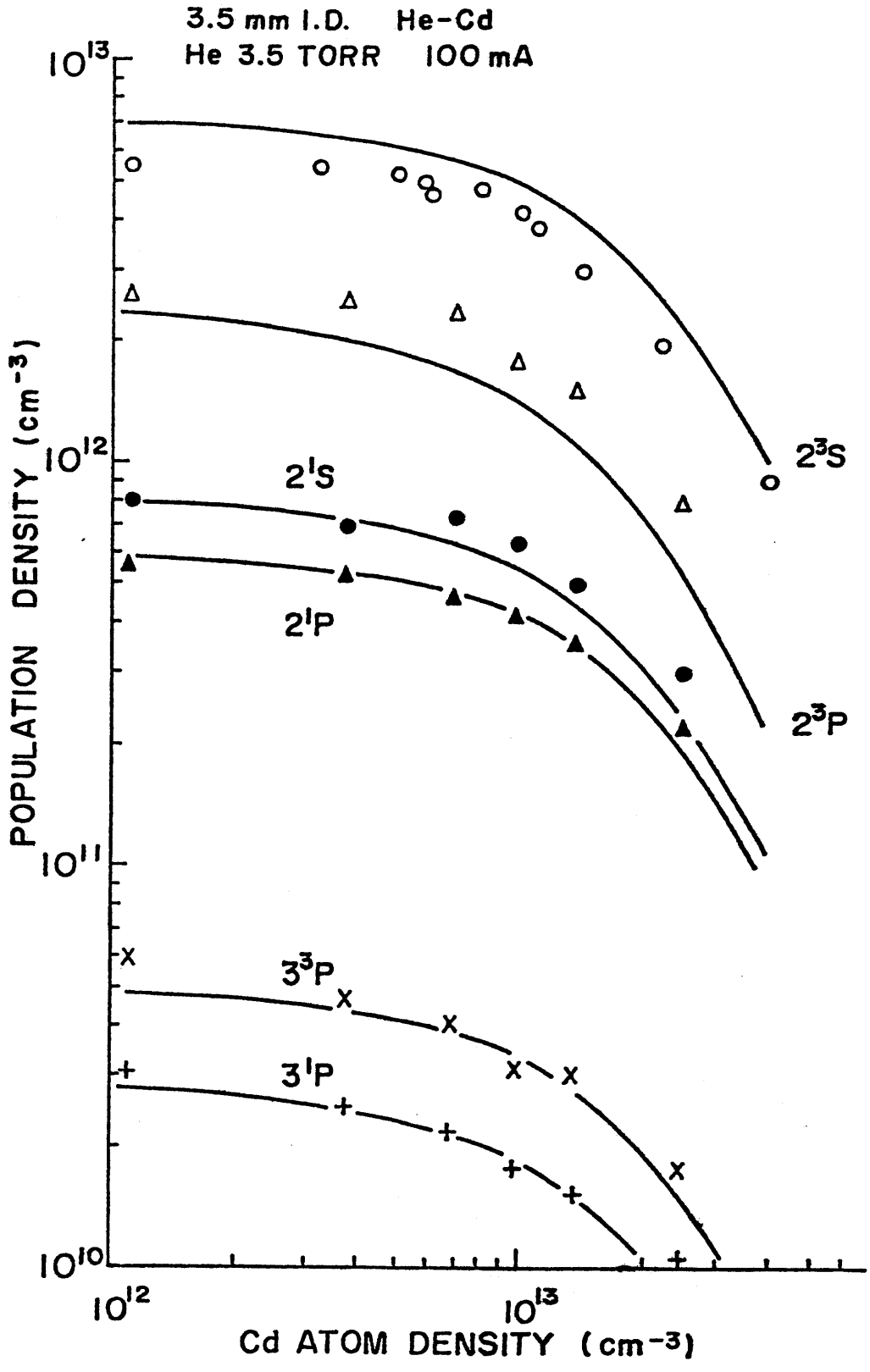

Fig.6-4. Population densities of He(I) excited states in the He-Cd discharge as a function of Cd atom density. The solid lines represent the results calculated with non-Maxwellian EDF.

Table 6-2. Rate coefficients in the He-Cd discharge as a function of Cd atom density; 3.5 mm I.D., discharge current of 100 mA, initial He pressure of 3.5 Torr.

	N_{Cd} (cm^{-3})	0.0	1.1^{12}	6.6^{12}	1.5^{13}	4.0^{13}	1.0^{14}
	n^e (cm^{-3})	8.0^{11}	8.0^{11}	9.0^{11}	9.8^{11}	1.1^{12}	1.4^{12}
Population Density(cm^{-3})	N_1	8.8^{11}	8.1^{11}	6.5^{11}	4.4^{11}	1.1^{11}	1.8^{9}
	N_2	6.6^{11}	6.0^{11}	4.9^{11}	3.5^{11}	9.7^{10}	1.8^{9}
	N_3	7.6^{12}	7.1^{12}	5.8^{12}	4.0^{12}	1.1^{12}	1.6^{10}
	N_4	2.6^{12}	2.3^{12}	1.7^{12}	1.1^{12}	2.2^{11}	3.5^{9}
Rate Coefficient (cm^3/sec)	S_{0-1}	8.2^{-12}	8.0^{-12}	6.1^{-12}	3.9^{-12}	8.7^{-13}	1.1^{-14}
	S_{1-2}	3.2^{-6}	3.2^{-6}	3.2^{-6}	3.2^{-6}	3.2^{-6}	3.0^{-6}
	S_{1-3}	3.9^{-5}	3.9^{-7}	4.0^{-7}	4.1^{-7}	4.6^{-7}	5.6^{-7}
	S_{1-C}	8.6^{-8}	8.5^{-8}	8.1^{-8}	7.5^{-8}	5.7^{-8}	2.6^{-8}
	S_{0-2}	1.5^{-11}	1.4^{-11}	1.0^{-11}	6.2^{-12}	1.3^{-12}	1.4^{-14}
	S_{2-1}	6.6^{-7}	6.6^{-7}	6.6^{-7}	6.6^{-7}	6.7^{-7}	6.7^{-7}
	S_{2-3}	1.3^{-7}	1.3^{-7}	1.3^{-7}	1.4^{-7}	1.8^{-7}	2.9^{-7}
	S_{2-4}	6.6^{-7}	6.7^{-7}	6.8^{-7}	7.0^{-7}	7.7^{-7}	9.5^{-7}
	S_{2-C}	1.3^{-7}	1.2^{-7}	1.2^{-7}	1.1^{-7}	8.9^{-8}	4.7^{-8}
	S_{0-3}	2.4^{-11}	2.3^{-11}	1.8^{-11}	1.2^{-11}	3.3^{-12}	5.9^{-14}
	S_{3-1}	9.3^{-8}	9.3^{-8}	9.4^{-8}	9.5^{-8}	1.0^{-7}	1.0^{-7}
	S_{3-2}	1.1^{-7}	1.1^{-7}	1.2^{-7}	1.3^{-7}	1.6^{-7}	2.2^{-7}
	S_{3-4}	1.7^{-6}	1.7^{-6}	1.7^{-6}	1.6^{-6}	1.6^{-6}	1.3^{-6}
	S_{3-C}	5.3^{-8}	5.3^{-8}	5.0^{-8}	4.5^{-8}	3.2^{-8}	1.3^{-8}
	S_{0-4}	1.8^{-11}	1.7^{-11}	1.3^{-11}	8.8^{-12}	2.2^{-12}	3.3^{-14}
	S_{4-2}	1.9^{-7}	1.9^{-7}	1.9^{-7}	2.0^{-7}	2.1^{-7}	2.5^{-7}
	S_{4-3}	3.7^{-7}	3.7^{-7}	3.7^{-7}	3.7^{-7}	3.7^{-7}	3.5^{-7}
	S_{4-C}	1.1^{-7}	1.1^{-7}	1.0^{-7}	9.5^{-8}	7.4^{-8}	3.7^{-8}

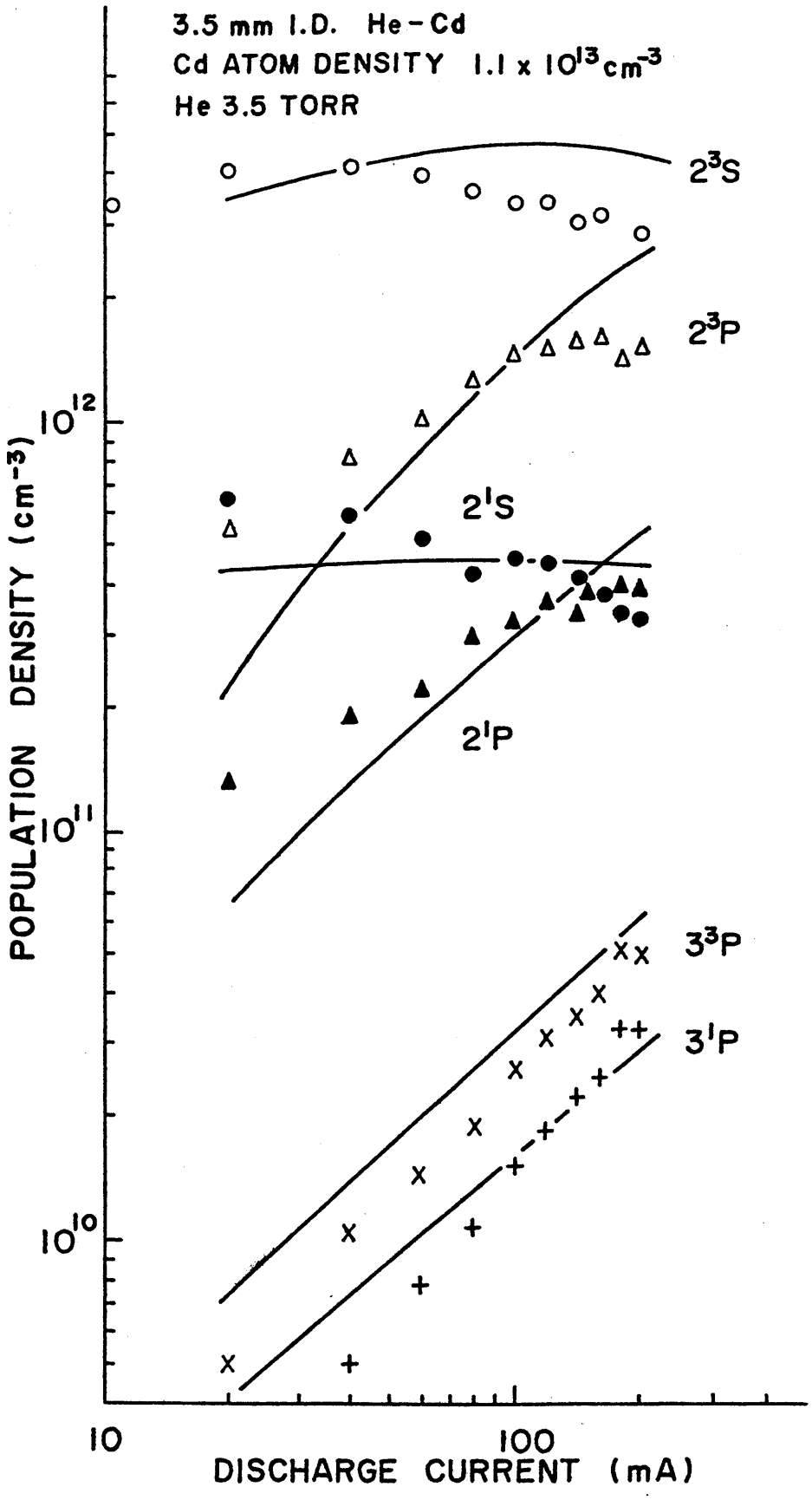

Fig.6-5. Population densities of He(I) excited states in the He-Cd discharge as a function of discharge current. The solid lines represent the results calculated with non-Maxwellian EDF.

The population density of the He(I) 2^3S state is saturated at the discharge current below 20 mA, while the sidelight intensity of the Cd(II) 4416 Å line increases with the discharge current up to 140 mA.[15] On the other hand, population densities of the He(I) excited states of n = 3 and 4 increase almost linearly with the discharge current as expected from the rate equations.

The population densities of the He(I) excited states in the He-Cd discharge were measured as a function of the initial He pressure at the constant Cd atom density of 1.1×10^{13} cm^{-3} and discharge current of 100 mA also. They were similar to those in the pure He discharge shown in Fig.6-2, while their absolute values were smaller by about a factor 2 than those in Fig.6-2.

In the discharge tube of 3 mm in diameter, the results similar to those in Figs.6-2 ~ 6-5 were obtained and the experimental results coincided with the calculated ones well.

§ 6.5. Saturation Mechanisms of He(I) Metastable States

Mewe calculated the population densities of the He(I) first excited states in the pure He discharge with neglecting the effects of the radiative cascadings from the higher lying excited states and could explain the experimental data well.[12] As the diameter of the discharge tube used in ref.12 was large (22 mm) and the discharge current density was very low in comparison with those in the present experiment, the effects of the radiative cascadings could be neglected probably.

However, the calculation shows that the radiative cascadings from those states of n = 3 and 4 to the He(I) first excited states cannot be neglected under the present experimental condition.

Figures 6-3 and 6-5 show that the population densities of the He(I) 2^3S and 2^1S states are saturated at the low discharge currents. According to the rate equations, this can be attributed to the following facts. Among the excitation rates to the He(I) 2^3S state, the radiative cascading rate $T_{4-3}N_4A_{4-3}$ by the transition $He(2^3P) \rightarrow He(2^3S) + h\nu$ and the direct excitation rate $N_0n^eS_{0-3}$ are large. On the other hand, the destruction rate of the He(I) 2^3S state is determined mainly by the diffusion to the wall in the low discharge current region of $I < 10$ mA. The population density N_3 of the He(I) 2^3S state is given by

$$N_3 \sim \frac{T_{4-3}N_4A_{4-3} + N_0n^eS_{0-3}}{D_3/\Lambda^2} . \qquad (6.3)$$

When we take into account that the population density N_4 of the He(I) 2^3P state is roughly proportional to the discharge current, we see from eq.(6.3) that N_3 increases almost linearly with the discharge current in this region. In the region of $I > 10$ mA, however, the electronic de-excitation rates become dominant in the destruction rate of the He(I) 2^3S state. Especially, the de-excitation rate $n^eN_3S_{3-4}$ by the electronic collision $He(2^3S) + e \rightarrow He(2^3P) + e$ is the largest. It is about 20 times larger than the de-excitation rate $n^eN_3S_{3-c}$ by the ionizing

collision $He(2^3S) + e \rightarrow He^+ + 2e$ and about 35 times larger than the de-excitation rate by the Penning collision $He(2^3S) + Cd(5^1S) \rightarrow He(1^1S) + (Cd^+)^* + e$ at the initial He pressure of 3.5 Torr, the discharge current of 100 mA, and the Cd atom density of 1.1×10^{13} cm^{-3}. Therefore, we must not neglect any of those three rates ($N_0 n^e S_{0-3}$, $T_{4-3} N_4 A_{4-3}$, and $n^e N_3 S_{3-4}$) in the discharge current region of $I > 10$ mA. In this case, N_3 is given roughly by

$$N_3 \sim \frac{T_{4-3}(N_4/n^e)A_{4-3} + N_0 S_{0-3}}{S_{3-4}} . \qquad (6.4)$$

As the population density of the He(I) 2^3P state N_4 is roughly proportional to the discharge current, N_3 is not considerably dependent on the discharge current in the pure He and also He-Cd discharges. The relative change of the population density N_1 of the He(I) 2^1S state with the discharge current can be interpreted in the similar way by taking into account the electronic collision process $He(2^1S) + e \rightarrow He(2^1P) + e$.

On the contrary, in refs.6 and 7, only the diffusion, stepwise ionization, and Penning collision processes were took into account as the destruction processes of the He(I) 2^3S state in the calculation. The stepwise ionization rate $n^e N_3 S_{3-c}$ becomes comparable with the diffusion loss rate D_3/Λ^2 at a discharge current higher than 100 mA. Then N_3 is given by eq.(6.3) in the region of $I < 100$ mA in this case. When we take into account the electronic collision $He(2^3S) + e \rightarrow He(2^3P) + e$, N_3 is saturated in the region of $I < 10$ mA, because the de-excitation rate

$n^e N_3 S_{3-4}$ is larger by one order of mgnitude than the stepwise ionization rate $n^e N_3 S_{3-c}$.

The dominant excitation processes to the He(I) 2^1P and 2^3P states are the direct excitations and the stepwise excitations from the He(I) 2^1S and 2^3S states. The destruction rates are mainly determined by the radiative decay rates, which are independent of the discharge current. Therefore, the population densities of the He(I) 2^1P and 2^3P states, N_2 and N_4, respectively, increase almost linearly with the discharge current. The situation is the same also for the He(I) excited states of n = 3 and 4.

In Figs.6-3 and 6-5, the calculated population densities of the He(I) 2^3S and 2^1S states decrease at discharge currents above 120 mA. This is caused by the decrease of the direct excitation rates and radiative cascading rates to those states, because the electric field strength decreases with the discharge current. Slight discrepancies between the calculated and measured results probably come from the following;(i) the assumption that the radial distribution of the population density of each He(I) excited state is the Bessel function of zero order does not hold valid completely, and (ii) the trapping coefficients for the transitions $He(2^3P) \rightarrow He(2^3S) + h\nu$ and $He(2^1P) \rightarrow He(2^1S) + h\nu'$ are affected to some extent by the fact mentioned in (i).

The discharge current dependences of the population densities of the He(I) first excited states in this experiment are qualitatively in good agreement with those in ref.5. The comparison of our results with those in ref.4 is difficult

because the shapes of the tubes used are not the same. However, they coincided at the point that the population density of the He(I) 2^3S state is saturated in the low discharge current region.

As shown in Figs.6-2~6-5, the present calculated results of the population densities agree with the experimental results in their absolute values, and also in the initial He pressure, Cd atom density, and discharge current dependences generally. When we assume the Maxwellian EDF of the electron temperature determined with the conventional double probe method, however, the calculated results deviate from the experimental ones considerably in their absolute values and the initial He pressure dependences as shown in Fig.6-2. The unified theory of the electron temperature in ref.26 gives a lower electron temperature than the Schottky theory does for a given product of the He pressure and the tube radius. However, the population densities calculated on the basis of the unified theory again increased monotonically up to the initial He pressure around 8 Torr. On the contrary, in the case of the non-Maxwellian EDF obtained from the Boltzmann equation, the higher energy part of EDF decreased rapidly with the increase of the initial He pressure, and therefore the direct and stepwise excitation rates decreased very rapidly. Consequently, the calculated population densities decreased at higher initial He pressures.

In order to explain the population densities in the pure He and He-Cd discharges consistently, therefore, it has to be taken into account that EDF is non-Maxwellian.

§6.6. Conclusion

The initial He pressure, Cd atom density, and discharge current dependences of the population densities of the He(I) excited states in the pure He and He-Cd discharges were explained theoretically and consistently by taking into account the non-Maxwellian EDF and the new electronic collision process; $He(2^3S \text{ or } 2^1S) + e \rightarrow He(2^3P \text{ or } 2^1P) + e$.

It has been confirmed experimentally and theoretically that the population densities of the He(I) 2^3S and 2^1S states are saturated at the low discharge currents in the pure He and He-Cd discharges. As the excitation processes to the upper states of the Cd(II) 4416 and 3250 Å lines, therefore, we must take into account other excitation processes in addition to the Penning collision process between He atoms in the He(I) 2^3S or 2^1S state and Cd atoms in the ground state. A further discussion on the excitation mechanisms in the PC $He-Cd^+$ laser discharge will be given in Chapter 8.

References in Chapter 6.

1) M.Mori, T.Goto, and S.Hattori,"Population densities of He excited states in a positive column discharge used for the He-Cd^+ laser,"submitted to J.Phys.Soc.Japan.

2) W.T.Silfvast,"Efficient CW laser oscillation at 4416 Å in Cd(II),"Appl.Phys.Lett.,vol.13,pp.169-171,Sep.1968.

3) G.J.Collins, R.C.Jensen, and W.R.Bennett,Jr.,"Charge-exchange excitation in the He-Cd laser,"Appl.Phys.Lett.,vol.19,pp.125-128,Sep.1971.

4) P.G.Browne and M.H.Dunn,"Metastable densities and excitation processes in the He-Cd laser discharge,"J.Phys.B.Atom.Molec. Phys.,vol.6,pp.1103-1117,June 1973.

5) K.Miyazaki, Y.Ogata, T.Fujimoto, and K.Fukuda,"Excitation mechanism of 3250 and 4416 Å laser lines in the cataphoretic He-Cd laser discharge,"Japan.J.Appl.Phys.,vol.13,pp.1866-1874,Nov.1974.

6) J.K.Mizeraczyk,"On saturation mechanisms in PC He-Cd^+ lasers," IEEE J.Quantum Electron.,vol.QE-11,pp.218-220,May 1975.

7) S.Watanabe, K.Kuroda, and I.Ogura,"Linewidth measurement and population calculation of a He-Cd laser,"J.Appl.Phys., vol.47,pp.4887-4895,Nov.1976.

8) N.A.Vorob'era, Yu.M.Kagan, and V.M.Milenin,"Electron velocity distribution function in the positive column in a mixture of gases,"Sov.Phys.-Tech.Phys.,vol.9,pp.632-634,Nov.1964.

9) D.Barbiere,"Energy distribution, drift velocity, and temperature of slow electrons in helium and argon,"Phys.Rev., vol.84,pp.653-658,Nov.1951.

10) K.Mašek and E.Vokatý,"Solution of the Boltzmann equation for electrons in the discharges in metal vapour-helium mixtures," Czech.J.Phys.,vol.B24,pp.267-283,1974.

(As to EDF in the discharges at medium pressures, the reader should refer to refs.6-12 in Chapter 4 in pp.74-75 also.)

11) M.Mori, T.Goto, and S.Hattori,"On the determination of the electron density in a positive column He-metal laser discharge having a non-Maxwellian electron energy distribution," J.Phys.Soc.Japan,vol.43,pp.662-668,Aug.1977.

12) R.Mewe,"On the positive column of discharges in helium at intermediate pressures, I.Ionization mechanism and atomic level populations,"Physica,vol.47,pp.373-397,1970.

13) R.Mewe,"On the positive column of discharges in helium at intermediate pressures, II. Plasma particle balance and discharge characteristics,"Physica,vol.47,pp.398-411,1970.

14) T.Goto, M.Mori, and S.Hattori,"Modified absorption method to determine level population densities in a cataphoresis type of He-metal laser discharge,"Appl.Phys.Lett.,vol.29, pp.358-360,Sep.1976.

15) M.Mori, K.Takasu, T.Goto, and S.Hattori,"Ion densities in a positive column He-Cd^+ laser discharge,"J.Appl.Phys.,vol.48, pp.2226-2230,June 1977.

16) T.Holstein,"Imprisonment of resonance radiation in gases," Phys.Rev.,vol.15,pp.1212-1233,Dec.1947.

17) J.D.Jobe and R.M.St.John,"Absolute measurements of the 2^1P and 2^3P electron excitation cross sections of helium atoms,"Phys.Rev.,vol.164,pp.117-121,Dec.1967.

18) B.L.Moiseiwitsch and S.J.Smith,"Electron impact excitation of atoms,"Rev.Mod.Phys.,vol.40,pp.238-353,April 1968.

19) D.R.Long and R.Geballe,"Electron-impact ionization of He(2s ^{3}S),"Phys.Rev.,vol.A1,pp.260-265,Feb.1970.

20) S.Trajmar,"Differential and integral cross sections for the excitation of the 2^1S, 2^3S, and 2^3P states of He by electron impact at 29.6 and 40.1 eV,"Phys.Rev.,vol.A8,pp.191-203, July 1973.

21) M.R.Flannery, W.F.Morrison, and B.L.Richmond,"Excitation in electron-metastable helium collisions," J.Appl.Phys.,vol.46, pp.1186-1190,March 1975.

22) J.G.Showalter and R.B.Kay,"Absolute measurement of total electron-impact cross sections to singlet and triplet levels in helium,"Phys.Rev.,vol.A11,pp.1899-1910,June 1975.

23) A.V.Phelps,"Absorption studies of helium metastable atoms and molecules,"Phys.Rev.,vol.99,pp.1307-1313,Aug.1955.

24) R.A.Buckingham and A.Dalgarno,"Diffusion and excitation transfer of metastable helium in normal gaseous helium," Proc.Roy.Soc.,vol.A213,pp.506-519,1952.

25) T.Dote,"A new method for determination of plasma electron temperature from the current-voltage characteristic of a floating double probe,"Reports of the Institute of Physical and Chemical Research,vol.44,pp.119-127,1968.

26) T.Dote and Y.Ichikawa,"Unified theory of the electron temperature in positive columns,"J.Phys.Soc.Japan,vol.40, pp.1217-1218,April 1976.

Chapter 7. Saturation Mechanism of the Cd(II) 4416 Å Laser Output Power

§7.1. Introduction

Generally, the saturation of the laser output power is related to the population density of the laser lower state as well as that of the laser upper state. It has been shown that the population density of the laser lower state plays significant role in the saturation of the laser gain in the He-Ne laser.[1] On the other hand, in the PC He-Cd^+ laser discharge, the effects of the population densities of the laser lower states on the laser output powers have been neglected up to the present,[2-4] because it has been observed that the behavior of the Cd(II) 4416 Å laser output power is analogous to that of the Cd(II) 4416 Å sidelight intensity. However, it seems difficult to interpret the discharge current or initial He pressure dependence of the Cd(II) 4416 Å or 3250 Å laser output power taking only the population density of the laser upper state into account. To interpret it, probably we need to measured the population density of the laser lower state accurately under various experimental conditions. The only data on the population densities of the laser lower states were reported by Hodges.[5] They were determined only at the optimum condition for the laser action with the absolute line-intensity measurement using the standard lamp. Therefore, the errors may be very large and, moreover, the data are insufficient to discuss the saturation mechanisms of the laser output powers.

It is difficult to determine the population densities of the laser lower states from the absolute intensities of the

Cd(II) 2144 and 2265 Å lines in a manner described in Chapter 3, because of the limitations of the tungsten-iodine standard lamp.

In this chapter, the population densities of the upper and lower states of the Cd(II) 4416 Å line were determined by combining the laser gain measurement with the modified absorption method, and it will be shown that the influence of the population density of the laser lower state on the laser output power is considerable, and we cannot interpret the saturation of the laser output power by neglecting it.[6)]

§7.2. Determination of the Population Densities of the Upper and Lower States, and Calculation of the Laser Output Power

In this chapter and next chapter, the population densities of the upper and lower states of the Cd(II) 4416 Å line in the discharge tube of 3.5 mm ID (inner diameter) under the various experimental conditions without lasing are denoted by n_2 and n_1 respectively. Moreover, n_{20} and n_{10} are defined as n_2 and n_1 under the near optimum condition for the laser action; the initial He pressure of 3.5 Torr, the Cd atom density of 1.5×10^{13} cm^{-3}, and the discharge current of 100 mA.

We can obtain n_2 and n_1 from n_{20} and n_{10} by measuring the relative changes of the Cd(II) 4416 and 2144 Å sidelight intensities, respectively. In determining them, the effects of the resonance trapping were taken into account. The trapping coefficient of the Cd(II) 2144 Å line was calculated in a manner similar to that in Chapter 3 assuming that the radial

distributions of the population densities of the upper and lower states of the Cd(II) 2144 Å line were of the Bessel function of the zeroth order. It is shown in Fig.7-1.

n_{20} and n_{10} were determined in the following manner.

With the method described in Chapter 3, n_{20} was determined from the absolute intensities of the spontaneous emissions of the Cd(II) 4416 Å and the Cd(I) 3261 Å lines. The ratio of the sidelight intensities was measured using the quartz laser tube. The population densities of other Cd(II), Cd(I), and He(I) excited states, from which optical transitions of wavelengths longer than 3000 Å were allowed, were also determined in the same manner.

The determination of n_{10} from the Cd(II) 2144 Å sidelight intensity with the above method was difficult because of the large uncertainty involved in the calibration of the relative spectral sensitivity of the optical detection system and the difficulty in estimating exactly the transmissivity of the tube wall at 2144 Å. Therefore, n_{10} was determined from the difference of the measured n_{20} and population inversion density $n_{20}-(g_2/g_1)n_{10}$ ($= \Delta n_0$). The population inversion density was obtained from the gain measurement in the following way.

In the case of the Cd(II) 4416 Å line of the natural isotopic abundance, the line profile is complicated due to the isotope shifts and hyperfine splittings.[7] Assuming that each component in the profile has a Doppler broadened profile and also that the natural width $\Delta\nu_N$ is very small compared with the Doppler width $\Delta\nu_D$, the saturated gain in the single frequency operation is given by the same formula as that derived for a single Doppler broadened profile.[8] When the coupling

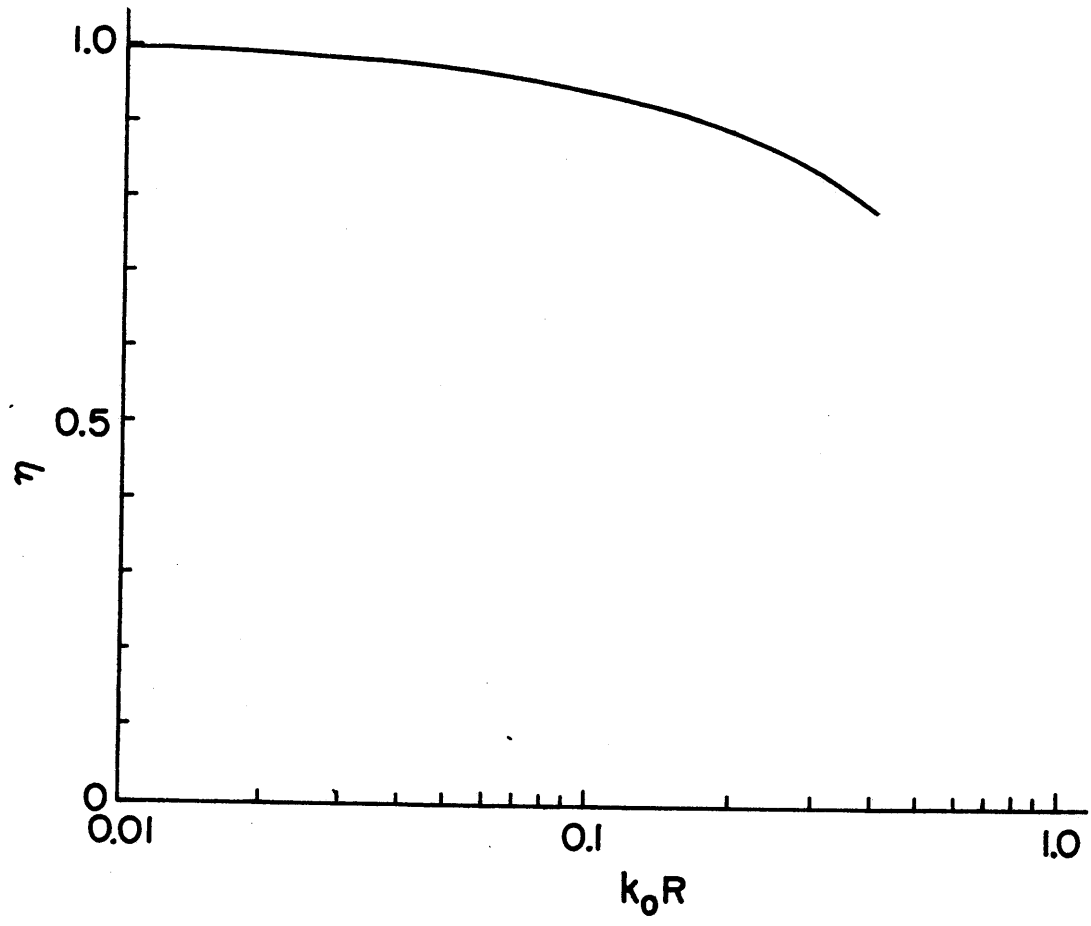

Fig.7-1. Trapping coefficient η of the Cd(II) 2144 Å line as a function of k_0R.

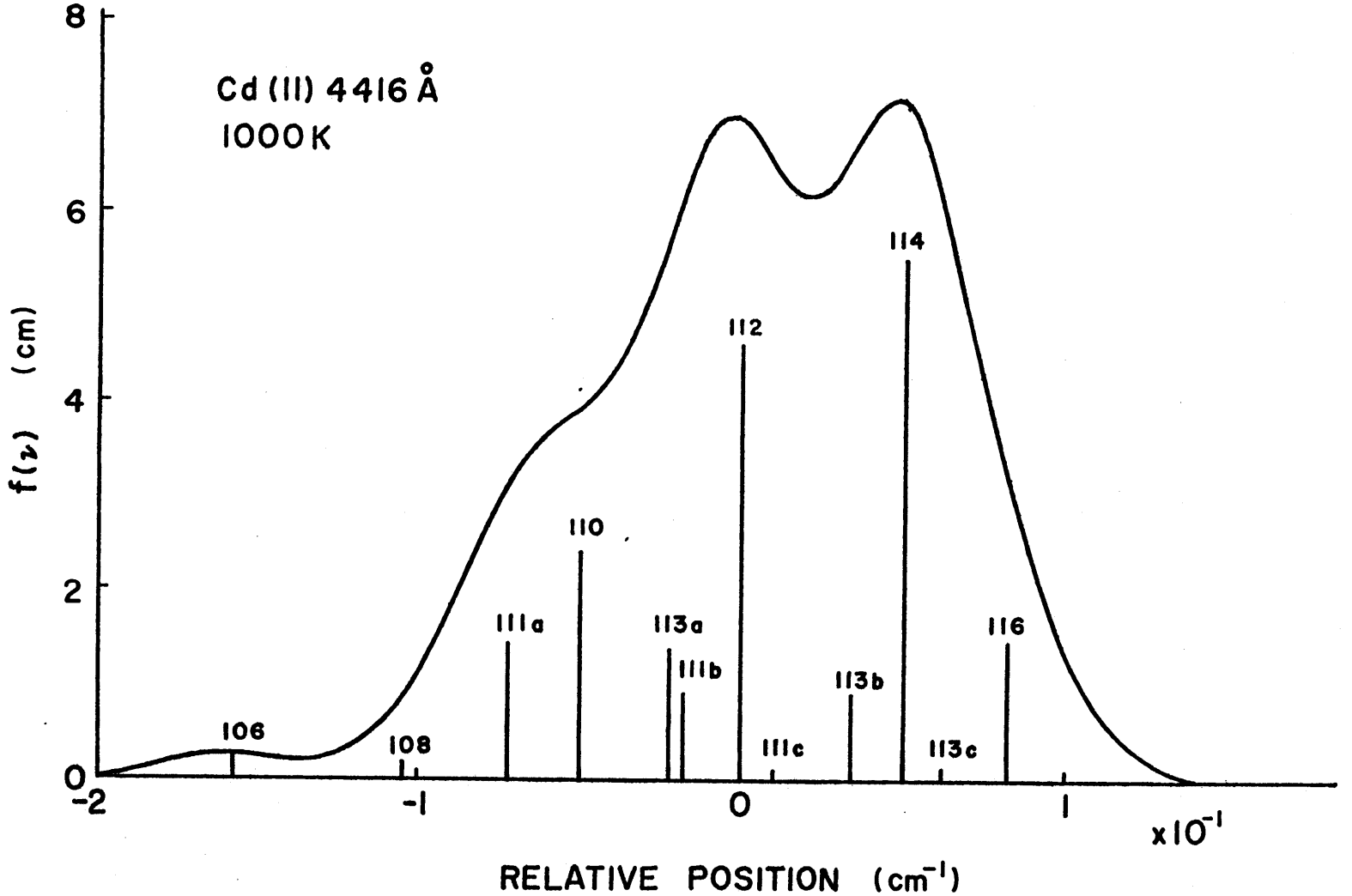

Fig.7-2. Line profile of the Cd(II) 4416 Å line. The number adjacent to each component is the mass number. The components due to the odd isotopes are labelled by a, b, and c.

plate of the total surface reflectivity R is used to take out the laser output power from the cavity, the laser output power density can be calculated by equating the gain to the loss per pass, and it is given by eq.(28) in ref.9.

In the case of the multi-frequency operation, the laser output power W taken from the coupling plate can be calculated by assuming that; 1) the number of the longitudinal modes is very large, and 2) the gain is saturated independently at each frequency. By summing up the laser output powers over all the longitudinal modes, one obtains that

$$W \propto NR\left[\left(\frac{G_0 \ell}{L + R}\right)^2 - 1\right], \tag{7.1}$$

where

$$G_0 = \left(n_{20} - \frac{g_2 n_{10}}{g_1}\right)\left(\frac{\lambda_{21}^2 A_{21}}{8\pi\nu_m}\right)\sqrt{\nu_m \int_{\nu_{min}}^{\nu_{max}} f^2(\nu')\,d\nu'}. \tag{7.2}$$

Here, $f(\nu)$ is the line profile shown in Fig.7-2,[7] and it is normalized as

$$\int_0^\infty f(\nu')\,d\nu' = 1, \tag{7.3}$$

In eqs.(7.1) and (7.2), ℓ is the active length, L is the loss per pass. The subscripts 1 and 2 denote the lower and upper states, respectively, and g is the statistical weight. N and ν_m are the number and frequency bandwidth of the longitudinal modes, respectively, and $\nu_m = \nu_{max} - \nu_{min}$. In case $f(\nu)$ is the

single Doppler broadened profile, eq.(7.2) is reduced to the small signal gain at the center of the profile.

The relation between the incident angle and the reflectivity R of the quartz coupling plate is shown in Fig.7-3[10] for the wave with the polarization in the parallel direction of the incident plane. Turning the coupling plate, the reflectivity R changes, and we can obtain the R dependence of the laser output power W. By fitting eq.(7.1) to the measured W versus R curve, G_0 and L can be determined. The population inversion density Δn_0 can be determined from eq.(7.2) with the measured G_0 when ν_m and $\sqrt{\nu_m \int_{\nu_{min}}^{\nu_{max}} f^2(\nu')\,d\nu'}$ are evaluated.

When the coupling plate is not inserted into the cavity, the laser output power W' taken out from the mirror of the transmissivity T is given by eq.(7.4) assuming that the radial field distribution is a Gaussian of the beam radius w_0.

$$W' = \pi w_0^2 P_s T \sum_{i=1}^{N} \left[\left\{ \frac{\lambda_{21}^2 A_{21} \Delta n \ell}{8\pi L} f(\nu_i) \right\}^2 - 1 \right], \tag{7.4}$$

where, $\Delta n = n_2 - (g_2/g_1) n_1$, and P_s is the saturation parameter, and is given by

$$P_s = \frac{4\pi^2 h c \Delta\nu_N}{\lambda_{21}^3}, \tag{7.5}$$

In eq.(7.4), the summation is taken over all the longitudinal modes. In eq.(7.5), h is the Planck constant and c is the light velocity. Using the measured loss L and population inversion density Δn on the tube axis, W' can be calculated from eq.(7.4) under the various experimental conditions.

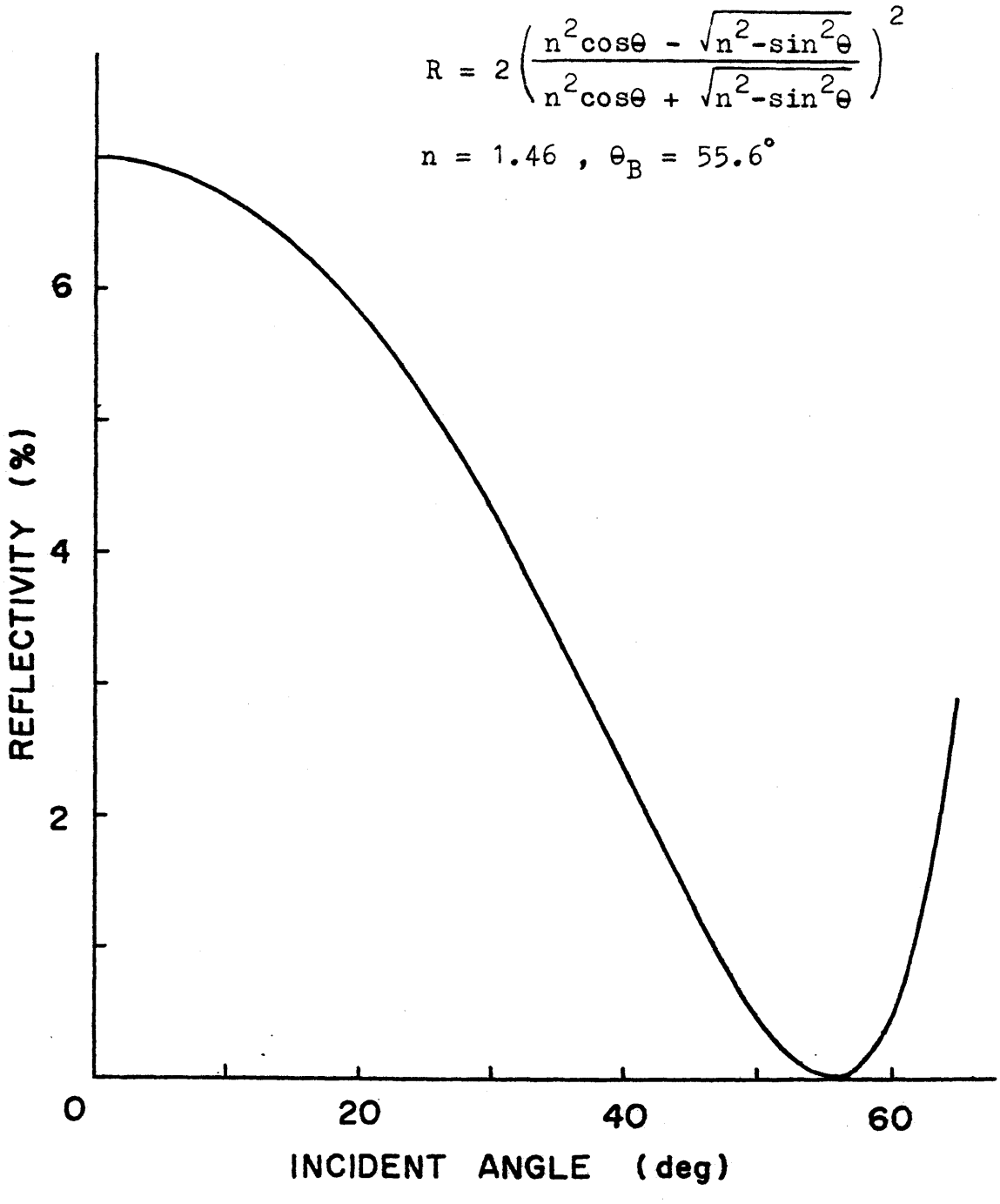

Fig.7-3. Reflectivity R of the quartz coupling plate for the wave with the polarization in the parallel direction of the incident plane as a function of incident angle.

§7.3. Experimental Procedure

The experimental arrangements are shown in Fig.7-4. A cataphoresis type quartz laser tube was used in this experiment. Also a cataphoresis type Pyrex discharge tube was used for the absorption measurement. Both tubes were of 3.5 mm I.D.. The capillary part of each tube was put in an oven of 600 K and the tube was connected to a flask of large volume.

G_0 in eq.(7.1) was measured by varying the angle between the quartz coupling plate and the tube axis in the way similar to that in ref.10. A typical data on the R dependence of W is shown in Fig.7-5. The transverse mode of the laser oscillation was TEM_{00}.

The laser output power was measured with the 40X opto-meter (United Detector Technology, Inc.). The transmissivity of the mirror from which the laser output power was taken out was measured with the laser beam. It was estimated to be $0.95(1\pm0.02)$ %.

Generally, it is difficult to determine accurately the Cd atom density N_{Cd} in the laser tube or the discharge tube only from the Cd oven temperature, because N_{Cd} is influenced by the oven structure and the discharge current. In the discharge tube, N_{Cd} was determined directly with the modified absorption method described in Chapter 2. In the laser tube, N_{Cd} was determined with the method described in ref.11 and, in addition to it, by monitoring the ratio of the sidelight intensities I_{3261}/I_{5016} or I_{4800}/I_{5016}, where the subscripts are the wavelengths in Å of the used He(I) and Cd(I) lines.

A quartz discharge tube of 3 mm I.D. was also used for the

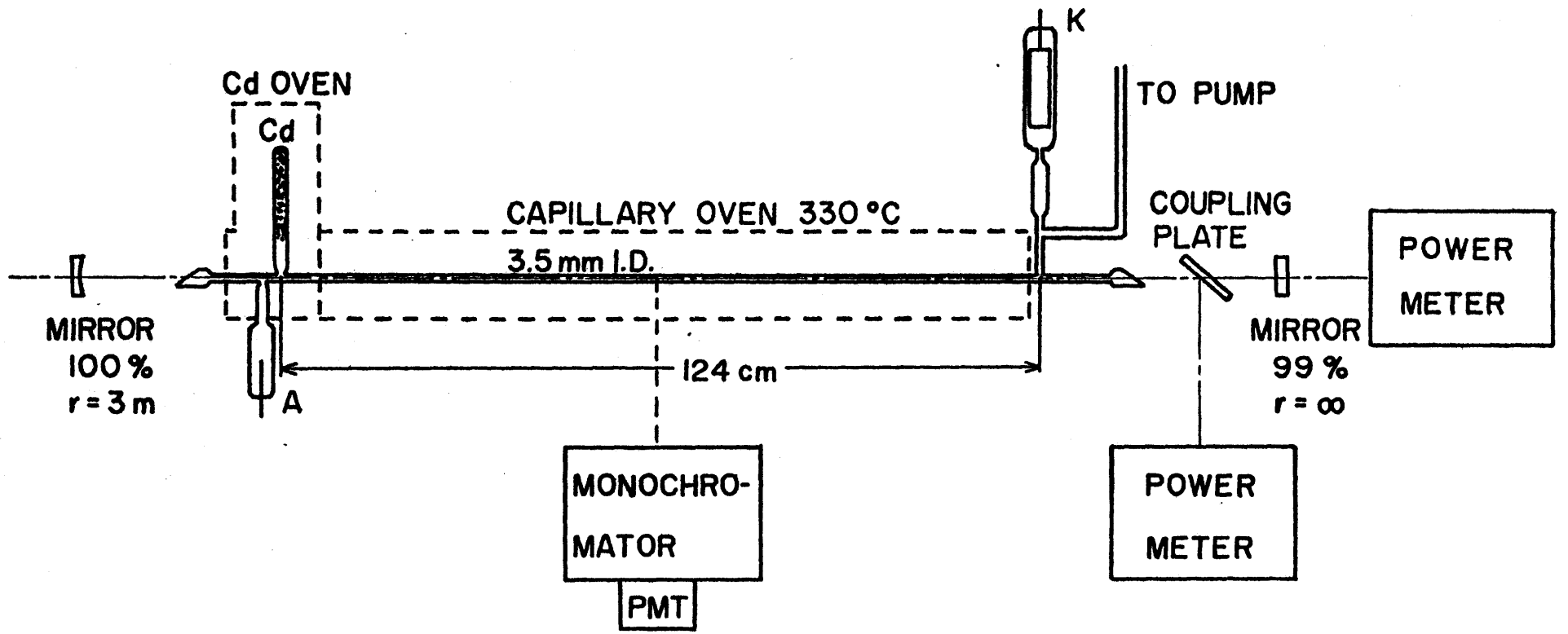

Fig.7-4. Schematic diagram of experimental arrangements for laser gain measurement.

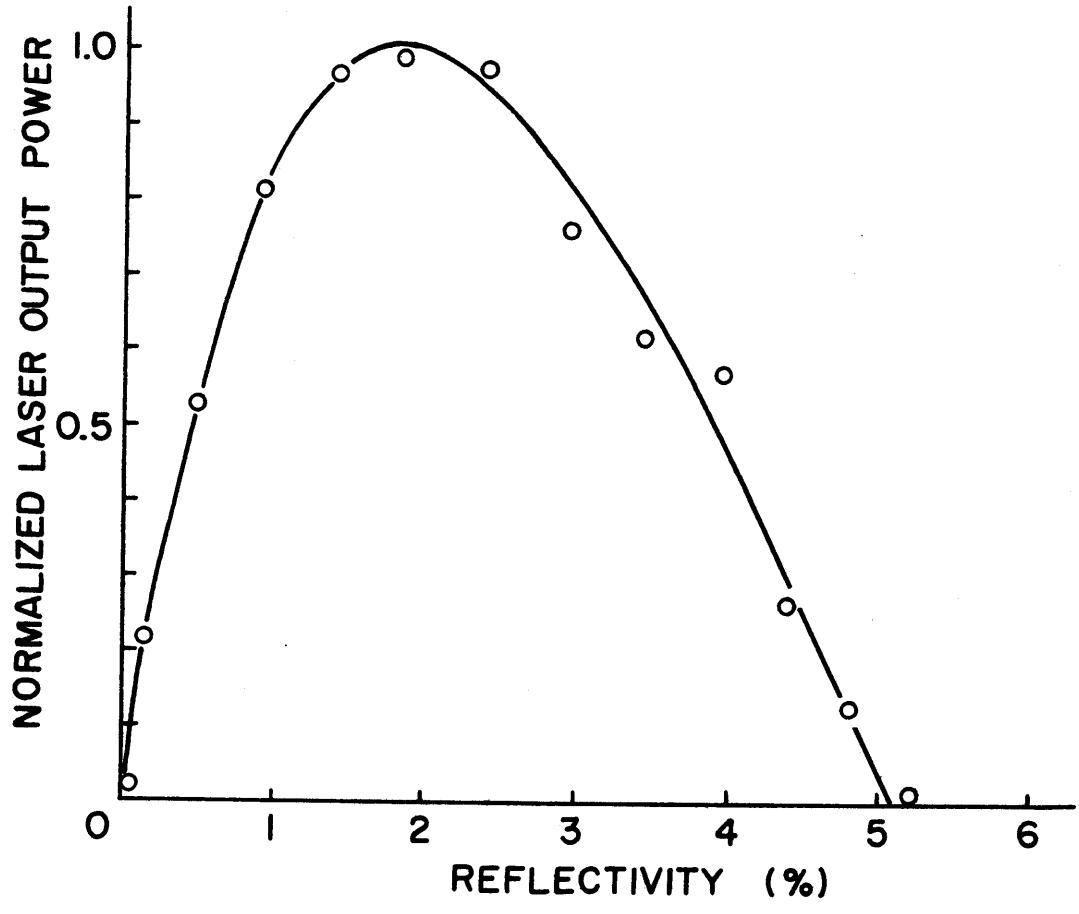

Fig.7-5. Laser output power as a function of reflectivity of quartz coupling plate.

measurements of the population densities of the laser upper states and the He(I) excited states. The discharge tube had the same structure as used for the absorption measurement in Chapter 2.

§7.4. Experimental and Calculated Results

The results in the tube of 3.5 mm I.D. are as follows. n_{20} defined in §7.2 was estimated to be 7.7×10^{10} cm^{-3}. The average value of ten measured values of G_0 was 8.4 %/m. From eq.(7.2), $\Delta n_0 = n_{20}-(g_2/g_1)n_{10} = 4.8 \times 10^{10}$ cm^{-3}. In obtaining Δn_0, we put $\gamma_m = 0.17$ cm^{-1} and $\sqrt{\gamma_m \int_{\gamma_{min}}^{\gamma_{max}} f^2(\gamma)\,d\gamma} = 0.98$, which was estimated roughly from the measured loss L by assuming that the ion temperature was 1000 K.[12,13] Then, $n_{10} = 1.9 \times 10^{10}$ cm^{-3}.

Figure 7-6 shows n_1, n_2, Δn, and the laser output power as a function of the discharge current. Δn was calculated from the measured n_1 and n_2. The initial He pressure was 3.5 Torr and the Cd atom density was 1.5×10^{13} cm^{-3}. At high discharge currents, n_2 is saturated while n_1 increases monotonically with the discharge current. On the other hand, Δn and the laser output power have maxima at a discharge current around 140 mA and then decrease with the discharge current.

Figure 7-7 shows n_1, n_2, Δn, and the laser output power as a function of the Cd atom density. The initial He pressure was 3.5 Torr and the discharge current was 100 mA. As the Cd atom density N_{Cd} increases, n_2 has a maximum at N_{Cd} around 1.5×10^{13} cm^{-3} and then decreases, while n_1 has a maximum

at N_{Cd} around 6 x 10^{13} cm^{-3}. In this case, there is no essential difference between the Cd atom density dependence of n_2 and that of Δn.

Figure 7-8 shows n_1, n_2, Δn, and the laser output power as a function of the initial He pressure. The discharge current was 100 mA and the Cd atom density was 1.5 x 10^{13} cm^{-3}. At high initial He pressures, n_2 is saturated while n_1 increases monotonically with the initial He pressure. On the other hand, Δn and the laser output power have maxima at the initial He pressure of 4 Torr. The influence of n_1 on the laser output power becomes more considerable at high initial He pressures.

The laser output power was calculated from eq.(7.4) using the measured values of Δn, T, L, and the beam radius w_0. The calculated results are shown in Figs.7-6(b), 7-7(b), and 7-8(b). They agree with the measured laser output power over the experimental conditions investigated well.

Also with the discharge tube of 3 mm I.D., the population density of the upper state of the Cd(II) 4416 Å line was measured. At the initial He pressure of 3 Torr and the Cd atom density of 1.4 x 10^{13} cm^{-3}, it was saturated at a discharge current around 150 mA. On the other hand, in the discharge tube of 3.5 mm I.D., it can be seen from Fig.7-6(a) that n_2 is saturated at the discharge current of 200 mA. The discharge current densities corresponding to these discharge currents are nearly equal with each other. In the initial He pressure dependence of the population density of the upper state of the Cd(II) 4416 Å line, it was observed that the similarity rule for the reduced tube radius pR held well between the discharge tubes of 3 and 3.5 mm I.D..

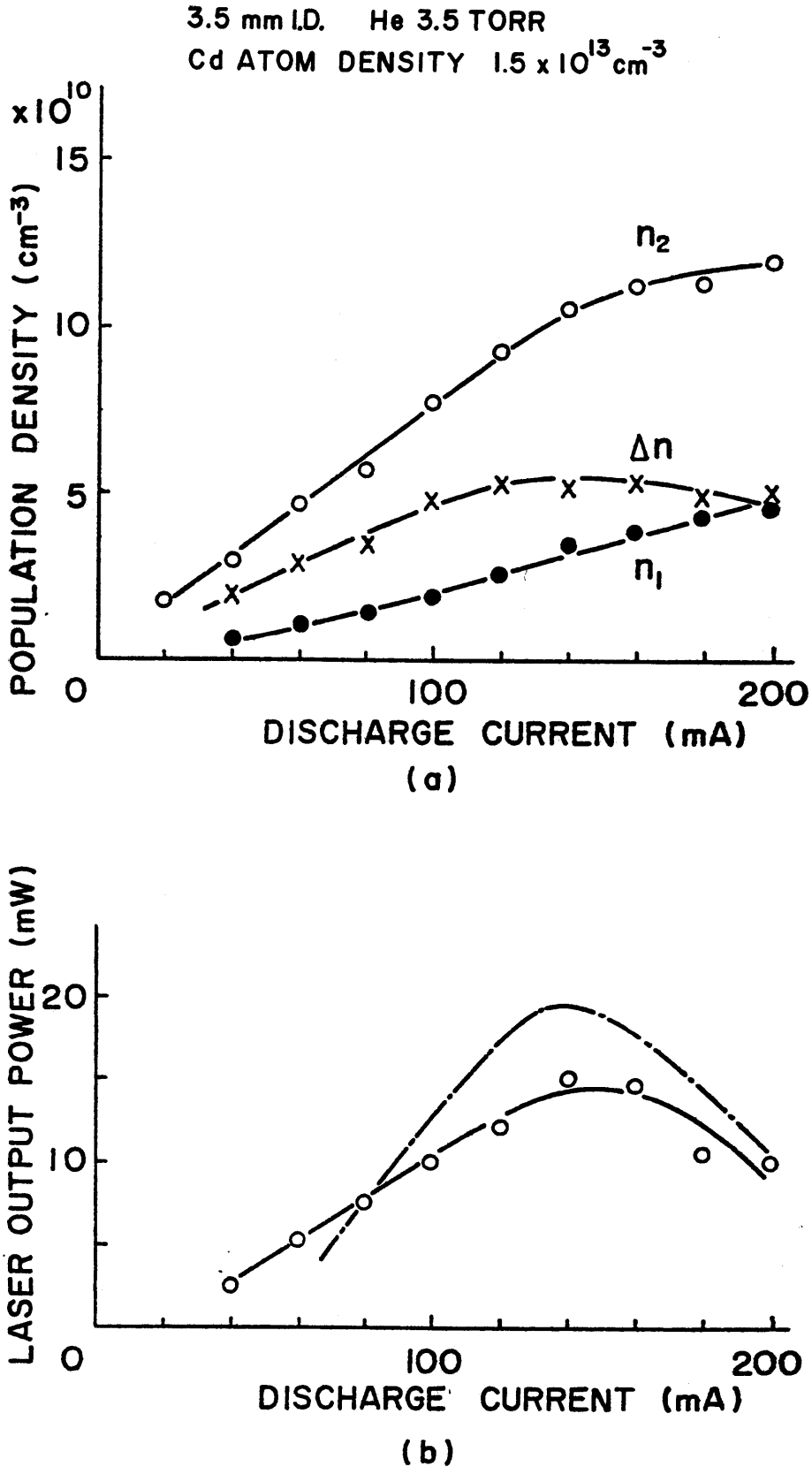

Fig.7-6. Population densities of laser upper and lower states, population inversion density, and laser output power as a function of discharge current. The dash-dot line represents the calculated laser output power.

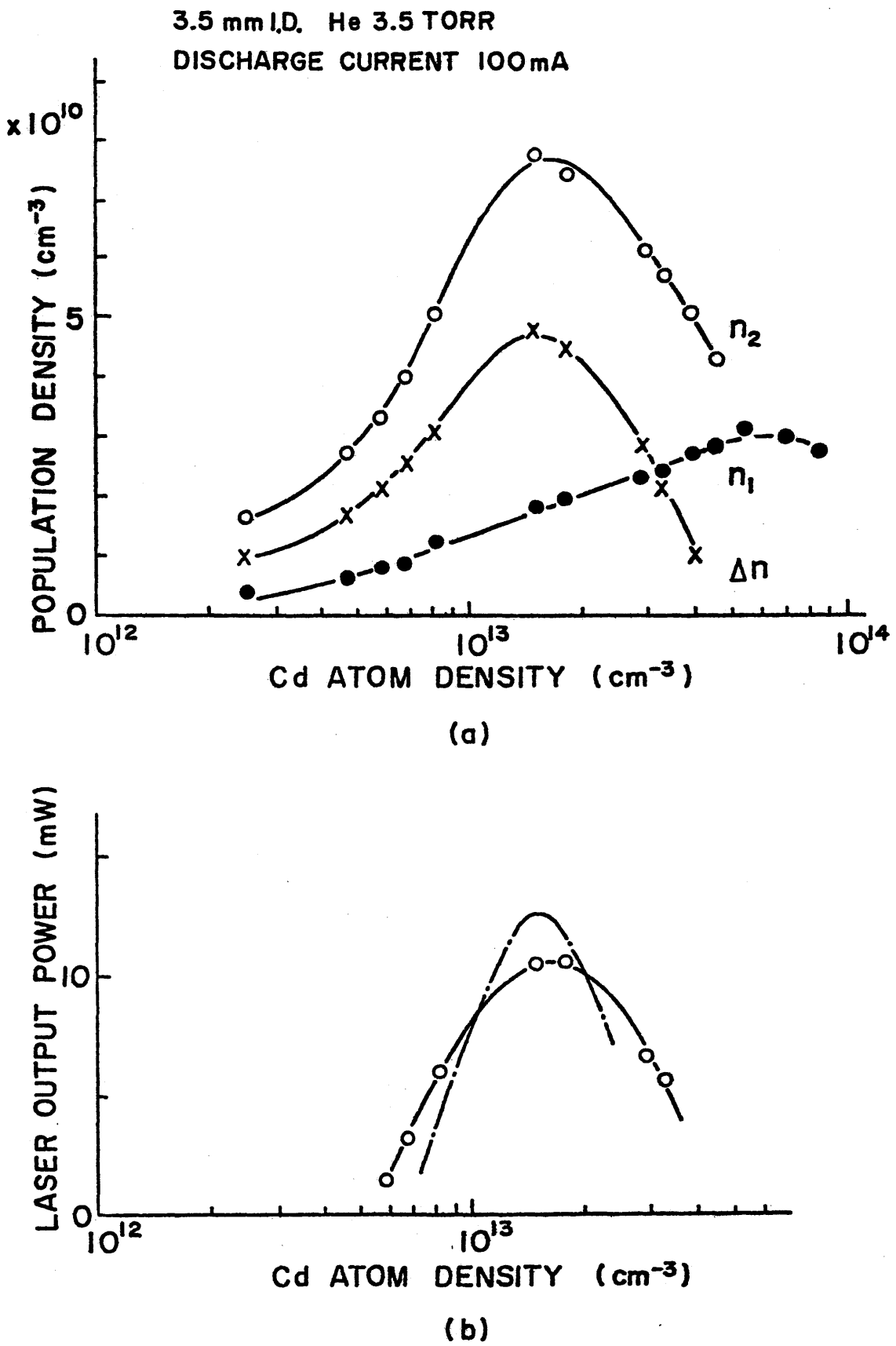

Fig.7-7. Population densities of laser upper and lower states, population inversion density, and laser output power as a function of Cd atom density. The dash-dot line represents the calculated laser output power.

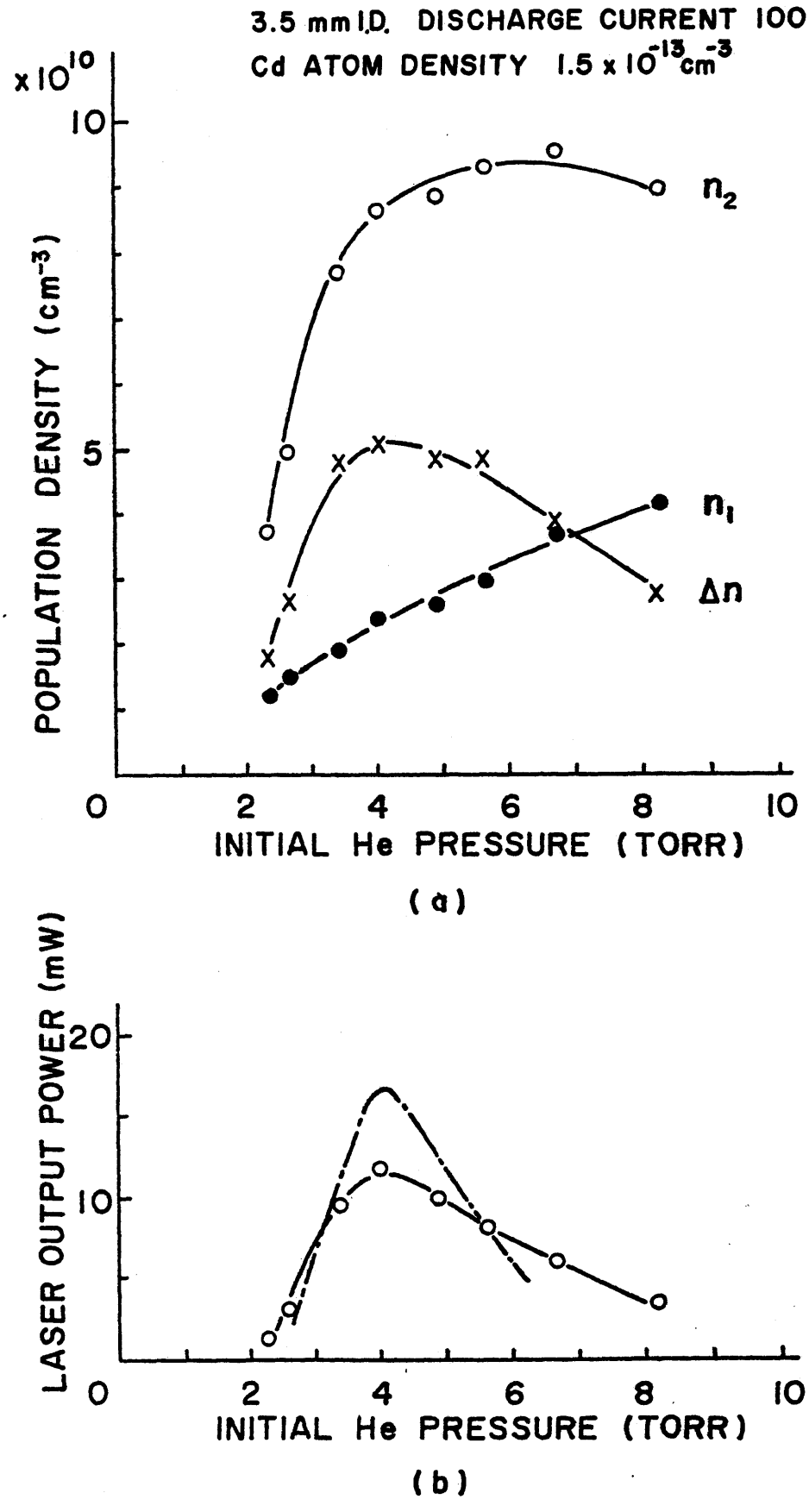

Fig.7-8. Population densities of laser upper and lower states, population inversion density, and laser output power as a function of initial He pressure. The dash-dot line represents the calculated laser output power.

§7.5. Reliability of Experimental Results

The relative changes of the Cd(II) 4416 and 2144 Å sidelight intensities can be measured directly with the optical detection system. Moreover, the effects of the imprisonment of radiation on the sidelight intensities can be estimated exactly over the experimental conditions in Figs.7-6 ~ 7-8, because the population density of the Cd(II) ground state can be measured with the modified absorption method. Therefore, the uncertainties of n_1 and n_2 are determined mainly by those of n_{10} and n_{20}.

As the relative spectral sensitivity of the optical detection system can be calibrated accurately in the wavelength region from 3000 to 7000 Å using the ordinary standard lamp, the uncertainty of n_{20} is determined mainly by the uncertainty involved in the population density n_s of the upper state of the Cd(I) 3261 Å line measured with the modified absorption method. The measurement of n_s was repeated using the Cd(I) 3261 and 4800 Å lines under the various Cd atom densities at the initial He pressure of 3.5 Torr and the discharge current of 100 mA.[11] The resultant uncertainty of n_{20} is estimated to be less than ±20 %.

The maximum value of the population density of the upper state of the Cd(II) 4416 Å line was 1.2×10^{11} cm^{-3} in the discharge tube of 3.5 mm I.D., and it was 1.1×10^{11} cm^{-3} in the discharge tube of 3 mm I.D.. They are nearly equal with each other. On the other hand, the population densities of the He(I) excited states in the two tubes were in good agreement with

those calculated on the basis of a simple collisional-radiative model in the pure Ne and Ne-Cd discharges as discussed in Chapter 6.[14] Moreover, the maximum value of the population density of the upper state of the Cd(II) 4416 Å line in the discharge tube of 3 mm I.D. agreed with the value obtained with the absolute line-intensity measurement by Hodges[5] within a factor 1.6. These facts show that n_2 obtained here is reliable.

The uncertainty of the value of G_0 measured repeatedly was ±14 %. This is equal to the uncertainty of the population inversion density $n_{20}-(g_2/g_1)n_{10}$ because the factor $\sqrt{\nu_m \int f^2(\nu)d\nu}/\nu_m$ only slightly depends on ν_m. Silfvast et al. obtained the unsaturated gain of 4.0 % in the single-Cd-segmented laser tube of 2 mm I.D. and 26 cm long under the optimum condition for the laser action.[15] When the inverse radial dependence of the gain is taken into account and the similarity rule for the reduced tube radius pR is applied, this corresponds to 8.6 %/m under our experimental condition. This value is close to G_0 obtained here.

n_{10} was also cross-checked with the following two methods. One method is to determine n_{10} from the ratio of the Cd(II) 2144 Å to the Cd(II) 2288 Å sidelight intensities in a manner similar to that stated in Chapter 3. The population density of the upper state of the Cd(I) 2288 Å line can be obtained from the absorption coefficient of the Cd(I) 5155 Å line measured with the modified absorption method. The other method is to employ the technique of the perturbation spectroscopy.[16] The values of n_{10} obtained with those two methods agreed with that obtained here within a factor 2. Moreover, the present

value of n_{10} is relatively close to the population density of the lower state of the Cd(II) 4416 Å line in the discharge tube of 3 mm I.D. obtained by Hodges,[5] when the discharge current dependence of n_1 is taken into account. These show that n_{10} obtained here is reliable.

Figure 7-6(b), 7-7(b), and 7-8(b) show that the laser output power calculated from eq.(7.4) is very close to the measured one. This means that the population inversion density Δn (and therefore n_{10}) is reliable. The slight differences between the calculated and measured laser output powers are caused by the change in the loss L or the beam radius w_0 in the course of the experiments probably.

As n_{10} is determined from the difference between n_{20} and $n_{20}-(g_2/g_1)n_{10}$ here, n_{10} may include a larger uncertainty than that of n_{20}. Even if n_1 is the half of the value obtained here, however, the term $(g_2/g_1)n_1$ can never be neglected in the population inversion density, especially in the high discharge current region, in the high Cd atom density region, or in the high initial He pressure region. The influence of n_1 on the laser output power can be easily seen from Figs.7-6 and 7-8. At the high discharge currents in Fig.7-6, n_2 is saturated but does not decrease, while the laser output power decreases. At the higher initial He pressures in Fig.7-8, n_2 decreases slightly while the laser output power decreases very rapidly. Also the laser output power calculated from eq.(7.4) accounts for the measured results well. Therefore, it can be concluded that the contribution of the population density of the laser

lower state to the saturation of the Cd(II) 4416 Å laser output power is very large.

In the course of the experiments, it was observed that the Cd atom density in the capillary part of the laser tube, N_{Cd}, decreased gradually with the discharge current or the initial He pressure when the Cd oven temperature was kept constant. The decrease in N_{Cd} with the discharge current, for instance, could be observed easily from the reduction of the rate of the increase in the Cd(I) 3261 Å sidelitht intensity. When the Cd oven temperature was kept constant, n_2 was saturated at a discharge current around 120 mA, and then it decreased at higher discharge currents. The laser output power appeared to follow a bahavior similar to that of n_2, and the saturation of the laser output power appeared to be caused only by the saturation of n_2. On the contrary, when N_{Cd} was kept constant, n_2 was saturated at the discharge current around 200 mA, but the laser output power had a maximum at the discharge current around 140 mA. Therefore, the experimental results that the laser output power shows the bahavior similar to that of the Cd(II) 4416 Å sidelight intensity (or n_2) in the discharge current characteristic[3] is caused by the decrease in N_{Cd} at high discharge currents probably.

7.6. Conclusion

A formula to determine the population inversion density from the unsaturated gain has been derived for a laser line

whose line profile consists of the superposition of several inhomogeneously broadened components. On the basis of this formula, the population densities of the upper and lower states of the Cd(II) 4416 Å line in the PC He-Cd^+ laser discharge were determined experimentally by combining the laser gain measurement and the modified absorption method. The reliabilities of the measured results were checked in several ways. It turns out that the influence of the population density of the laser lower state on the laser output power is considerable and must not be neglected, especially in the high discharge current region, in the high Cd atom density region, or in the high initial He pressure region.

The excitation mechanisms to the laser upper and lower states will be discussed in the following chapter.

References in Chapter 7.

1) A.D.White and E.I.Gordon,"Excitation mechanisms and current dependence of population inversion in He-Ne lasers,"Appl. Phys.Lett.,vol.3,pp.197-199,Dec.1963.

2) W.T.Silfvast,"Penning ionization in a He-Cd dc discharge," Phys.Rev.Lett.,vol.27,pp.1489-1492,Nov.1971.

3) T.G.Giallorenzi and S.A.Ahmed,"Saturation and discharge studies in the He-Cd laser,"IEEE J.Quantum Electron., vol.QE-7,pp.11-17,Jan.1971.

4) L.Csillag, M.Jánossy, K.Kántor, K.Rózsa, and T.Salamon, "Investigation on a continuous wave 4416 Å cadmium ion laser," J.Phys.D:Appl.Phys.,vol.3,pp.64-68,1970.

5) D.T.Hodges,"Helium-cadmium laser parameters,"Appl.Phys. Lett.,vol.17,pp.11-13,July 1970.

6) M.Mori, M.Murayama, T.Goto, and S.Hattori,"Excitation mechanism of the Cd(II) 441.6 nm laser in the positive column He-Cd discharge,"submitted to IEEE J.Quantum Electron.

7) H.G.Kuhn and S.A.Ramsden,"Isotope shifts and hyperfine structure in the atomic spectrum of cadmium,"Proc.Roy.Soc. (London),vol.A237,pp.485-495,1956.

8) A.Maitland and M.H.Dunn, Laser Physics (North-Holland, Amsterdam,1969),pp.176-181.

9) W.W.Rigrod,"Gain saturation and output power of optical masers,"J.Appl.Phys.,vol.34,pp.2602-2609,Sep.1963.

10) E.Spiller,"Ausgangsleistung und Anpassung des He-Ne-Lasers," Phys.Lett.,vol.9,pp.125-127,April 1964.

11) M.Mori, K.Takasu, T.Goto, and S.Hattori,"Ion densities in a positive column He-Cd^+ laser discharge,"J.Appl.Phys.,vol.48,

pp.2226-2230,June 1977.

12) W.T.Silfvast and P.W.Smith,"Mode locking of the He-Cd laser at 4416 and 3250 Å,"Appl.Phys.Lett.,vol.17,pp.70-73,July 1970.

13) J.P.Goldsborough, Laser Handbook, edited by F.T.Arecchi and E.O.Schulz-DuBois (North-Holland, Amsterdam,1972),vol.1,p.620.

14) M.Mori, T.Goto, and S.Hattori,"Population densities of He excited states in a positive column discharge used for the $He-Cd^+$ laser,"submitted to J.Phys.Soc.Japan.

15) W.T.Silfvast and L.H.Szeto,"Simplified low-noise He-Cd laser with segmented bore,"Appl.Phys.Lett.,vol.19,pp.445-447,Nov.1971.

16) M.Murayama, T.Goto, and S.Hattori,"Determination method of population densities of laser upper and lower states from perturbation and gain measurements,"Paper of Technical Meeting on Plasma,I.E.E.J.,EP-77-19(1977).

Chapter 8. Excitation Mechanisms to the Upper and Lower States of the Cd(II) 4416 Å Line

§8.1. Introduction

Many papers about the excitation mechanisms in the PC He-Cd^+ laser have been published.[1-4] Since it has been thought that the population densities of the laser lower states are negligibly small compared with those of the laser upper states, only the excitation mechanisms to the laser upper states have been discussed so far. Silfvast has suggested that the Penning excitation process between He atoms in the metastable states and Cd atoms in the ground state is the dominant excitation process to the upper states of the Cd(II) 4416 and 3250 Å laser lines.[1] When it is assumed that only the Penning excitation process is dominant, however, it is difficult to explain the experimental results that the population densities of the He metastable states are saturated in the low discharge current region while those of the upper states and the laser output powers of the Cd(II) 4416 and 3250 Å laser lines are saturated in the much higher discharge current region.[4] To explain it, Miyazaki et al. have supposed that He atoms in the He(I) 2^3P and 2^1P states also come into the Penning collisions with Cd atoms in the ground state, and proposed to take the sum N_m of the population densities of the He(I) first excited states. But there was still rather large discrepancies between the discharge current dependence of N_m and those of the population densities of the laser upper states. The discrepancy with respect to the Cd(II) 4416 Å line became larger when the non-radiative decay rate of the upper state of

the Cd(II) 4416 Å line was taken into account.[5-7]

Jánossy et al. proposed that the stepwise excitation process from the Cd(II) ground state was the dominant excitation process at high discharge currents.[3] They assumed that the Cd(II) ground state was excited most dominantly by the Penning excitation process and, therefore, the population density n_{Cd^+} of the Cd(II) ground state was saturated in the low discharge current region. However, experimentally determined n_{Cd^+} increased linearly with the discharge current and was not saturated.[8] n_{Cd^+} also increased monotonically with the Cd atom density. Our calculations have shown that the direct ionization of Cd atoms by electron impacts is much more dominant than that by the Penning collisions as described in Chapter 5.

There is still the large ambiguity on the excitation mechanism to the upper state of the Cd(II) 4416 Å line as mentioned above. On the laser lower state, which plays an important role in the saturation of the laser output power, the excitation mechanism has never been discussed yet. In this chapter, the excitation mechanisms not only to the upper state of the Cd(II) 4416 Å line but also to the lower state are discussed on the basis of the measured parameters.[9]

§8.2. Rate Equations

Although the dominant excitation process to the upper state of the Cd(II) 4416 Å line, the Cd(II) $5s^2{}^2D_{5/2}$ state, has been assumed to be the Penning collision process between He atoms in the metastable states and Cd atoms in the ground

state,[1,2] the discharge current dependence of the population density of the upper state of the Cd(II) 4416 Å line, n_2, shown in Fig.7-6 is quite different from those of the population densities of the He(I) metastable states shown in Fig.6-5. Here, we examine whether the discharge current dependence of n_2 can be interpreted with the total Penning excitation rate including all the He(I) excited states or not. Although there is no data on the collision cross sections for the Penning ionizations between Cd atoms and He atoms in the non-metastable states, it has been reported that those between Ar atoms and He atoms in the He(I) 3^3S and 3^3P (or 2^1P, 3^1S, and 3^1P) states are not different by a factor of more than 2 from that between Ar atoms and He atoms in the He(I) 2^3S (or 2^1S) state.[10-13] Therefore, it is not unreasonable to assume that collision cross sections for the Penning ionizations between Cd atoms and He atoms in various He(I) triplet (or singlet) excited states are identical in magnitude. In this case, the total Penning excitation rate to the laser upper state is given by $(n_T\overline{\sigma v}_T + n_S\overline{\sigma v}_S)N_{Cd}$. Here, n_T (or n_S) is the sum of the population densities of the He(I) triplet (or singlet) excited states of the principal quantum number n = 2 to 6 determined experimentally. The sum of the population densities of the He(I) excited states of $n \geq 7$ was negligibly small compared with n_T or n_S. $\overline{\sigma v}_T$ (or $\overline{\sigma v}_S$) is the rate coefficient of the Penning collision of He atoms in the triplet (or singlet) excited states. We used 2.5×10^{-10} cm^3/sec for $\overline{\sigma v}_T$ and 6.3×10^{-10} cm^3/sec for $\overline{\sigma v}_S$.[14-16] In Fig.8-1, the total Penning excitation rate $(n_T\overline{\sigma v}_T + n_S\overline{\sigma v}_S)N_{Cd}$ is shown as a function of the discharge current. The discharge current

dependence of the total Penning excitation rate is still quite different from that of n_2. Therefore, it is difficult to explain the discharge current dependence of n_2 by taking only the Penning excitation process into account.

It was confirmed that the direct excitation rate calculated with the collision cross section in ref.17 was smaller by one order of magnitude than the Penning excitation rate under the experimental conditions investigated here. If it is assumed that the direct excitation process is dominant, the collision cross section of it must be of the order of 10^{-15} cm^2. This is not probable, because the total ionization cross section is of the same order. Also it was estimated from the measured He^+ ion densities that the radiative cascading rates from the high lying Cd(II) states,which were excited by the thermal energy charge transfer excitation process,could be negligible compared with the Penning excitation rate. On the other hand, the rate of the stepwise excitation from the Cd(II) ground state is large probably, because the population density of the Cd(II) ground state is rather large at the optimum condition for the laser action,[8] the threshold energy is low, and the collision cross section between electrons and ions may be large due to the Coulomb interaction.[18] Therefore, as the excitation processes in the rate equation, the stepwise and Penning excitation processes are taken into account.

As the destruction process of the upper state, only the radiative transition ($5s^2{}^2D_{5/2} \rightarrow 5p^2P_{3/2}$) has been assumed before. However, it has been shown experimentally that the non-radiative decay rate of the state due to the electron

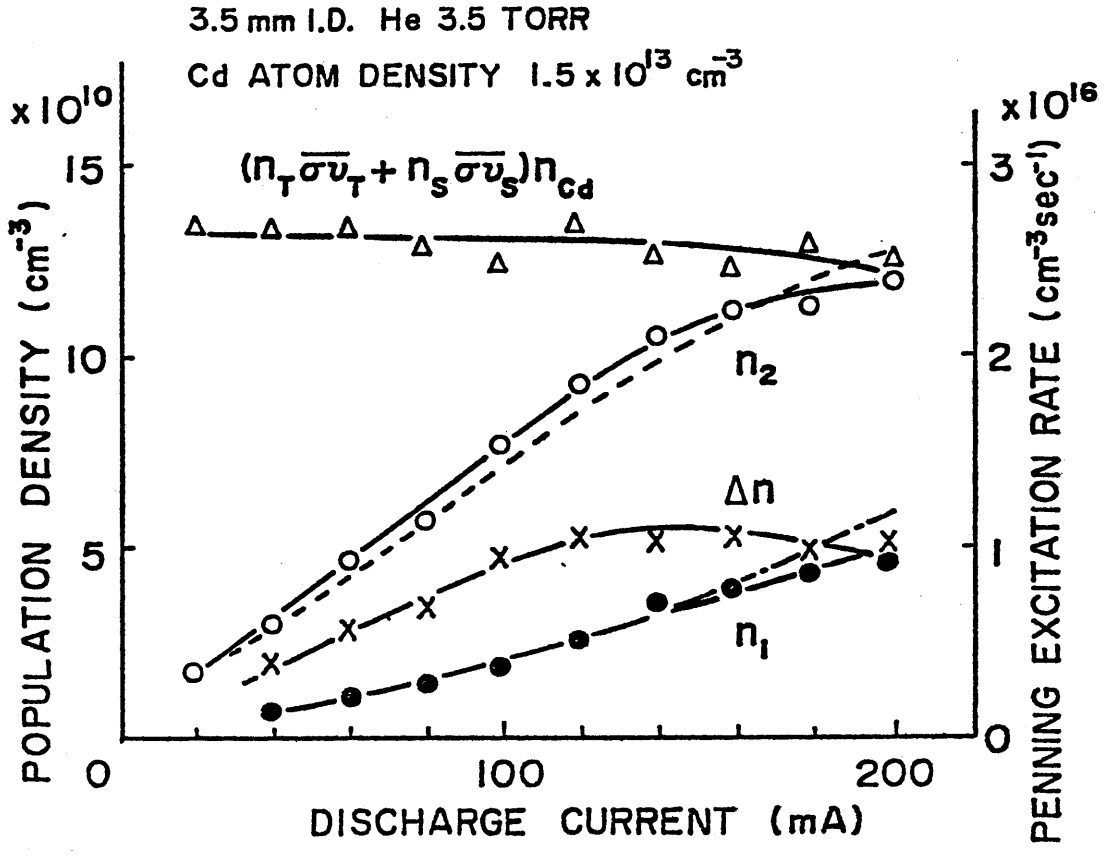

Fig.8-1. Penning excitation rate and calculated population densities of the laser upper and lower states as a function of discharge current. The calculated results are shown by the dotted and dash-dot lines.

Table 8-1. Excitation rates in the He-Cd discharge as a function of discharge current; 3.5 mm I.D., initial He pressure of 3.5 Torr, Cd atom density of 1.5×10^{13} cm^{-3}.

	I (mA)	20	40	60	80	100	140	180	200
	$N_2{}^3S+2{}^3P$ (cm^{-3})	5.0^{12}	4.9^{12}	5.1^{12}	4.8^{12}	4.6^{12}	4.6^{12}	4.6^{12}	4.4^{12}
	$N_2{}^1S+2{}^1P$ (cm^{-3})	8.7^{11}	8.5^{11}	7.4^{11}	7.2^{11}	6.8^{11}	7.0^{11}	7.3^{11}	6.4^{11}
	n^e (cm^{-3})	2.0^{11}	3.9^{11}	5.9^{11}	7.8^{11}	9.8^{11}	1.4^{12}	1.8^{12}	2.0^{12}
	N_{Cd^+} (cm^{-3})	1.0^{11}	1.9^{11}	2.8^{11}	3.6^{11}	4.3^{11}	5.5^{11}	6.4^{11}	6.7^{11}
Upper State	Penning ex. rate ($cm^{-3}sec^{-1}$)	2.7^{16}	2.6^{16}	2.6^{16}	2.5^{16}	2.5^{16}	2.4^{16}	2.4^{16}	2.3^{16}
Upper State	Stepwise ex. rate ($cm^{-3}sec^{-1}$)	7.3^{15}	2.8^{16}	6.1^{16}	1.1^{17}	1.7^{17}	2.8^{17}	4.2^{17}	4.9^{17}
Upper State	A_{21} (sec^{-1})	1.2^6	-	-	-	-	-	-	-
Upper State	γ_{dif} (sec^{-1})	3.0^5	-	-	-	-	-	-	-
Upper State	γ_{de} (sec^{-1})	2.4^5	4.8^5	7.2^5	9.6^5	1.2^6	1.7^6	2.2^6	2.4^6
Upper State	N_u (cm^{-3})	2.0^{10}	2.7^{10}	3.7^{10}	5.2^{10}	7.2^{10}	9.5^{10}	1.2^{11}	1.3^{11}
Lower State	Stepwise ex. rate ($cm^{-3}sec^{-1}$)	2.3^{17}	8.7^{17}	1.9^{18}	3.3^{18}	5.0^{18}	8.8^{18}	1.3^{19}	1.5^{19}
Lower State	A_{10} (sec^{-1})	3.0^8	-	-	-	-	-	-	-
Lower State	Trapping Coefficient	0.97	0.95	0.93	0.90	0.87	0.85	0.83	0.82
Lower State	N_1 (cm^{-3})	8.0^8	3.0^9	6.8^9	1.2^{10}	1.9^{10}	3.4^{10}	5.3^{10}	6.2^{10}

de-excitation process and the diffusion process is of the same order of magnitude as the radiative one.[5,6,19,20] This is also expected from the results obtained with the flowing afterglow technique in ref.7. The transition probability of the Cd(II) 4416 Å line is rather small because the transition $5s^2{}^2D_{5/2} \rightarrow 5p^2{}^2P_{3/2}$ involves a change of two electrons in the orbital quantum number, which is forbidden according to the selection rule. The non-radiative decay rate can be of the same order as the radiative decay rate in this case.[7]

Then in the steady state, n_2 is given by

$$n_2 = \frac{(n_T\overline{\sigma v}_T + n_S\overline{\sigma v}_S)N_{Cd} + n^e n_{Cd^+}M_2}{A_{21} + D_{Cd^+}/(\Lambda^2 p_0/2) + n^e\overline{\sigma v}_{de}} . \qquad (8.1)$$

Here, n_{Cd^+} is the population density of the Cd(II) ground state, M_2 is the rate coefficient of the stepwise excitation from the Cd(II) ground state, which was obtained with the collision cross section and the electron energy distribution function (EDF) calculated in Chapters 5 and 6.[21] n^e is the electron density, D_{Cd^+} is the ambipolar diffusion coefficient of the Cd^+ ions, Λ is the diffusion length, p_0 is the initial He pressures, and $\overline{\sigma v}_{de}$ is the rate coefficient of the electronic de-excitation.

In eq.(8.1), as n_T, n_S, N_{Cd}, and n_{Cd^+}, the values obtained in Chapters 4 - 6 were used. D_{Cd^+} and $\overline{\sigma v}_{de}$ were calculated from the data in refs.5, 6, 19, and 20. As the measured or calculated collision cross section for the stepwise excitation as a function of the electron energy, $\sigma_{M2}(u)$, was not available, its value was assumed in the following way. The measured collision cross

sections for the stepwise excitations from the Hg(II) ground state in ref.22 can be well approximated by Drawin's formula.[23] As the electron configuration of the Cd^+ ion is similar to that of Hg^+ ion, it can be assumed that the functional form of $\sigma_{M2}(u)$ is given by Drawin's formula. The peak value of $\sigma_{M2}(u)$ was assumed so that n_2 calculated from eq.(8.1) agreed with the measured one at the optimum condition for the laser action. Figure 8-2(a) shows $\sigma_{M2}(u)$ obtained in this manner.

The excitation mechanism to the lower state of the Cd(II) 4416 Å line, the Cd(II) $5p^2P_{3/2}$ state, is somewhat different from that to the upper state. The sums of the population densities of the He(I) excited states, n_T and n_S, decrease slightly with the discharge current, decrease with the Cd atom density, and decrease slwoly at initial He pressures higher than 4 Torr.[21] On the contrary, the population density of the lower state, n_1, increases monotonically in any case as shown in Figs.7-6(a), 7-7(a), and 7-8(a). Therefore, the Penning excitation process is never dominant. The direct excitation rate from the Cd(I) ground state is much smaller than the Penning excitation rate according to the calculation with the collision cross section in ref.17. When it is assumed that Cd^+ ions in the laser upper state are de-excited only to the laser lower state by the electronic collisions, the cascading rate from the laser upper state to the laser lower state is given by $n_2(A_{21} + n^e\overline{\sigma v}_{de})$. In the Cd atom density dependence of the cascading rate, it has a maximum at the Cd atom density N_{Cd} of 2×10^{13} cm^{-3}. But n_1 has a maximum at N_{Cd} of 6×10^{13} cm^{-3} as shown in Fig.7-7(a). Therefore, either the cascading from the laser upper state cannot be dominant.

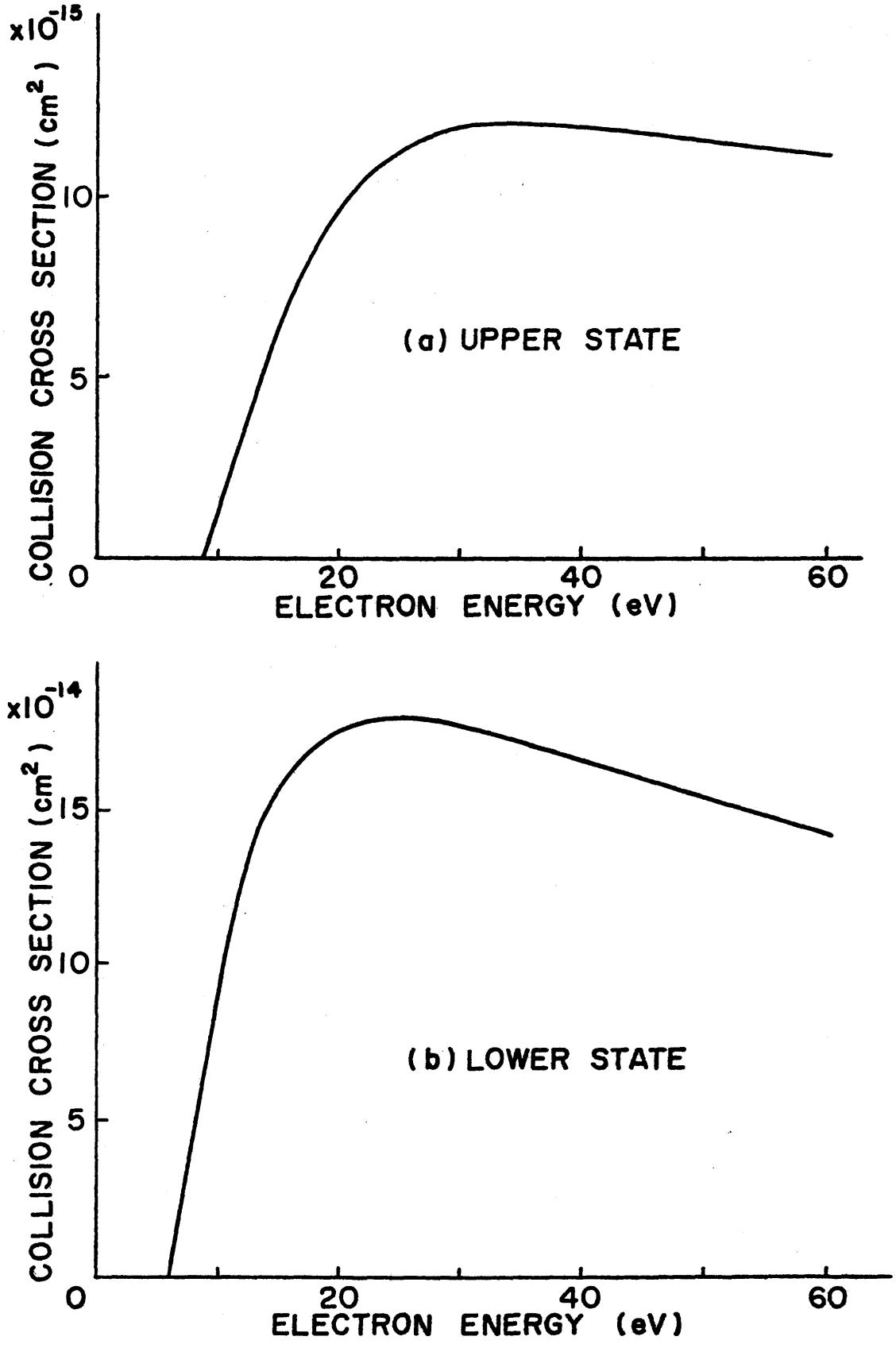

Fig.8-2. Estimated collision cross sections for stepwise excitations from Cd(II) ground state as a function of electron energy.

On the other hand, the stepwise excitation rate from the Cd(II) ground state is large probably, because the electronic collision cross section for the optically allowed transition $5p^2P_{3/2} - 5s^2S_{1/2}$ is expected to be large and the threshold energy is low (5.8 eV). As the transition probability A_{10} of the Cd(II) 2144 Å line is very large (3×10^8 sec^{-1}),[24,25] the non-radiative decay rate can be negligible compared with the radiative one. Then, in the steady state, n_1 is given by

$$n_1 = \frac{n^e n_{Cd^+} M_1}{\eta_1 A_{10}}, \tag{8.2}$$

where M_1 is the rate coefficient of the stepwise excitation from the Cd(II) ground state. η_1 is the trapping coefficient due to the imprisonment of the Cd(II) 2144 Å line, and it is shown in Fig.7-1 as a function of the optical depth k_0R. With the measured population density of the Cd(II) ground state, η_1 could be calculated. η_1 was not less than 0.72 in our experimental conditions. The collision cross section $\sigma_{M1}(u)$ was calculated in the same way as in the case of the laser upper state. It is shown as a function of the electron energy in Fig.8-2(b). The rate coefficient M_1 was calculated from $\sigma_{M1}(u)$ with the non-Maxwellian EDF.

§ 8.3. Comparison of Calculated and Experimental Results

The calculated n_1 and n_2 are shown by the dash-dot and dotted lines, respectively, in Figs.8-1, 8-3, and 8-4, and are tabulated in Tables 8-1 ~ 8-3. It can be seen from the figures

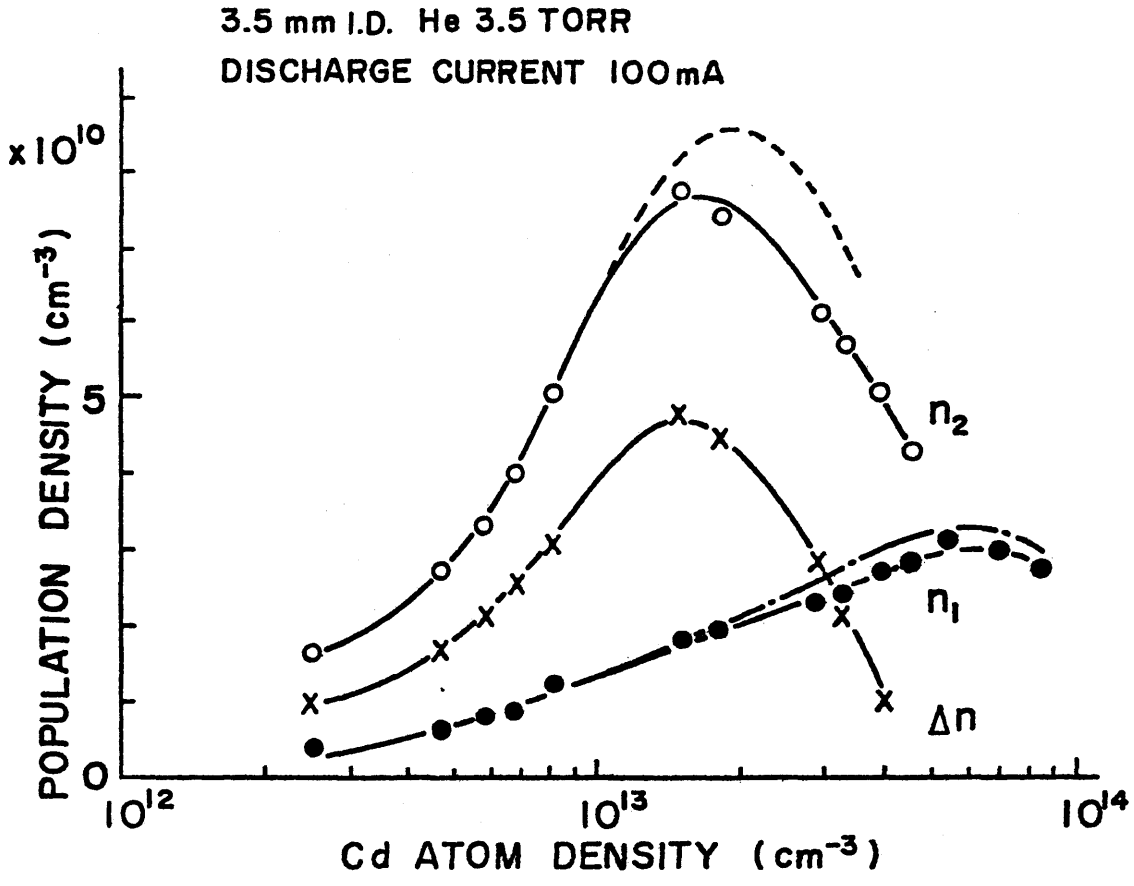

Fig.8-3. Calculated population densities of laser upper and lower states as a function of Cd atom density. The calculated results are shown by dotted and dash-dot lines.

Table 8-2. Excitation rates in the He-Cd discharge as a function of Cd atom density; 3.5 mm I.D.,initial He pressure of 3.5 Torr, discharge current of 100 mA.

	N_{Cd} (cm^{-3})	1.1^{12}	3.8^{12}	6.6^{12}	1.0^{13}	1.5^{13}	2.5^{13}	4.0^{13}
	$N_{2^3S+2^3P}$ (cm^{-3})	8.2^{12}	7.9^{12}	7.1^{12}	6.0^{12}	4.6^{12}	2.7^{12}	1.2^{12}
	$N_{2^1S+2^1P}$ (cm^{-3})	1.4^{12}	1.3^{12}	1.2^{12}	1.1^{12}	6.8^{11}	5.0^{11}	2.0^{11}
	n^e (cm^{-3})	8.0^{11}	8.6^{11}	9.0^{11}	9.4^{11}	9.8^{11}	1.1^{12}	1.1^{12}
	N_{Cd^+} (cm^{-3})	3.4^{10}	1.2^{11}	1.8^{11}	3.4^{11}	4.3^{11}	6.7^{11}	7.6^{11}
Upper State	Penning ex. rate $(cm^{-3}sec^{-1})$	3.3^{15}	1.1^{16}	1.7^{16}	2.2^{16}	2.5^{16}	2.5^{16}	1.7^{16}
Upper State	Stepwise ex. rate $(cm^{-3}sec^{-1})$	1.3^{16}	5.0^{16}	7.0^{16}	1.4^{17}	1.7^{17}	2.3^{17}	1.5^{17}
Upper State	A_{21} (sec^{-1})	1.2^6	-	-	-	-	-	-
Upper State	γ_{dif} (sec^{-1})	3.0^5	-	-	-	-	-	-
Upper State	γ_{de} (sec^{-1})	9.6^5	1.0^6	1.1^6	1.1^6	1.2^6	1.3^6	1.3^6
Upper State	N_u (cm^{-3})	6.6^9	2.4^{10}	3.3^{10}	6.1^{10}	7.2^{10}	9.1^{10}	6.0^{10}
Lower State	Stepwise ex. rate $(cm^{-3}sec^{-1})$	3.4^{17}	1.3^{18}	1.8^{18}	3.6^{18}	5.0^{18}	6.8^{18}	6.9^{18}
Lower State	A_{10} (sec^{-1})	3.0^8	-	-	-	-	-	-
Lower State	Trapping Coefficient	0.99	0.97	0.95	0.91	0.87	0.82	0.80
Lower State	N_1 (cm^{-3})	1.1^9	4.5^9	6.2^9	1.3^{10}	1.9^{10}	2.7^{10}	2.9^{10}

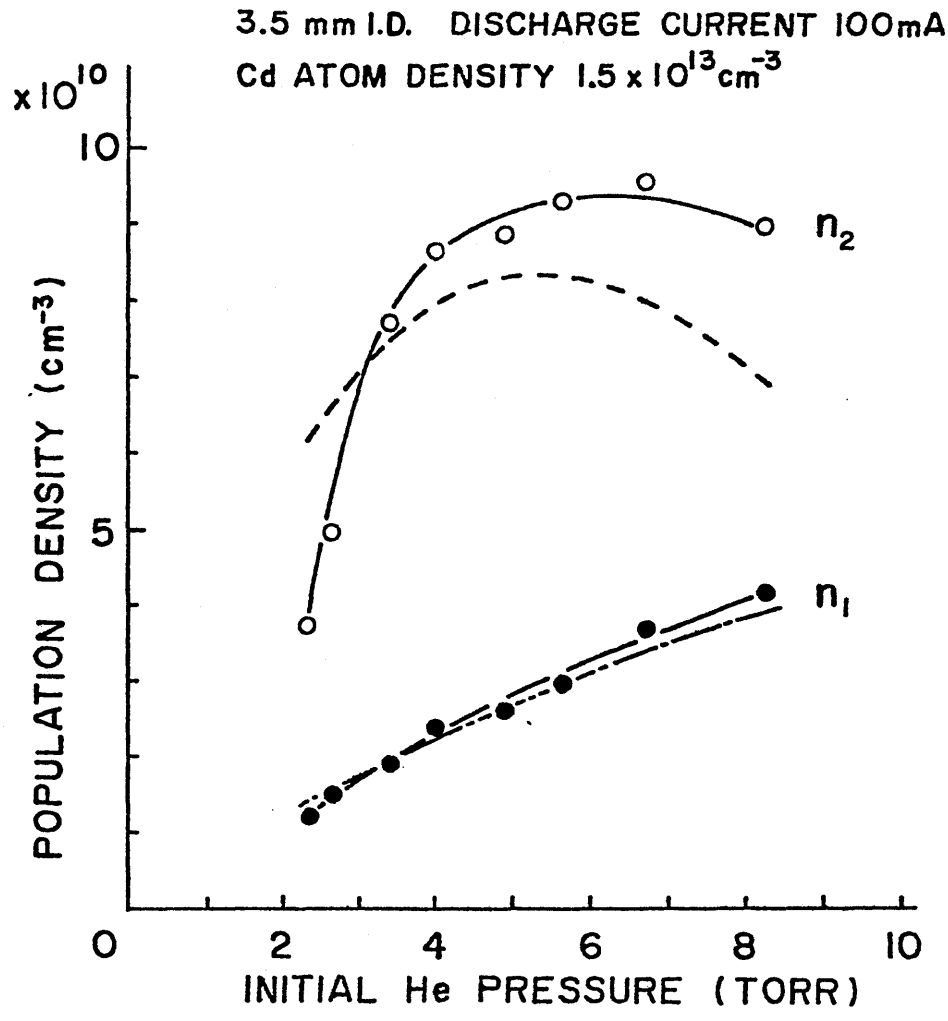

Fig.8-4. Calculated population densities of laser upper and lower states as a function of initial He pressure. The calculated results are shown by the dotted and dash-dot lines.

Table 8-3. Excitation rates in the He-Cd discharge as a function of initial He pressure; 3.5mm I.D., Cd atom density of 1.5×10^{13} cm^{-3}, discharge current of 100 mA.

	p_0 (Torr)	1.5	2.3	3.5	4.8	6.7	9.6
	$N_2{}^3S+2{}^3P$ (cm^{-3})	2.1^{12}	3.1^{12}	4.6^{12}	5.8^{12}	5.2^{12}	3.1^{12}
	$N_2{}^1S+2{}^1P$ (cm^{-3})	2.2^{11}	3.7^{11}	6.8^{11}	8.0^{11}	7.3^{11}	4.1^{11}
	n^e (cm^{-3})	4.4^{11}	7.0^{11}	9.8^{11}	1.4^{12}	2.2^{12}	3.4^{12}
	N_{Cd^+} (cm^{-3})	4.2^{11}	4.2^{11}	4.3^{11}	4.3^{11}	4.3^{11}	4.7^{11}
Upper State	Penning ex. rate ($cm^{-3}sec^{-1}$)	1.0^{16}	1.5^{16}	2.5^{16}	2.9^{16}	2.6^{16}	1.5^{16}
Upper State	Stepwise ex. rate ($cm^{-3}sec^{-1}$)	1.0^{17}	1.4^{17}	1.7^{17}	2.3^{17}	2.8^{17}	2.9^{17}
Upper State	A_{21} (sec^{-1})	1.2^6	-	-	-	-	-
Upper State	γ_{dif} (sec^{-1})	7.0^5	4.6^5	3.0^5	2.2^5	1.6^5	1.1^5
Upper State	γ_{de} (sec^{-1})	5.3^5	8.4^5	1.2^6	1.7^6	2.6^6	4.1^6
Upper State	N_u (cm^{-3})	4.6^{10}	6.3^{10}	7.2^{10}	8.4^{10}	7.9^{10}	5.7^{10}
Lower State	Stepwise ex. rate ($cm^{-3}sec^{-1}$)	2.8^{18}	4.1^{18}	5.0^{18}	7.2^{18}	9.7^{18}	8.3^{18}
Lower State	A_{10} (sec^{-1})	3.0^8	-	-	-	-	-
Lower State	Trapping Coefficient	0.89	0.89	0.87	0.89	0.89	0.87
Lower State	N_1 (cm^{-3})	1.0^{10}	1.5^{10}	1.9^{10}	2.7^{10}	3.6^{10}	3.2^{10}

that the calculated results account for the dependences of the measured n_1 and n_2 on various experimental parameters well.

In Fig.8-1, n_2 increased almost linearly up to the discharge current of 140 mA. The Penning excitation rate $(n_T\overline{\sigma v}_T + n_S\overline{\sigma v}_S)N_{Cd}$ in eq.(8.1) is saturated at the discharge current below 20 mA and remains almost constant at the higher discharge currents, because n_T and n_S are saturated in the low discharge current region as shown in Fig.6-5. On the contrary, n^e and n_{Cd^+} increase linearly with the discharge current and the stepwise excitation rate $n^e n_{Cd^+} M_2$ increases monotonically. The ratio $n^e n_{Cd^+} M_2/(n_T\overline{\sigma v}_T + n_S\overline{\sigma v}_S)N_{Cd}$ is about 9 at the discharge current of 100 mA. If the absolute value of the collision cross section for the stepwise excitation is smaller by one order of magnitude than the present one, n_2 calculated from eq.(8.1) is saturated in the low discharge current region and the measured discharge current dependence of n_2 cannot be interpreted. This means that the stepwise excitation process as well as the Penning excitation process is dominant in the excitation processes to the laser upper state. The saturation of n_2 at high discharge currents in Fig.8-1 is caused by the increase in $n^e\overline{\sigma v}_{de}$ and by the decreases in n_T, n_S, and M_2 due to the reduction of the electric field strength.

In Fig.8-3, n_2 increases with the Cd atom density and is saturated at the Cd atom density around 1.5×10^{13} cm^{-3}. The stepwise excitation rate $n^e n_{Cd^+} M_2$ in eq.(8.1) shows a behavior similar to that of n_2. The decrease in $n^e n_{Cd^+} M_2$ at the high Cd atom density is caused by the decrease in M_2 due to the reduction of the high energy part of EDF. The Cd atom density

dependence of $(n_T\overline{\sigma v}_T + n_S\overline{\sigma v}_S)N_{Cd}$ is also analogous to that of n_2 in this case. Slight discrepancies between the Cd atom density dependence of the measured n_2 and that of the calculated one may come from the uncertainty of the electron energy dependence of the cross section $\sigma_{M2}(u)$.

In Fig.8-4, n_2 increases with the initial He pressure and is saturated at the initial He pressure around 5 Torr. $n^e n_{Cd^+} M_2 / \{A_{21} + D_{Cd^+}/(\Lambda^2 p_0/2) + n^e\overline{\sigma v}_{de}\}$ follows the same behavior as n_2. The slow change in $n^e n_{Cd^+} M_2$ is caused by that the increase in n^e cancels the decrease in M_2 and, moreover, n_{Cd^+} is almost constant ($\sim 5 \times 10^{11}$ cm^{-3}) in the initial He pressure region concerned. On the contrary, when it is assumed that only the Penning excitation process is dominant, the calculated n_2 decreases rapidly at high initial He pressures because $(n_T\overline{\sigma v}_T + n_S\overline{\sigma v}_S)N_{Cd}$ is saturated at the initial He pressure around 4 Torr and $n^e\overline{\sigma v}_{de}$ increases.

The assumed value of $\sigma_{M2}(u)$ as to the laser upper state is of the order of 10^{-15} cm^2. It can be reasonable because the collision cross sections for the stepwise excitations from the Ca(II) and Ba(II) ground states are of the order of 10^{-15}cm^2,[26,27] and that from the Hg(II) ground state is of the order of 10^{-16} cm^2.[22]

The above facts show that the stepwise excitation process from the Cd(II) ground state is the dominant excitation process to the Cd(II) $5s^2{}^2D_{5/2}$ state as well as the Penning excitation process.

It is very interesting to note that there is not a very considerable difference between the Cd atom density dependence of

the Penning excitation rate and that of the stepwise excitation rate. Although it has been assumed from the similarity among the Cd atom density dependences of the product $(n_T + n_S)N_{Cd}$ and n_2 that the Penning excitation process is the most dominant,[1] calculations show that the Cd atom density dependences of the stepwise excitation rate, the charge transfer excitation rate, and the direct excitation rate are similar to that of n_2 also. Therefore, we can conclude that it is impossible to make clear which process is dominant among the excitation processes to the Cd(II) $5s^2{}^2D_{5/2}$ state only from the data concerning the Cd atom density dependence of n_2.

The excitation mechanism to the upper state of the Cd(II) 3250 Å line, the Cd(II) $5s^2{}^2D_{3/2}$ state, is expected to be the same as that to the Cd(II) $5s^2{}^2D_{5/2}$ state because the Cd(II) 3250 Å sidelight intensity follows the same behavior as the Cd(II) 4416 Å sidelight intensity.

In Fig.8-1, 8-3, and 8-4, n_1 calculated from eq.(8.2) accounts for the dependences of the measured n_1 on various experimental parameters well. This means that the stepwise excitation process from the Cd(II) ground state is the most dominant one among several excitation processes to the lower state of the Cd(II) 4416 Å line. In Fig.8-3, n_1 has a maximum at N_{Cd} higher than 1.5×10^{13} cm^{-3} at which n_2 has a maximum. This difference is caused by that the threshold energy for the stepwise excitation to the laser lower state is smaller than that to the laser upper state. The stepwise excitation rate $n^e n_{Cd^+} M_1$ does not decrease until the energy part of $u \geq 5.8$ eV of EDF decreases considerably and the increase in n^e or n_{Cd^+} is canceled out by the decrease in M_1.

In the He-Cd discharge, Csillag et al. obtained laser oscillation at the Cd(II) 4416 Å line.[28] The laser output power in Ne-Cd was smaller by two orders of magnitude than that in He-Cd of the same discharge current and electron temperature.[3,28] This difference is caused partly by that the laser upper state is never excited by the Penning excitation process in Ne-Cd. However, it is caused mainly by the following probably. First, the electron density in Ne-Cd is smaller than that in He-Cd according to our preliminary experiment. Second, the high energy part of EDF in Ne-Cd is possibly smaller than that in He-Cd. In fact, the high energy part of EDF in Ne is smaller than that in He when the average electron energies are identical between them.[29-31] As a result of these two facts, the population densities of the laser upper and lower states decrease. Particularly, that of the laser upper state decreases considerably.

Even if the stepwise excitation process is dominant, helium is necessary for obtaining the stable discharge, and the combination of EDF, the average electron energy, electron density, Cd atom density, and Cd^+ ion density optimum for the laser action at the Cd(II) 4416 or 3250 Å line.

§8.4. Conclusion

The excitation mechanisms to the upper and lower states of the Cd(II) 4416 Å line have been discussed on the basis of the measured electron density, ion densities, and population densities of the He(I) excited states using the rate equations and the non-Maxwellian EDF.

The following points have been made clear: The dependences of the population density of the upper state of the Cd(II) 4416 Å laser line on various experimental parameters have been explained well by taking into account the stepwise excitation process from the Cd(II) ground state, the Penning excitation process, and the non-radiative decay process. It is concluded that the dominant excitation process to the laser upper state are the stepwise excitation process from the Cd(II) ground state and the Penning excitation process. On the other hand, it has been assured that the most dominant excitation process to the laser lower state should be the stepwise excitation process from the Cd(II) ground state.

References in Chapter 8.

1) W.T.Silfvast,"Penning ionization in a He-Cd dc discharge," Phys.Rev.Lett.,vol.29,pp.1489-1492,Nov.1971.

2) T.G.Giallorenzi and S.A.Ahmed,"Saturation and discharge studies in the He-Cd laser,"IEEE J.Quantum Electron.,vol. QE-7,pp.11-17,Jan.1971.

3) M.Jánossy, V.V.Itagi, and L.Csillag,"On the excitation mechanism and operation parameters of the 4416 Å He-Cd laser,"Acta Phys.Hungar.,vol.32,pp.149-163,Jan.1972.

4) K.Miyazaki, Y.Ogata, T.Fujimoto, and K.Fukuda,"Excitation mechanism of 3250 and 4416 Å laser lines in the cataphoretic He-Cd laser discharge,"Japan.J.Appl.Phys.,vol.13,pp.1866-1874,Nov.1974.

5) P.G.Browne and M.H.Dunn,"Perturbation spectroscopy of the He-Cd laser discharge,"J.Phys.B:Atom.Molec.Phys.,vol.7, pp.1113-1121,1974.

6) E.A.Korolev, A.I.Odintsov, T.V.Feofilaktova, and N.I.Kalinovskaya,"Investigation of several characteristics of a He-Cd laser,"Opt.Spectrosc.,vol.37,pp.669-670,Dec.1974.

7) J.M.Green and C.E.Webb,"Second-kind collisions of electrons with excited Cd^+, Ca^+, Ga^+, Tl^+ and Pb^+ ions,"J.Phys.B:Atom. Molec.Phys.,vol.8,pp.1484-1500,1975.

8) M.Mori, K.Takasu, T.Goto, and S.Hattori,"Ion densities in a positive column He-Cd^+ laser discharge,"J.Appl.Phys.,vol.48, pp.2226-2230,June 1977.

9) M.Mori, M.Murayama, T.Goto, and S.Hattori,"Excitation mechanism of the Cd(II) 441.6 nm laser in the positive column He-Cd discharge,"submitted to IEEE J.Quantum Electron..

10) C.H.Chen, H.Haberland, and Y.T.Lee,"Interaction potential and reaction dynamics of He(2^1S,2^3S)+Ne, Ar by the crossed molecular beam method,"J.Chem.Phys.,vol.61,pp.3095-3103, Oct.1974.

11) S.Kubota, C.Davies, and T.A.King,"Nonmetastable Penning ionization in He(3^1P)-Ne, Ar, Kr, Xe collisions,"Phys.Rev., vol.A11,pp.1200-1204,April 1975.

12) S.Kubota, C.Davies, and T.A.King,"Relaxation of He(3^1S, 3^3S, 3^3P) states in Ne, Ar, Kr, and Xe collisions,"J.Phys.B: Atom.Molec.Phys.,vol.8,pp.1220-1227,1975.

13) M.Kohmoto and T.Watanabe,"Penning ionization of optically allowed excited atoms: the He(2^1P) and Ar system,"J.Phys.B: Atom.Molec.Phys.,vol.10,pp.1875-1887,1977.

14) L.D.Schearer and F.A.Padovani,"De-excitation cross section of metastable helium by Penning collision with cadmium atoms,"J.Chem.Phys.,vol.52,pp.1618-1619,1970.

15) G.J.Collins, R.C.Jensen, and W.R.Bennett,Jr.,"Charge-exchange excitation in the He-Cd laser,"Appl.Phys.Lett.,vol.19,pp.125-128,Sep.1971.

16) V.Čermák,"Penning ionization electron spectroscopy,III Ionization of cadmium,"Collec.Czech.Chem.Commun.,vol.36, pp.948-950,1970.

17) S.P.Varshavskii, A.A.Mityureva, and N.P.Penkin,"Effective cross sections for the formation of excited cadmium ions during ionization of cadmium atoms by electron impacts," Opt.Spectrosc.,vol.29,pp.341-343,1970.

18) B.L.Moiseiwitsch and S.J.Smith,"Electron impact excitation of atoms,"Rev.Mod.Phys.,vol.40,pp.238-321,April 1968.

19) M.B.Klein and D.Maydan,"Measurement of the upper laser

level lifetime in the helium-cadmium laser by fast cavity dumping techniques,"Appl.Phys.Lett.,vol.15,pp.509-511, June 1970.

20) A.Dienes and T.P.Sosnowski,"Magnetic-field dip measurements on the He-Cd laser,"Appl.Phys.Lett.,vol.16,pp.512-514,June 1970.

21) M.Mori, T.Goto, and S.Hattori,"Population densities of He excited states in a positive column discharge used for the $He-Cd^+$ laser,"submitted to J.Phys.Soc.Japan.

22) D.H.Crandell, R.A.Phaneuf, and G.H.Dunn,"Electron impact excitation of Hg^+,"Phys.Rev.,vol.A11,pp.1223-1232,1975.

23) H.W.Drawin,"Collision and transport cross sections," Association Euratom-C.E.A.Report EUR-CEA-FC 383 (revised),1967.

24) S.R.Baumann and W.H.Smith,"Atomic transition probabilities: ultraviolet multiplets of Zn I,II and Cd I,II,"J.Opt.Soc. Am.,vol.60,pp.345-347,March 1970.

25) T.Andersen and G.Sørensen,"Systematic trends in atomic transition probabilities in neutral and singly-ionized zinc, cadmium and mercury,"J.Quant.Spectrosc.Radiat. Transfer,vol.13,pp.369-376,1973.

26) P.O.Taylor and G.H.Dunn,"Absolute cross sections and polarization for electron-impact excitation of the K and H resonance lines of the Ca^+ ion,"Phys.Rev.,vol.A8,pp.2304-2321,1973.

27) D.H.Crandall, P.O.Taylor, and G.H.Dunn,"Electron-impact excitation of the Ba^+ ion,"Phys.Rev.,vol.A10,pp.141-157,1974.

28) L.Csillag, V.V.Itagi, M.Jánossy, and K.Rozsa,"Laser oscillation at 4416 Å in Ne-Cd discharge,"Phys.Lett.,vol.34A,pp.110-111, Feb.1971.

29) J.Y.Wada and H.Heil,"Electron energy spectra in neon, xenon,

and helium-neon laser discharge,"IEEE J.Quantum Electron., vol.QE-1,pp.327-335,Nov.1965.

30) W.R.L.Thomas,"The determination of the total excitation cross section in neon by comparison of theoretical and experimental values of Townsend's primary ionization coefficient,"J.Phys.B:Atom.Molec.Phys.,vol.2,pp.551-561,1969.

31) A.J.Postma,"calculated electron energy distribution functions for discharges in helium and helium-argon mixtures,"Physica, vol.43,pp.581-595,1969.

Chapter 9. Conclusions

The excitation and saturation mechanisms in the PC He-Cd^+ laser discharge have been discussed quantitatively in this dissertation, and the following results have been obtained.

The modified absorption method developed here proved to be useful and accurate in determining the population densities of various excited states of He(I), Cd(I), and Cd(II) in a cataphoresis type of PC He-Cd^+ laser discharge. This method gives accurate absorption coefficients in the ultraviolet region as well as in the visible region. With this method, the population density of the Cd(II) ground state could be determined directly for the first time. The modified absorption method could also be applied to the determination of the absolute intensities of spontaneous emissions in the PC gas discharge.

The electron energy distribution function (EDF) in the PC He and He-Cd discharges were discussed by comparing the experimentally determined population densities of the He(I) excited states with the theoretically calculated ones. It has been concluded that the dependences of the population densities on various experimental parameters can be explained with the non-Maxwellian EDF calculated from the Boltzmann transport equation consistently. Therefore, the non-Maxwellian EDF has been used throughout this dissertation.

It has been shown that the electron density in the He-metal discharge at medium pressures can be determined conveniently with the modified double probe method even in the case of the non-Maxwellian EDF. The electron density determined with this

method is in good agreement with that obtained with the microwave cavity technique by other investigators.

The He^+ and Cd^+ ion densities in the PC He-Cd^+ laser discharge were separated by combining the modified absorption method with the modified double probe method. They are also checked with the theoretical calculations, and it has been found that the dominant ionization process of Cd atoms is the direct ionization process. The Penning ionization rate of Cd atoms is not more than 10 % of the total ionization rate of Cd atoms. This is a very interesting result about the ionization mechanisms in the PC He-Cd^+ laser discharge, where the Penning ionization process has ever been considered to be the most dominant ionization process of Cd atoms.

The population densities of the He(I) excited states were determined experimentally with the modified absorption method, and calculated theoretically with rate equations. Especially in the discharge current dependences of them, it has been made clear for the first time that the saturation of the population densities of the He(I) 2^3S and 2^1S states in the low discharge current region is caused by the fact that the electronic de-excitation rate of the process $He(2^3S \text{ or } 2^1S) + e \rightarrow He(2^3P \text{ or } 2^1P) + e$ dominates over the diffusion losses or the stepwise ionization rate $He(2^3S \text{ or } 2^1S) + e \rightarrow He^+ + 2e$ in the discharge current region of $I > 10 \sim 20$ mA. The Cd(II) 4416 and 3250 Å sidelight intensities, however, increased monotonically with the discharge current up to a discharge current around 140 mA. This suggests that we have to take into account other excitation processes to

the laser upper states in addition to the Penning excitation process.

The population densities of the upper and lower states of the Cd(II) 4416 Å line were determined by combining the laser gain measurement and the modified absorption method. It has been found that the population density of the laser lower state cannot be neglected compared with that of the laser upper state while it was neglected so far in the interpretation of metal vapor lasers generally. This was assured from the discharge current and initial He pressure dependences of the laser output power. Therefore, it has been shown that the saturation mechanism of the Cd(II) 4416 Å laser output power cannot be interpreted unless the population densities of the laser upper and lower states are taken into account.

The excitation mechanisms to the laser upper and lower states were discussed finally using the measured parameters. It has been found that the dominant excitation processes to the laser upper state are the stepwise excitation process from the Cd(II) ground state and the Penning excitation process. The most dominant excitation process to the laser lower state is the stepwise excitation process from the Cd(II) ground state. Also it has been pointed out that we cannot decide which process is dominant among the excitation processes to the laser upper states only from the Cd atom density dependence of the Cd(II) 4416 or 3250 Å sidelight intensity. Actually, also the Cd(II) 5337 Å sidelight intensity, whose upper state was excited by the different excitation processes, followed a behavior similar to the Cd(II) 4416 or 3250 Å sidelight intensity.

As mentioned above, most of the essential parts as to the excitation mechanisms in the PC He-Cd^+ laser have been made clear in this study. Nevertheless, in order to make the excitation mechanisms clear more quantitatively, it is necessary to solve the following problems.

In Chapter 4, we introduced the nominal electron temperature. However, its meaning was not given there because the calculation of the electron current to the double probe was difficult on account of the collisions of electrons with He atoms.

In Chapter 8, it has been concluded that the stepwise excitations from the Cd(II) ground state to the laser upper and lower states play significant roles in the population inversion mechanisms. At that time, we used the values of the collision cross sections of the stepwise excitations inferred from the measured population densities of the laser upper and lower states. In future, it is indispensable to measure those collision cross sections.

The radiative decay rate of the upper state of the Cd(II) 4416 Å line has been measured by several investigators. It is necessary, however, to measure accurately the total decay rate in the discharge condition suitable for the laser action because the electronic de-excitation rate and the diffusion loss rate cannot be neglected compared with the radiative decay rate.

As the population densities of various excited states and the electron density all have been determined on the tube axis and the excitation mechanisms have been discussed there, the radial distributions of those population densities scarcely influence on the results and conclusions described here. However, it is

necessary to measure the radial distribution of each density in investigating the excitation mechanisms more quantitatively in future.

Acknowledgments

The author would like to express his thanks to his research advisor, Professor Shūzo Hattori, Faculty of Engineering, Nagoya University, for his guidance and continuous encouragement, and vice-advisors, Professor Yasuo Akao, Professor Takayoshi Okuda, and Associate Professor Toshio Goto, Faculty of Engineering, Nagoya University, for their guidances and helpful suggestions. The author is grateful to Professor Susumu Takeda, Faculty of Engineering, Nagoya University, for his useful discussions. At the same time, he is deeply indebted to professors in Department of Electrical and Electronic Engineering, Faculty of Engineering, Nagoya University.

The author is heartily grateful to Professor Yoshisuke Hatta, Faculty of Engineering, Tohoku University, for his guidance in plasma physics. He is indebted to Dr. Toshihiko Dote, Institute of Physical and Chemical Research, and Dr. Hiroyuki Kano, who is now in Nippon Telegraph and Telephone Public Corporation, for their valuable discussions.

The author wishes to express his appreciation to Mr. Mitsuo Mori, Faculty of Engineering, Nagoya University, for his constructions of the discharge tubes used in this study. He is indebted to Messrs. Katsuji Takasu, Motoaki Murayama, and Teruo Matsuba in his room for their cooperation during this study.

The author thanks to Associate Professor Akira Nishiwaki in Chubu Institute of Technology, Associate Professor Katsumi Yoneda in Faculty of Science and Technology, Meijō University, Assistant Professor Seitetsu Chinen in Toyata

Technical College, Assistant Professor Masahiro Tawada in Faculty of Science and Technology, Meijō University, and Mr. Toshihiko Arai in Faculty of Engineering, Meiji University, for their useful suggestions. He especially thanks to teaching staffs, Mr. Yoshiyuki Uchida, Mr. Fumio Matsuda, and Mr. Akihiro Kono in his room for their helpful discussions.

Many people have given time to the reading and criticism of this dissertation, and to all of them the author is very grateful.

Papers Concerned with This Study

論文題目	発表機関及び時期	共同研究者
1) Modified absorption method to determine level population densities in a cataphoresis type of He-metal laser discharge	Appl.Phys.Lett., vol.29, No.6, pp.358-360, Sep. 1976.	T.Goto S.Hattori
2) Ion densities in a positive column He-Cd^+ laser discharge	J.Appl.Phys., vol.48, No.6, pp.2226-2230, June 1977.	K.Takasu T.Goto S.Hattori
3) On the determination of the electron density in a positive column He-metal laser discharge having a non-Maxwellian electron energy distribution	J.Phys.Soc.Japan, vol.43, No.2, pp.662-668, Aug. 1977.	T.Goto S.Hattori
4) Population densities of He excited states in a positive column discharge used for the He-Cd^+ laser	J.Phys.Soc.Japan, vol.44, No.5, May 1978.	T.Goto S.Hattori
5) Excitation mechanism of the Cd(II) 441.6 nm laser in the positive column He-Cd discharge	IEEE J.Quantum Electron., vol.QE-14, No.6, June 1978.	M.Murayama T.Goto S.Hattori